

STATISTICAL AND NUMERICAL ANALYSES OF PRESSUREMETER TESTS IN GLACIAL TILLS

by

Kanagaratnam Balachandran,

B.Eng. (Hons), University of Moratuwa, 1997

M.Eng, University of Moratuwa, 2009

A thesis

presented to Ryerson University

in partial fulfillment of the
requirements for the degree of
Master of Applied Science
in the program of
Civil Engineering

Toronto, Ontario, Canada, 2016

© (Kanagaratnam Balachandran) 2016

AUTHOR'S DECLARATION

I hereby declare that I am the sole author of this thesis. This is a true copy of the thesis, including any required final revisions, as accepted by my examiners.

I authorize the Ryerson University to lend this thesis to other institutions or individuals for the purpose of scholarly research.

I further authorize the Ryerson University to reproduce this thesis by photocopying or by other means, in total or in part, at the request of other institutions or individuals for the purpose of scholarly research.

STATISTICAL AND NUMERICAL ANALYSES OF PRESSUREMETER TESTS IN GLACIAL TILLS

Kanagaratnam Balachandran
Master of Applied Science, 2016
Department of Civil Engineering
Ryerson University, Toronto, Canada

ABSTRACT

This study is performed on pressuremeter tests (PMT) in glacial tills based on comprehensive geotechnical investigation programs for a light rail transit project in the City of Toronto. The main objectives are to establish a correlation between SPT-N values and PMT parameters, and the Menard “ α ” factors for glacial tills. Currently, there are no such relationships available. So first, the pairs of PMT data and SPT-N values are collected at the same depth and test area. With these paired data, two linear correlation equations are established. Then, the numerical simulation is performed for PMTs in glacial tills by using finite element software, Plaxis 2D. The Mohr-Coulomb material model is used to model the different types of soil. The Menard “ α ” factor is suggested based on the best match between numerical prediction and field PMT. Ranges of SPT-N, E_{PMT} and P_L are also suggested for glacial tills.

ACKNOWLEDGEMENTS

This thesis arose in part out of years of research. In that time, I worked with several people whose contributions to the research and the making of the thesis deserve special mention. It is a pleasure to convey my gratitude to them in this humble acknowledgement.

In the first place I would like to record my sincere thanks and gratitude to Dr.Jinyuan Liu for his supervision, advice and guidance from the very early stage of this research as well as giving me extraordinary experiences throughout the work. Above all and the most needed, he provided me encouragement and support in various ways. His truly engineering intuition has made him as a constant oasis of ideas and passion in geotechnical engineering, which exceptionally inspired and enriched my growth as a student, a researcher and geotechnical engineer want to be.

In the second place I would like to record my sincere thanks and gratitude to Dr. Laifa Cao for his supervision. He provided a continuous source of ideas relating to the technical approach, numerical modelling, and the practical applications of the research.

Many thanks go to the Dean, Faculty of Engineering, Head of the Department of Civil Engineering and Dr A.El-Rabbany Professor and Graduate Program Director, Civil Engineering Program, for making all the necessary arrangements to carry out the project.

I would like to thanks Rachel Harpley, Graduate Program Administrator, Department of Civil Engineering, for her continuous communication and support during this study.

I must also thank the Department of Civil Engineering and Natural Sciences and Engineering Research Council of Canada for financial assistance and Metrolinx and SPL Consultant Limited for granting permission to study the ECLRT project data.

It is a pleasure to pay tribute to the academic staff during the course studying stage for helping me in various ways for the successful completion of this thesis.

I would like to give sincere thanks to my wife and my children for their endless love, encouragements and patience throughout my educational career.

TABLE OF CONTENTS

AUTHOR’S DECLARATION	ii
ABSTRACT.....	iii
ACKNOWLEDGEMENTS	iv
TABLE OF CONTENTS	vi
LIST OF TABLES.....	ix
LIST OF FIGURES.....	x
CHAPTER 1: INTRODUCTION.....	1
1.1 RESEARCH BACKGROUND	1
1.2 ENGINEERING BACKGROUND.....	1
1.3 NEED FOR RESEARCH.....	4
1.4 OBJECTIVES OF THE STUDY	5
1.5 RESEARCH METHODOLOGY	5
1.6 THESIS OUTLINE.....	6
CHAPTER 2: LITERATURE REVIEW	8
2.1 INTRODUCTION.....	8
2.2 PREVIOUS RESEARCH ON STATISTICAL CORRELATION BETWEEN SPT AND PMT	8
2.2.1 STANDARD PENETRATION TEST (SPT)	8
2.2.1.1 Equipment and Test Procedure	9
2.2.1.2 SPT-N correction	10
2.2.1.3 Interpretation of SPT.....	13
2.2.2 PRESSUREMETER TEST (PMT).....	13
2.2.2.1 Equipment and Test Procedure	14
2.2.2.2 Calibration.....	16
2.2.2.3 Test results interpretation.....	17
2.2.2.4 Application of these two parameters.....	20
2.2.2.5 Pressuremeter test correlation in soils.....	21
2.2.3 CORRELATION BETWEEN SPT-N WITH PMT PARAMETERS.....	26
2.3 PREVIOUS RESEARCH ON NUMERICAL SIMULATIONS OF THE PMT	28
2.3.1 GEOMETRY AND BOUNDARY CONDITION OF THE MODEL.....	28
2.3.2 PROB LENGTH (L) TO DIAMETER (D) RATIO (L/D RATIO).....	31
2.3.3 TYPE OF MODEL.....	31

2.3.4 DEFORMED MESH AND ANALYSIS	33
2.3.5 ANALYSIS RESULTS AND GRAPHS.....	36
2.3.6 COMPARISON OF PM AND YOUNG MODULUS	39
2.3.7 CONVENTIONAL LIMIT PRESSURE.....	39
2.3.8 ANALYTICAL METHOD	41
2.4 SUMMARY.....	42
CHAPTER 3: STATISTICAL CORRELATION BETWEEN SPT-N VALUE WITH PMT PARAMETERS FOR GLACIAL TILLS	44
3.1 INTRODUCTION.....	44
3.2 DATA SELECTION, SPT-N VALUE CORRECTION AND FILTERING	44
3.3 GENERAL RANGE OF SPT-N, E_{PMT} AND P_L FOR GLACIAL TILLS	46
3.3.1 RANGE OF SPT-N VALUE	46
3.3.2 RANGE OF E_{PMT} VALUE	49
3.3.3 RANGE OF P_L VALUE	53
3.4 CORRELATION BETWEEN SPT-N AND E_{PMT} VALUE.....	56
3.5 CORRELATION BETWEEN SPT-N AND P_L VALUE.....	59
3.6 COMPARISON OF CORRELATION BETWEEN SPT-N VALUE AND BOTH E_{PMT} AND P_L	65
3.6.1 COMPARISON OF CORRELATION BETWEEN SPT-N VALUES AND E_{PMT} FOR SAND	65
3.6.2 COMPARISON OF CORRELATION BETWEEN SPT-N VALUES AND P_L FOR SAND	67
3.6.3 COMPARISON OF CORRELATION BETWEEN SPT-N VALUES WITH BOTH	
E_{PMT} AND P_L FOR GLACIAL TILL.....	68
3.6.4 COMPARISON OF CORRELATION BETWEEN SPT-N VALUES AND E_{PMT}/P_L	71
RATIO FOR SAND.....	71
3.6.5 COMPARISON OF CORRELATION BETWEEN SPT-N VALUES AND E_{PMT}/P_L	
RATIO FOR GLACIAL TILL	73
3.7 SUMMARY	75
CHAPTER4: FINITE ELEMENT SIMULATION OF PMT	77
4.1 INTRODUCTION.....	77
4.2 FINITE ELEMENT METHOD.....	77
4.2.1 CONSTITUTIVE BEHAVIOUR	77
4.2.2 STEPS INVOLVED IN THE FEM	81
4.3 MOHR-COULOMB MATERIAL MODEL	83
4.4 2D PMT MODELLING AND VERIFICATION.....	85
4.4.1 2D PMT MODELLING.....	85
4.4.2 VERIFICATION OF THE MODEL.....	86
4.5 SENSITIVITY STUDY	92

4.5.1 MESH COARSENESS	92
4.5.2 HORIZONTAL BOUNDARY CONDITION	93
4.5.3 VERTICAL BOUNDARY CONDITION	94
4.6 CASE STUDY AT MOUNT DENNIS STATION	96
4.6.1 FINITE ELEMENT ANALYSES.....	97
4.6.2 2D FINITE ELEMENT RESULTS AND ANALYSIS	102
4.6.3 COMPARISON OF PRESSURE VS RADIAL STRAIN CURVES FROM PMT AND PLAXIS.....	110
4.6.4 VALIDATE THE RESULTS	116
4.7 SUMMARY	117
CHAPTER 5: CONCLUSIONS AND RECOMMENDATIONS FOR FUTURE	
RESEARCH	119
5.1 MAIN CONCLUSIONS	119
5.2 RECOMMENDATIONS FOR FUTURE RESEARCH	120
REFERENCES.....	122
APPENDICES	127

LIST OF TABLES

Table 1.1 Layout of thesis.....	6
Table 2.1 Approximate correction factor for SPT-N values (after Skempton, 1986).....	12
Table 2.2 Compactness condition of sands from SPT	13
Table 2.3 Approximate common values of the PMT parameters for clay and sand	21
Table 2.4 Typical Menard PMT values	22
Table 2.5 Typical Menard α factor (Briaud, 1992)	24
Table 2.6 Typical Young's modulus for different types of soils (Bowles, 1996).....	25
Table 2.7 Review of the Literature survey regards FEM simulation of PMT	42
Table3.1 Summary of SPT-N value for different types of soils	47
Table3.2 Summary of E_{PMT} value for different types of soils	50
Table 3.3 Summary of P_L value for different types of soils	53
Table3.4 Summary of correlation between SPT-N value with both E_{PMT} and P_L value for different types of soils	64
Table 3.5 Summary of range of SPT-N, E_{PMT} and P_L for corrected and filtered data	76
Table 3.6 Summary of correlation equation for E_{PMT} and P_L for $N160$	76
Table 3.7 Summary of E_{PMT}/P_L ratio for filtered data	76
Table 4.1 Parameters used in the M-C model for dense Hostun sand	86
Table 4.2 Comparison of horizontal displacement related to mesh coarseness	93
Table 4.3 The values of volumetric strain related to horizontal boundary condition	94
Table 4.4 The value of volumetric strain related to vertical boundary condition	95
Table 4.5 Summary of soil parameters used in the FEM analysis	98
Table 4.6 Linear correlation equations for glacial till at MD Station	112
Table 4.7 Linear with intercept correlation equations for glacial till at MD Station	115
Table 4.8 Summary of predicted E and calculated and analytical E_{PMT} at MD Station.....	116
Table 4.9 Summary of the E_{PMT} , E and Menard " α " factor for MD Station.....	118

LIST OF FIGURES

Figure 1.1 Typical glacial till (http://www.free-stockillustration.com	2
Figure 1.2 Crosstown route map (http://www.thecrosstown.ca/the-project).....	3
Figure 2.1 Standard split barrel sampler used in SPT (ASTM, 2014)	9
Figure 2.2 The Menard pressuremeter equipment (ASTM, 2000).....	14
Figure 2.3 Sequences of the PMT (ASTM, 2000)	16
Figure 2.4 Calibration curves obtained before the PMT (Bowles, 1997)	17
Figure 2.5 Typical pressuremeter test curve (ASTM, 2000)	18
Figure 2.6 Determination of limit pressure from inverse of volume vs pressure curve.....	20
Figure 2.7 Correlation between SPT N and net limit pressure (P_L) (Briaud, 1992).....	26
Figure 2.8 Correlations between SPT N and E_p (Briaud, 1992).....	27
Figure 2.9 Correlation between SPT N and E_{PMT} for clays (Ohya et al., 1982).....	27
Figure 2.10 Correlation between SPT N and E_{PMT} for sands (Ohya et al., 1982).....	28
Figure 2.11 The 2D axisymmetric model and associated mesh diagram (Malecot et al.(2012)).....	30
Figure 2.12 The 2D axisymmetric model and associated mesh diagram (Levasseur et al.(2012)).....	30
Figure 2.13 Geometry model for PMT (Plaxis 2D (2012))	31
Figure 2.14 FE discretization of the calibration chamber (Schanz et al. (2000))	33
Figure 2.15 Points from which the displacements are read (Rita (2008)).....	34
Figure 2.16 The 2D axisymmetric model and associated mesh diagram (Malecot et al.(2009)).....	34
Figure 2.17 The 2D axisymmetric model and associated mesh diagram (Levasseur et al.(2009)).....	35
Figure 2.18 Deformed geometry of the PMT (Plaxis (2012)).....	35
Figure 2.19 Geometry of axisymmetric model (Fawaz (2014))	36
Figure 2.20 Comparison between experimental and numerical results of the PMT (Schanz et al.(20000) 37	37
Figure 2.21 Model and test curves at 500 kPa of effective vertical stress (Rita (2008))	37
Figure 2.22 Comparison of numerical results and PMT data (Plaxis (2012))	38
Figure 2.23 Experimental and numerical pressure-volume curves at different depth (Fawaz (2014)).....	38
Figure 3.1 Range of SPT-N value for cohesive glacial tills	48
Figure 3.2 Range of SPT-N value for cohesionless glacial tills	49
Figure 3.3 Range of E_{PMT} value for cohesive glacial tills	51
Figure 3.4 Range of E_{PMT} value for cohesionless glacial tills	52

Figure 3.5. Range of P_L value for cohesive glacial tills	54
Figure 3.6 Range of P_L value for cohesionless glacial tills	55
Figure 3.7 Correlation between SPT-N vs E_{PMT} for cohesive glacial tills	57
Figure 3.8 Correlation between SPT-N vs E_{PMT} for cohesionless glacial tills	59
Figure 3.9 Correlation between SPT-N vs P_L for cohesive glacial tills	61
Figure 3.10 Correlation between SPT-N vs P_L for Cohesionless glacial tills	63
Figure 3.11 Comparison of correlation between SPT- $(N_1)_{60}$ and E_{PMT} for sand	67
Figure 3.12 Comparison of correlation between SPT- $(N_1)_{60}$ and P_L for sand.....	69
Figure 3.13(a) Comparison of correlation between SPT- $(N_1)_{60}$ vs E_{PMT} for linear with intercept relationship for glacial till.....	70
Figure 3.13 (b) Comparison of correlation between SPT- $(N_1)_{60}$ vs P_L for linear with intercept relationship for glacial till.....	71
Figure 3.14 (a) Correlation between E_{PMT} vs P_L for sand.....	72
Figure 3.14 (b) Correlation between E_{PMT}/P_L vs SPT- $(N_1)_{60}$ for sand	73
Figure 3.15 (a) Correlation between E_{PMT} vs P_L for glacial till.....	74
Figure 3.15 (b) Correlation between SPT- $(N_1)_{60}$ vs E_{PMT}/P_L for glacial till.....	75
Figure 4.1 Stresses on a typical element	78
Figure 4.2 Example of axisymmetric co-ordinate axis	81
Figure 4.3 Stresses in the axisymmetric element.....	81
Figure 4.4 Mohr's circles of effective stress (Ports and Zdravkovic (2001)).....	84
Figure 4.5 Mohr - Coulomb yield surfaces in principal stress space (Ports and Zdravkovic (2001)).....	85
Figure 4.6 2D axisymmetric model and associated mesh (Levasseur et al. (2009)).....	87
Figure 4.7 Geometry of the PMT model	87
Figure 4.8 Deformed mesh diagrams.....	88
Figure 4.9 Zoomed view of deformed mesh diagram.....	89
Figure 4.10 Horizontal displacement diagram	90
Figure 4.11 Zoomed view of horizontal displacement diagram.....	91
Figure 4.12 Pressure (p) vs volumetric strain ($\Delta v/V$) curves for verification of the model.....	92
Figure 4.13 Pressure (p) vs volumetric strain ($\Delta v/V$) curves for horizontal boundary conditions.....	94
Figure 4.14 Pressure (p) vs volumetric strain ($\Delta v/V$) curves for vertical boundary conditions.....	94
Figure 4.15 Soil profile at MD Station according to borehole MD101-PMT and test @6.0m	100
Figure 4.16 Typical FE mesh for numerical simulation at MD Station	101

Figure 4.17 Water table diagram for soil profile at MD Station @ test depth 6m after generate the in-situ initial stress condition.	101
Figure 4.18 Typical deformed meshes @ 6.0 m depth at MD Station.....	103
Figure 4.19 Zoomed views of the deformed meshes diagram@ 6.0 m depth at MD Station.....	104
Figure 4.20 Typical horizontal displacements arrow diagram @ 6.0m depth at MD Station.....	105
Figure 4.21 Zoomed views of the horizontal displacements arrow diagram @ 6.0m depth at MD Station	106
Figure 4.22 Typical horizontal displacement shaded diagram @ 6 m depth at MD Station.....	107
Figure 4.23 Zoomed view of horizontal displacement shaded diagram @ 6 m depth at MD Station....	108
Figure 4.24 Typical horizontal displacement cross section @6.0m depth at MD Station.....	108
Figure 4.25 Zoomed view of horizontal displacement cross section (along the probe) @6.0m depth at MD Station	109
Figure 4.26 Pressure vs radial strain graph at 6m depth for MD Station.....	111
Figure 4.27 Linear relationship for E_{PMT} vs E for cohesionless glacial till at MD Station	114
Figure 4.28 Linear relationship for E_{PMT} vs E for cohesive glacial till at MD Station	115

CHAPTER 1: INTRODUCTION

1.1 RESEARCH BACKGROUND

Statistical correlations between in-situ soil testing results and soil parameters are increasingly used during various stages of geotechnical engineering work. Statistical correlation equations are used during the early stage of engineering design work since they are more practical ways to proceed than extensive in-situ testing programs. In geotechnical design work statistical correlations are widely used to predict unknown parameters from simple known parameters, and save the time and cost.

Many geotechnical design parameters of the soil can be derived from Standard Penetration Test (SPT) and SPT is widely used around the world. On the other hands, Pressuremeter Test (PMT) is becoming increasing more popular for site investigation and geotechnical design especially in estimating soil properties for foundation design.

The numerical simulation of the PMT in use of the Finite Element Method (FEM) becomes more and more popular in geotechnical engineering. This method assumes to model the soil behavior by constitutive equation. A lot of soil constitutive models deal with a large variety of geotechnical problems. Nevertheless, these constitutive models have most of the time a large number of parameters whose values are unknown.

1.2 ENGINEERING BACKGROUND

This study is performed in the Eglinton Crosstown Light Rail Transit (ECLRT) project in Toronto. The site is situated along Eglinton Avenue from the existing Kennedy Subway Station in the east to the Mount Dennis Station in the west, in Toronto, Ontario, Canada.

The Toronto area acquired at least three glacial and two interglacial periods from the published geological data (Karrow (1967) and Sharpe (1980)). The geological history of the Toronto area

has included several advances and retreats of glaciers of Illinoian and Wisconsinan age (Karrow and White (1998)). The glacial tills in this area were generally deposited during the early to late Wisconsinan periods, represented by the Sunnybrook, Seminary, Meadowcliffe, Newmarket and Halton tills (Sharpe et al. (1999)). The glacial till deposits in Toronto can be divided into low plasticity cohesive glacial tills (silty clay to clayey silt glacial till) and cohesionless glacial tills (sandy silt to silty sand glacial till) (Manzari et al. (2014)). This kind of soil is derived due to the wearing away and entrainment of material as a result of the moving ice of a glacier. As shown in Figure 1.1, this type of soil can be described as high variability materials in both horizontal and vertical axis, and it normally contains complex non-linear stress-strain characteristics (Baker et al. (1998)).



Figure 1.1 Typical glacial till (Source- Mark Clark, <http://www.free-stockillustration.com>)

In addition to that, the tills consist of a heterogeneous mixture of gravel, sand, silt and clay size particles in varying proportions. Cobbles and boulders are common in these deposits (Robert et al. (2011)). The recorded maximum boulder size founded in Toronto so far has been about 3m in

the maximum dimension. Boulder volume ratios (BVR) (total boulder volume per volume of excavated earth material) of 0.12% and 0.17% for interglacial deposits and glacial tills respectively have been recommended for TTC Subway projects such as the Sheppard Subway (Boone and Shirlaw (1996)) and the Toronto – York Spadina Subway extension (Boone and Westland (2008)).

The proposed ECLRT is approximately 33 km in length and located approximately 7 km north of Lake Ontario. There are 25 proposed stations along the alignment as shown in Figure 1.2.

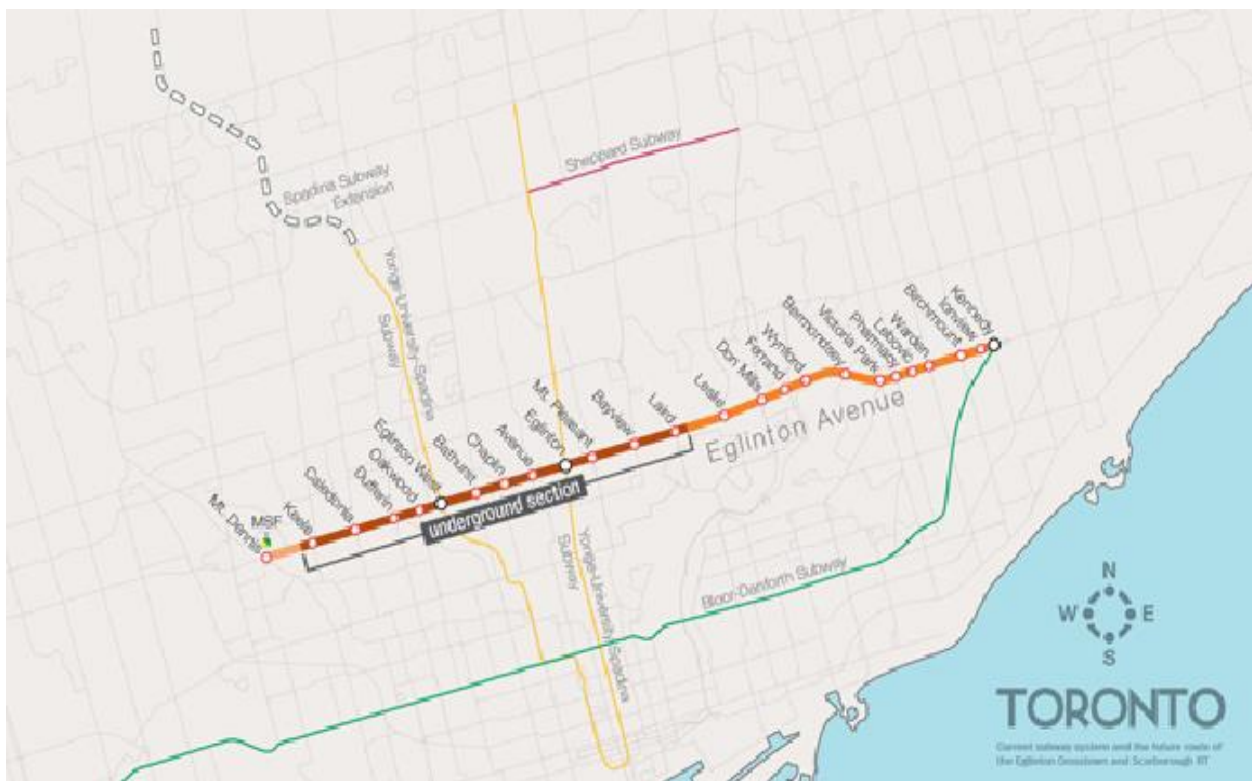


Figure 1.2 Crosstown route maps (<http://www.thecrosstown.ca/the-project>)

A series of laboratory and in-situ tests were conducted in advance at the above stations. The in-situ tests included SPTs, field vane shear tests, pre-bored TEXAM PMTs and seismic tests. The laboratory tests included density and moisture content measurements, grain size and hydrometer analysis, consistency (Atterberg) limit tests, consolidation tests, consolidated undrained and drained triaxial compression tests.

Based on these tests, the soil is classified as a glacial till which further classified as low plasticity cohesive glacial till and cohesionless glacial till according to the current version of TTC geotechnical standards (2014). In this area, the low plasticity cohesive glacial till mostly consists of the following soil types such as (i) silty clay till (ii) clayey silt till. The cohesionless glacial till mostly consists of following soil types such as (iii) sandy silt till (iv) silty sand till. The glacial tills are interbedded with silty clay, clayey silt, sandy silt, sand and silt and silty sand. However, the behavior of glacial tills in southern Ontario is not fully understood.

1.3 NEED FOR RESEARCH

The SPT is a well-established method of investigating soil properties. The differences in testing practices can be at least partly compensated by changing the measured N to $(N_1)_{60}$. There are many possible applications to correct the field measured SPT- N . There is no any general agreements on these applications of corrections of field measured SPT- N . In contrast to heavy criticisms about the SPT- N correction, there is strong needed to recommend a suitable correction method for more suitable for local conditions.

Estimation of the PMT parameters such as PM modulus (E_{PMT}) and pressure limit (P_L) from SPT $-N$ value has been studied by a few researchers in the past. Attempted correlations have usually been weak because of the differences in the methods and uncertainties involved in the tests. Even though, they are widely used in practice to get an idea about the level of the geotechnical parameters used in the design. The most of the correlation work done in the past was for sand and clay. There is almost no correlative work on glacial till especially Toronto glacial till. Hence research is needed to avoid these short comes and recommended a suitable relationship more suitable for local condition especially glacial tills in the city of Toronto.

In the case of numerical simulation of PMT, there is bulk of information available but none of these simulations is performed for real soil profile. The length to diameter ratio of the probe is influenced in the plain strain condition of the probe. A very little information is available on back calculating the PM modulus from pressure-volume curve which is obtained from simulation. However, this modulus differs from the elastic Young's modulus (E) which is the

principal soil parameter. The deduction of the Young's modulus from PM modulus is still under research. Menard developed ratio of $\frac{E_{PMT}}{E}$ for peat, clay, silt, sand, sand and gravel. Currently there is no such a relationship available for glacial tills in the city of Toronto. Hence there is a strong need for an in-depth research to develop and recommend suitable relationship for glacial tills in the city of Toronto.

1.4 OBJECTIVES OF THE STUDY

The main objectives of this thesis are listed below.

- (i) To correct the field measured SPT-N and develop a ratio of corrected SPT-N ($(N_1)_{60}$) to field measured SPT-N (N_F) which is ratio of ($\frac{(N_1)_{60}}{N_F}$) for glacial tills.
- (ii) To establish the ranges of SPT-N, E_{PMT} and P_L for glacial tills.
- (iii) To develop the statistical correlation relationships between SPT – N values with PMT parameters such as PM modulus (E_{PMT}) and pressure limit (P_L) for glacial tills.
- (iv) To develop the statistical correlation equations between PM modulus (E_{PMT}) with Young's modulus (E) for glacial tills by using Finite Element Method (FEM).
- (v) To develop the Menard's "α" factors which is the ratio of $\frac{E_{PMT}}{E}$ for glacial tills.

1.5 RESEARCH METHODOLOGY

Statistical analysis is carried out to investigate the relationship between SPT-N values with PMT parameters such as PM modulus (E_{PMT}) and pressure limit (P_L) for glacial tills in the city of Toronto based on soil investigation for the ECLRT project, Canada. The first step is to collect the pairs of PMT data and SPT-N value at the same depth in the same test area. After collect these data, the field measured SPT-N values are corrected and filtered. Then an attempt is made to develop a correlation between corrected and filtered SPT-N values with PMT parameters. As emphasized by Phoon and Kulhawy (1999), local correlations that are developed within a specific geologic setting generally are preferable to generalized global correlations because they are significantly more accurate.

Numerical analysis of PMT is performed using Plaxis 2D software. The Mohr–Coulomb (M–C) material model is used in this simulation. The appropriate parameters required are grasped from ECLRT geoengineering factual data reports for different types of soils. Those identified and extracted values are used in M-C material model which is in the constitutive model. The pressure-radial strain curve obtained from this simulation is used to compute the PM modulus (E_{PMT}). This is determined from the quasi-linear part of the pressure vs radial strain curve. However, this modulus differs from the elastic Young’s modulus (E) which is the principal soil parameter. The PM modulus has been related to the elastic Young’s modulus for the glacial tills. Then Menard’s rheological factors “ α ” which is the ratio of $\frac{E_{PMT}}{E}$ are derived for glacial tills.

These findings will help geotechnical community in evaluating and interpreting geotechnical parameters for their clients.

1.6 THESIS OUTLINE

This thesis consists of five chapters including references and annex. The thesis outline is shown in Table1.1.

Table1.1 Layout of thesis

Chapter	Title	Content
Chapter 1	Research background	Introduction, engineering background, need for research, objectives and methodology.
Chapter 2	Literature review	Literature review on SPT, PMT, correlation between SPT and PMT, and simulation of PMT.
Chapter 3	Statistical correlation between SPT-N and PMT for glacial tills	Correction for field measured SPT-N and SPT-N correction ratio. Develop the ranges of SPT-N, E_{PMT} and P_L for glacial tills. Develop correlation equations between SPT-N values with PMT parameters such as E_{PMT} and P_L for glacial tills.

		Compare these values and correlation equations with literature.
Chapter 4	Finite Element Method simulation of PMTs in glacial tills	FEM simulation is performed for PMTs by using Plaxis 2D. The M-C material model is adopted in this simulation. Develop correlation between PM modulus (E_{PMT}) and Young's modulus (E) for glacial tills. Develop Menard " α " factors for glacial tills.
Chapter 5	Conclusions and Recommendations	Content of conclusions and recommendations for future research.
References		
Appendices		Content of borehole reports, PMTs results, SPT-N corrections calculation sheets.

CHAPTER 2: LITERATURE REVIEW

2.1 INTRODUCTION

This chapter presents the results of the literature review conducted during the study. Information available from specific research studies on statistical correlation between SPT with PMT are very few, as only a few researchers have studied for sand and clay, even rare for Toronto glacial till. Such information, as it was considered very valuable, is presented in the first part of this chapter. Further literature survey was conducted on numerical simulations of the PMT. As a bulk of information on modelling has been emanated through actual practice and through available theory in the past researchers, the information gathered from those sources are presented in the second part of this chapter. This literature survey provided the background information for the formulation and execution of the research study.

2.2 PREVIOUS RESEARCH ON STATISTICAL CORRELATION BETWEEN SPT AND PMT

2.2.1 STANDARD PENETRATION TEST (SPT)

Standard penetration test (SPT) was first introduced in early 1900's by driving an open end pipe into soil during wash boring process and it has become the most extensively used in-situ test in site investigation practice.

Originally, the test was used to determine the relative density of granular soils. The idea of the SPT at the beginning was the comparison of blows required to penetrate the tested soil. If the number of blows for a tested location was larger than another tested location, it was concluded that the denser soil is the one with the largest blow count. Although SPT had been performed only for granular soils in the past, it is executed in almost all kinds of soil today including weak rock.

2.2.1.1 Equipment and Test Procedure

The SPT is a well-established method for soil investigation. As many forms of the test are in use worldwide, standardization is essential to facilitate the comparison of results from different investigations, even at the same site (Thorburn (1986)). In 1958, the test method was standardized by ASTM D1586. This means that the test standardized using a 50 mm outside diameter split spoon sampler with dimensions shown in Figure 2.1, is driven into soil with a 64 kg weight having a free fall of 760 mm auto hammer. The blows required to drive the split-barrel sampler a distance of 305 mm, after an initial penetration of 152 mm, is referred as the SPT-N value. Procedure is repeated after the drilling to the depth of the next test. (Conventionally test is performed at every 1.0 to 1.5 m intervals). In this study, SPT is performed in accordance with the ASTM D 1586 method.

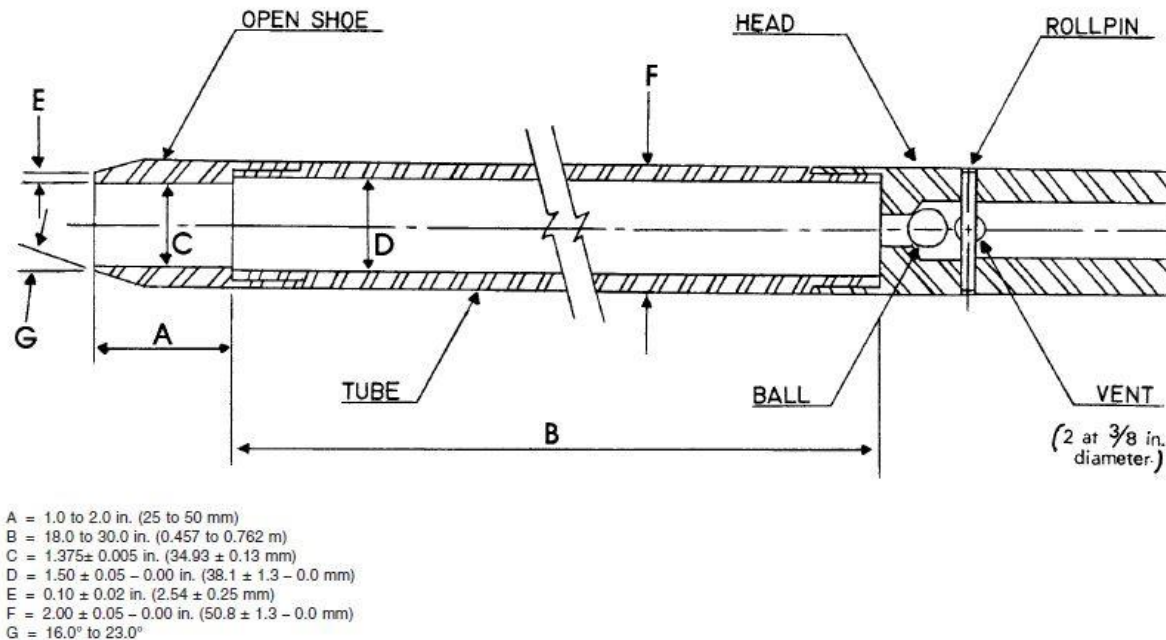


Figure 2.1 Standard split barrel sampler used in SPT (ASTM (2014))

2.2.1.2 SPT-N correction

The main reasons for extensive use of SPT in the site exploration can be related to many factors such as availability of equipment, simplicity of the operation, applicability in the type of soils and process of sampling. Due to all of these practical aspects, the results of SPT–N value can be dramatically affected by drilling operation, the type of equipment, capability of the operator, presence of size of particles (such as gravels, cobbles and boulders) and ground water conditions.

The SPT is usually stopped on the following situation where 50 or more blows are required for 150mm penetration, 100 blows are obtained to drive the required 300 mm and 10 successive blows produce no advance. If any of the above situations is encountered during the test, SPT-N value for the relevant depth is recorded as “refusal” and indicated with the letter “R” in the borehole logs.

In the above refusal situation the recorded field SPT-N value has to be corrected using Equation 2.1 according to Cao et al. (2015) with measured penetration depth.

$$N_F = \frac{305 N}{\Delta s} \quad [2.1]$$

Where N_F - Corrected SPT-N value
 N - Field recorded SPT-N value
 Δs - Measured penetration depth in mm

Because of the variability in equipment and operating conditions, the direct use of SPT results for geotechnical design is not recommended. As a result, many corrections shall be done on the field SPT-N values. These corrections can be summarized in an equation formatted as given below according to the Canadian Foundation Engineering Manual (2006).

$$(N_1)_{60} = C_E C_N C_R C_B C_S N_F \quad [2.2]$$

$$(N_1)_{60} = C_N N_{60} \quad [2.3]$$

$$N_{60} = C_E N_F \quad [2.4]$$

$$C_N = \left(\frac{P}{\sigma' } \right)^{0.5} \quad [2.5]$$

$$C_E = \frac{ER_R}{60} \quad [2.6]$$

Where C_E - Hammer energy correction factor

ER_R – Rod energy ratio

C_N - Overburden pressure correction factor

P - Atmospheric pressure

σ' - Effective overburden pressure

C_R - Rod length correction factor

C_B - Borehole diameter correction factor

C_S - Sampler correction factor

N_F - Corrected SPT-N value for penetration depth

N_{60} - SPT-N value corrected to 60% of theoretical free fall hammer energy

$(N_1)_{60}$ - SPT-N value correctd for both vertical effective stress and input energy

In the literature, most researchers express their concerns regards energy correction which was elaborated as follows. The energy delivered to the rods during a SPT expressed as a ratio of the theoretical free fall potential energy, can vary from 30% to 90% (Kovacs and Salomone (1982) and Robertson et al. (1983)). Schmertmann and Palacios (1979) have shown that the SPT blow count is inversely proportional to the delivered energy. Kovacs et al. (1984), Seed et al. (1984) and Robertson et al. (1983) have recommended that the SPT-N value has to be corrected to an energy level of 60% (CFEM (2006)). The SPT N-values corresponding to 60% efficiency are termed N_{60} . The practice in the United States/Canada the SPT N-value measured to an average energy ratio of 60% ($ER_R=60\%$) according to ASTM D1586-11 (2014). In this study energy ratio of 60% ($ER_R=60\%$) is adopted.

Other correction factors such as C_R , C_S and C_B are mentioned in Table 2.1 according to CFEM (2006) (after Skempton (1986)) is adopted in this study.

Table 2.1 Approximate correction factors for SPT-N values (after Skempton (1986))

Correction factor	Item	Correction factor value
C_R	Rod length (below anvil)	
	>10 m	1.0
	6 – 10 m	0.95
	4 – 6 m	0.85
	3 – 4 m	0.70
C_S	Standard sampler	1.0
	US sampler without liner	1.2
C_B	Borehole diameter	
	65 – 115 mm	1.0
	150 mm	1.05
	200 mm	1.15

Bowles (1997) suggested that there are three possible approaches about correction of SPT-N value.

- (i) Do nothing on the field recorded N value
- (ii) Adjust only for overburden pressure
- (iii) Apply all of the mention corrections

Since there is no any general agreement on the application of corrections to the field record SPT-N value, many of the correlation with SPT-N value only suggests energy correction, in some cases overburden correction was recommended. However, overburden correction for fine grained soils is still considered as controversial issue and not preferred in practice (Sivrikaya and Togrol, (2007)).

In contrast to serious criticisms about SPT for being destructive and sensitive to many factors, it is still most commonly used in-situ test in the geotechnical engineering practices.

2.2.1.3 Interpretation of SPT

A term describing the compactness condition of a cohesionless soil is often interpreted from the results of a SPT. Compactness and penetration values are often related to Table 2.2, which was proposed by Terzaghi and Peck (1967). Notice that the term “compactness condition” replaces the earlier term “relative density” used in the past according to CFEM (2006).

Table 2.2 Compactness condition of sands from SPT

Compactness condition	SPT-N Index (blows per 0.3 m)
Very loose	0 – 4
Loose	4 – 10
Compact	10 – 30
Dense	30 – 50
Very dense	Over 50

2.2.2 PRESSUREMETER TEST (PMT)

The PMT was invented by German Kogler (1930) in order to measure a soil deformation modulus. Due to the technology of that time, the unit was not operational. Furthermore, the inventor has failed to correctly interpret the results and the unit was abandoned.

In 1954 a young French engineer, Louis Menard, took up the idea in the refining the inflatable cylinder Kogler, he added two guard cells to the central measuring cell, avoiding the expansion of the drilling and thus making interpretable test. The unit became operational quickly because of advances in technology.

Now a day the PMT is becoming more popular in Ontario for site investigation and geotechnical design especially in estimating soil properties for foundation design. Louis Menard developed the pre-bored PMT device and considered it to be one of the most precise testing methods available for almost any type of soil (Menard (1965)).

2.2.2.1 Equipment and Test Procedure

Equipment

The pressuremeter consists of three main parts which are a probe, a control unit and tubing for inflation as shown in Figure 2.2.

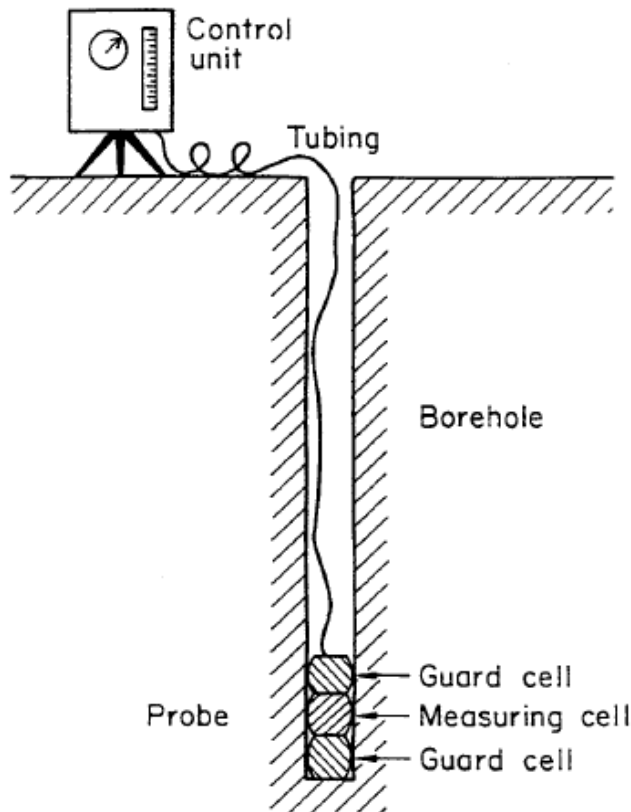


Figure 2.2 The Menard pressuremeter equipment (ASTM (2000))

- (i) **Probe:** A typical Menard type PM probe includes three separate cells namely as top cell, loading cell and bottom cell. Top and bottom cells are usually called “guard” cells which are filled with gas before the test in order to isolate the loading cell from end condition effects. Load cell is a flexible membrane (usually made from rubber) that is filled with water after the guard cells are inflated. The two guard cells are used to reduce end effects on the middle cell which will produce predominantly radial strains in the soil. Lateral displacements are measured only in the middle cell.

- (ii) **Control unit:** A metal case that houses the main cylinder, four quick connectors and the control valve. It consist a manual actuator to operate the piston and digital pressure gauge. It is used for both controlling the pressure given to the probe and monitoring the volume changes with respect to pressure increase by the dial gauges.
- (iii) **Tubing:** A high pressure single conduit fitted with a shut off quick connector to keep the probe and tubing saturated.

Currently, many types of PMs have been developed besides original Menard type PM such as self -boring and push in PMs which can be used for different in-situ soil conditions.

Borehole preparation

It is extremely important to minimize disturbance of the borehole wall during, the drilling process. Drilling methods should be selected to prevent collapse of the borehole wall, minimize erosion of the soil and prevent softening of the soil (Finn et al. (1984)). Good test results begin with a high quality borehole having minimal disturbance to its side walls, typically requiring mud wash rotary techniques which was recommended (Briaud (2013)). Maintain the drilling mud level at or near the top of the borehole minimizes the horizontal stress release from drilling. During drilling, the operator should carefully monitor the rotation rate, advance rate and mud flow to obtain a high quality borehole.

Test procedure

PMT is performed either by application of pressure in equal increments (stress controlled) or equal volume increments (strain controlled). In stress control test, apply the pressure on the control unit in about equal increments, until the expansion of the probe during one load increment exceeds about $\frac{1}{4}$ of V_0 . Generally 25, 50, 100 or 200 kPa pressures are selected for testing soils. Too small steps will result in an excessively long test, too large steps may yield result with inadequate accuracy. The pressure steps should be determined in such a way that about 7 to 10 load increments are obtained. In a strain control test, increase the volume of the probe on volume increments of 0.05 to 0.1 times the volume V_0 until the limit of the equipment is

reached. For both procedures, take readings after 30s and 1 min after the pressure or volume increment have been applied. Volume readings are recorded to an accuracy of 0.2% of V_0 and pressure readings to an accuracy of 5% of the limit pressure. The sequences of the PMT are shown in Figure 2.3.

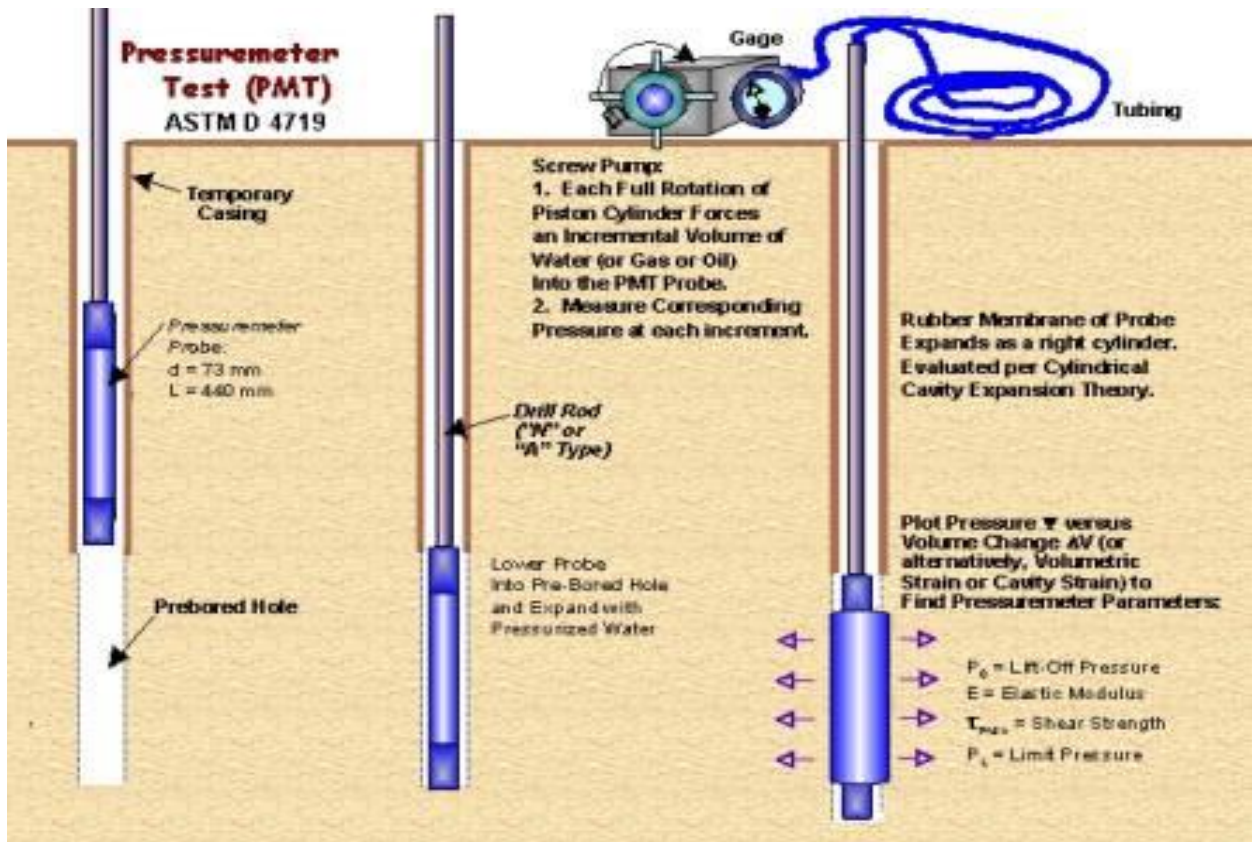


Figure 2.3 Sequences of the PMT (ASTM (2000))

2.2.2.2 Calibration

Before the test, two main calibration namely as volume and pressure calibration are required in order to correct the raw data obtained during the test. Those calibrations are explained below.

Volume calibration: Volume calibration is performed for detection of the leaks in the system and making necessary adjustments about system compressibility. PM probe is usually placed in a steel tube before the volume calibration and the pressure is increased in steps. For a given

pressure, the volume lost is determined since the probe is confined by the tubes. A typical volume calibration curve is given in Figure 2.4.

Pressure calibration: Pressure calibration is performed to determine the self - resistance of the rubber membrane to expansion. Before the pressure calibration, probe is taken out from the steel tube and calibration is performed in atmospheric pressure condition. A typical pressure calibration curve is given in Figure 2.4.

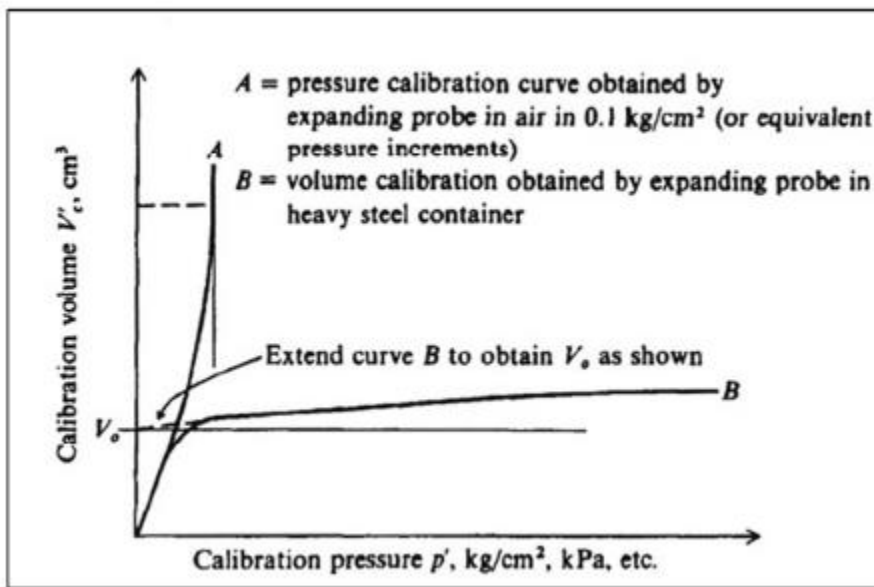


Figure 2.4 Calibration curves obtained before the PMT (Bowles (1997))

Calibration in the PMT is essential for obtaining accurate results from the test and if the calibrations are not carried out properly, and then the data obtained from the test can be considered as useless.

2.2.2.3 Test results interpretation

Plot the pressure–volume curve by entering corrected volume and corrected pressure on a coordinate system. Connect the points by a smooth curve. This curve is the corrected PMT curve which is shown in Figure 2.5 and used in to determine the PMT modulus.

The PMT modulus can also be calculated as represented by the slope of the pressure vs radial strain curve along its linear portion is shown in Equation 2.8.

$$E_{\text{PMT}} = (1 + \nu)(p_2 - p_1) \frac{\left[1 + \left(\frac{\Delta R}{R_0}\right)_2\right]^2 + \left[1 + \left(\frac{\Delta R}{R_0}\right)_1\right]^2}{\left[1 + \left(\frac{\Delta R}{R_0}\right)_2\right]^2 - \left[1 + \left(\frac{\Delta R}{R_0}\right)_1\right]^2} \quad [2.8]$$

Where p and $\frac{\Delta R}{R_0}$ are the pressure and the corresponding radial strain recorded at the beginning (subscript 1) and at the end (subscript 2) of the linear portion of the PMT pressure vs radial strain curve respectively. The Poisson's ratio is given by ν . For soils under drained conditions (ie, zero excess pore pressure) a Poisson's ratio of 0.33 is typically used, in which case the PMT modulus is designated as the Menard's modulus E_{PMT} (Baguelin et al. (1978)).

Conventional limit pressure is determined as follows, the limit pressure (P_L) is defined as the pressure where the probe volume reaches twice the original soil cavity volume, defined as the volume $V_0 + V_i$ (see Fig 2.5) where V_i is the corrected volume reading at the pressure where the probe made contact with the borehole. The volume reading at twice the original soil cavity volume is $(V_0 + 2V_i)$. The limit pressure is usually not obtained by direct measurements during the test due to limitation in the probe expansion or excessively high pressure.

If the test was conducted to read sufficient plastic deformation, the limit pressure can be determined by a $1/V$ to P plot, as shown in Figure 2.6. Points from the plastic range of the test generally fall in an approximate straight line. The extension of this line to twice the original probe volume will give the limit pressure (P_L) on the plot.

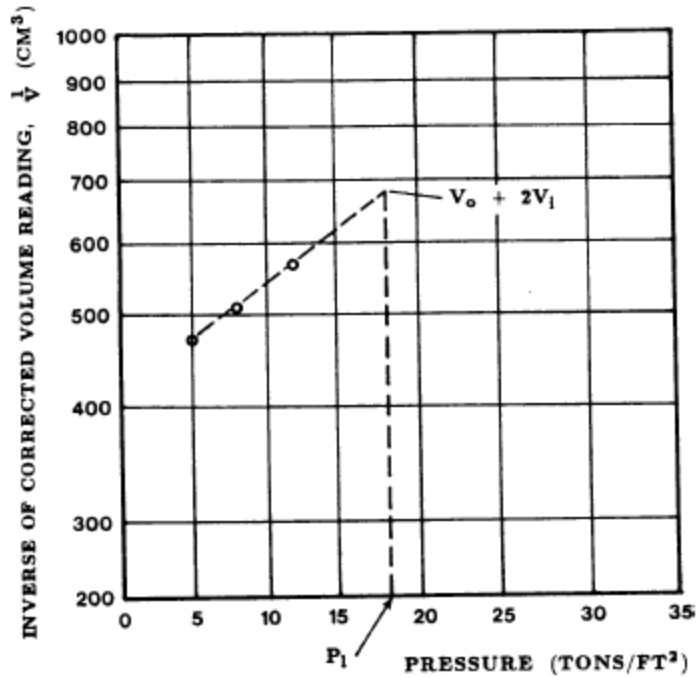


Figure 2.6 Determination of limit pressure from inverse of volume vs pressure curve (ASTM (2000))

2.2.2.4 Application of these two parameters

These two parameters are directly used in the Menard method (1965) to design the foundation. It is assumed that the ultimate bearing capacity is related to the pressure limit (P_L) and the settlement is related to PM modulus (E_{PMT}). The relationships have been shown below. The pressuremeter bearing capacity factor, k , is defined by following equation.

$$k = \frac{q_u - \sigma_v}{P_L - \sigma_h} \quad [2.9]$$

Where q_u – Ultimate bearing capacity

σ_v - Total vertical stress at the formation level

σ_h - Total horizontal stress at the pressuremeter test level

The Menard method for settlement is based on a modulus of elasticity which is expressed in terms of the PM modulus, E_{PMT} . The settlement is given by following equation.

$$S = \left(\frac{q - \sigma_v}{9E_{PMT}} \right) \times \text{a shape factor} \quad [2.10]$$

Where q is the total bearing capacity

In this study the PMT was performed accordance with Procedure B, volume-controlled loading, as outlined in the ASTM D 4719-00, Pre-bored PMT was completed using a TEXAM unit.

2.2.2.5 Pressuremeter test correlation in soils

Pressuremeter test results are used for identification of the soils. Briaud (1992) developed an approximate common value of the pressuremeter parameters for clay and sand are given in Table 2.3 below.

Table 2.3 Approximate common values of the PMT parameters for clay and sand

Sand					
Soil type	Loose	Compact	Dense	Very dense	
P_L (kPa)	0-500	500-1500	1500-2500	>2500	
E_p (kPa)	0-3500	3500-12000	12000-22500	>22500	
Clay					
Soil type	Soft	Medium	Stiff	Very stiff	Hard
P_L (kPa)	0-200	200-400	400-800	800-1600	>1600
E_p (kPa)	0-2500	2500-5000	5000-12000	12000-25000	>25000

Yield pressure (P_y)

The yield pressure indicates the end of the linear pseudo – elastic deformation and the onset of plasticity. This yield pressure is useful in indicating beyond which pressure significant creep deformation may occur.

Two useful ratios, such as $\frac{E_{PMT}}{P_L}$ and $\frac{P_L}{P_y}$ can be used as a general guideline for soil identification, as follows (Briaud (1992)).

For sand $7 < \frac{E_{PMT}}{P_L} < 12$

For clay $12 < \frac{E_{PMT}}{P_L}$

Typical Menard PMT values are presented in the CFEM (2006) is shown in Table 2.4.

Table 2.4 Typical Menard PMT values

Types of soil	Limit pressure (kPa)	$\frac{E_{PMT}}{P_L}$
Soft clay	50 – 300	10
Firm clay	300 – 800	10
Stiff clay	600 – 2500	15
Loose silty sand	100 – 500	5
Silt	200 – 1500	8
Sand and gravel	1200 – 5000	7
Till	1000 – 5000	8
Old fil	400 – 1000	12
Recent fill	50 – 300	12

For most soil types the ratio between the limit and the yield pressures may be expressed as

(Briaud (1992)) $1.3 < \frac{P_L}{P_y} < 2.0$

Deformation modulus of soils (Es)

The slope of the PMT curve in the elastic range is defined as PMT modulus or Menard modulus (E_P or E_M) of the soil. PMT modulus is commonly used in geotechnical practice for foundation design because in many cases, the soil or rock shows elastic behavior before the failure conditions. This deformation modulus is one of the most important parameters in any geotechnical engineering projects. Its determination is not a fully solved theoretically. (Serrano and Romana(2002)).

Expansion of a cylindrical cavity in an infinite elastic medium can be defined from cavity expansion theory (Lame (1852) cited in Baguelin et al. (1978)) as

$$G=V\left(\frac{\Delta P}{\Delta V}\right) \quad [2.11]$$

Where G – Shear modulus

V - Volume of the cavity

P – Pressure in the cavity

Shear modulus can be substituted with Young's modulus by using the equation obtained from theory of elasticity as follows.

$$G=\frac{E_S}{2(1+\nu)} \quad [2.12]$$

The critical parameter in the equation above is the Poisson's ratio (ν) which varies with the type of soil. For practical purposes a value of 0.33 is commonly selected for the Poisson's ratio. However, it is not appropriate to use for the undrained behavior of cohesive soils because volume of the soil does not change during the loading. Thus, saturated clay would have a Poisson's ratio of 0.45. Since Menard accepted the ν as 0.33 in his original study, PMT modulus is calculated as follows.

$$E_M=2(1+0.33) G \quad [2.13]$$

$$E_M=2.66G \quad [2.14]$$

Even though PMT modulus describes elastic behavior of a soil, it shall be used cautiously for design purposes because of the reasons listed below (Briaud (1992)).

- (i) Strains on the soil are generally in large ranges which may not be realistic for the real loading conditions.

- (ii) Tensile stresses are likely to occur in the circumferential direction during the test. In spite the PM is a compression test, since the soil is known to be weak under tension; measured modulus is reduced due to tensile stresses.
- (iii) Disturbances on the walls of borehole significantly reduce the modulus.
- (iv) Aspect ratio (L/D) of the probe has been found to be a factor that can be affecting the modulus.
- (v) Loading of the soil is relatively fast and in short time duration whereas the real superstructure loads act slowly during a larger time span.
- (vi) PMT modulus is a horizontal modulus. For vertical loading on the soil vertical modulus should be considered which differs from horizontal modulus especially in anisotropic soils.

As above reasons, the PMT modulus can be considered as a relatively low value compared with Young's modulus. Menard (1975) proposed that the PMT modulus should be divided by a correction factor α in order to relate with Young's modulus (Briaud (1992)). Typical α value is proposed by Menard for different types of soil and rock are given in Table 2.5.

Table 2.5 Typical Menard α factors (Briaud (1992))

Soil type	Peat		Clay		Silt		Sand		Sand and gravel	
	E/p_L^*	α	E/p_L^*	α	E/p_L^*	α	E/p_L^*	α	E/p_L^*	α
Over-consolidated			> 16	1	> 14	2/3	> 12	1/2	> 10	1/3
Normally consolidated	For all values	1	9-16	2/3	8-14	1/2	7-12	1/3	6-10	1/4
Weathered and/or remoulded			7-9	1/2		1/2		1/3		1/4
Rock	Extremely fractured $\alpha = 1/3$		Other $\alpha = 1/2$			Slightly fractured or extremely weathered $\alpha = 2/3$				

The pressuremeter modulus has been related empirically to the elastic modulus of the soil as $E_M/E = \alpha$, (Menard (1995)), in which α is termed by Menard as the rheological coefficient and has a value between 0 and 1.

Elastic Young's modulus of soil

Soil Young's modulus (E), commonly referred to as soil elastic modulus, is an elastic soil parameter and a measure of soil stiffness. It is defined as the ratio of the stress along an axis over the strain along that axis in the range of elastic soil behavior. The elastic modulus is often used for estimation of soil settlement and elastic deformation analysis. Soil elastic modulus can be estimated from laboratory or in-situ tests or based on correlation with other soil properties. In laboratory, it can be determined from triaxial test or indirectly from oedometer test. On field, it can be estimated from SPT, CPT and PMT.

Typical Young's modulus was recommended for different types of soils by Bowles (1996) were shown in Table 2.6.

Table 2.6 Typical Young's modulus for different types of soils (Bowles (1996))

Soil type		Young's modulus (Mpa)
Clay	Very stiff	2 – 15
	Soft	5 – 25
	Medium	15 – 50
	Hard	50 – 100
	Sandy	25 – 250
Sand	Silty	5 – 20
	Loose	10 – 25
	Dense	50 – 81
	Silt	2 – 20
Glacial till	Loose	10 – 150
	Dense	150 – 720
	Very dense	500 – 1440

2.2.3 CORRELATION BETWEEN SPT-N WITH PMT PARAMETERS

Estimation from SPT-N value of the two pressuremeter parameters such as pressuremeter modulus (E_{PMT}) and pressure limit (P_L) has been studied by a few researchers in the past (Briaud (1992) and Ohya et al. (1982)). Attempted correlations have usually been weak because of the differences in the methods and uncertainties involved in the tests. Even though, they are widely used in practice to get an idea about the level of the geotechnical parameters used in the design. One linear relationship with zero intercept was proposed by Briaud (1992) for the E_{PMT} and P_L from SPT-N value for sands (Figure 2.7 and Figure 2.8), while one non-linear relationship was proposed by Ohya et al. (1982) on the basis of data obtained from alluvial and dilluvial deposits in Japan (Figure 2.9 and Figure 2.10). Both researches indicated the wide scatter of data.

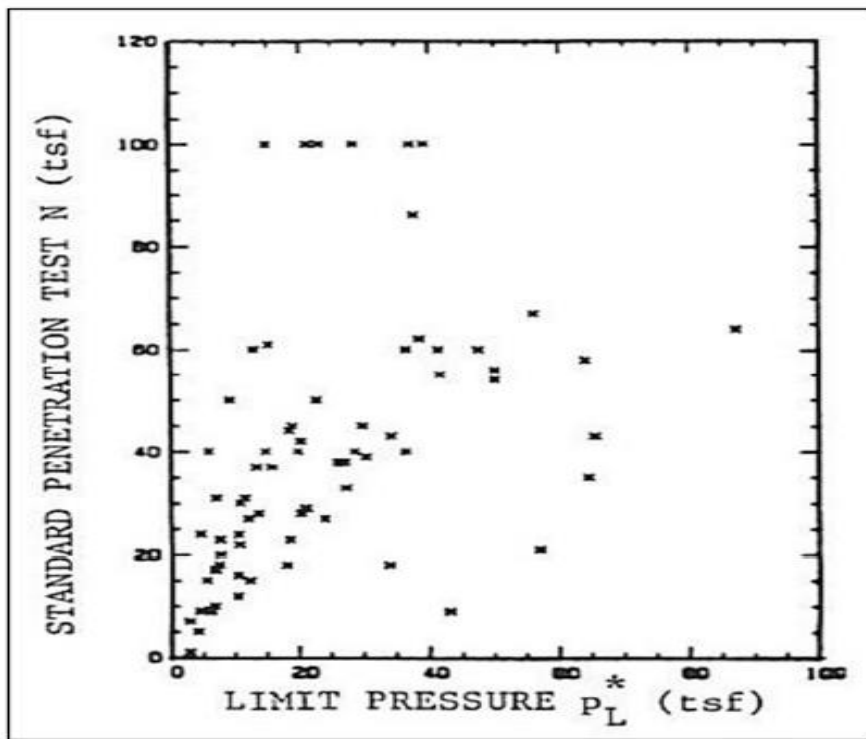


Figure 2.7 Correlation between SPT N and limit pressure (P_L) (Briaud (1992))

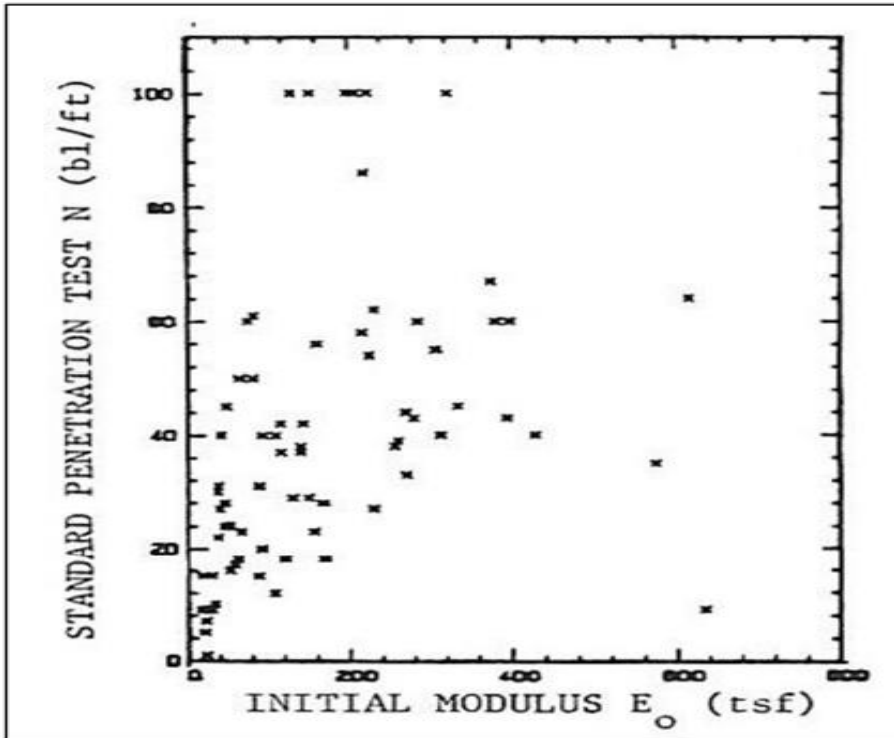


Figure 2.8 Correlations between SPT N and E_p (Briaud (1992))

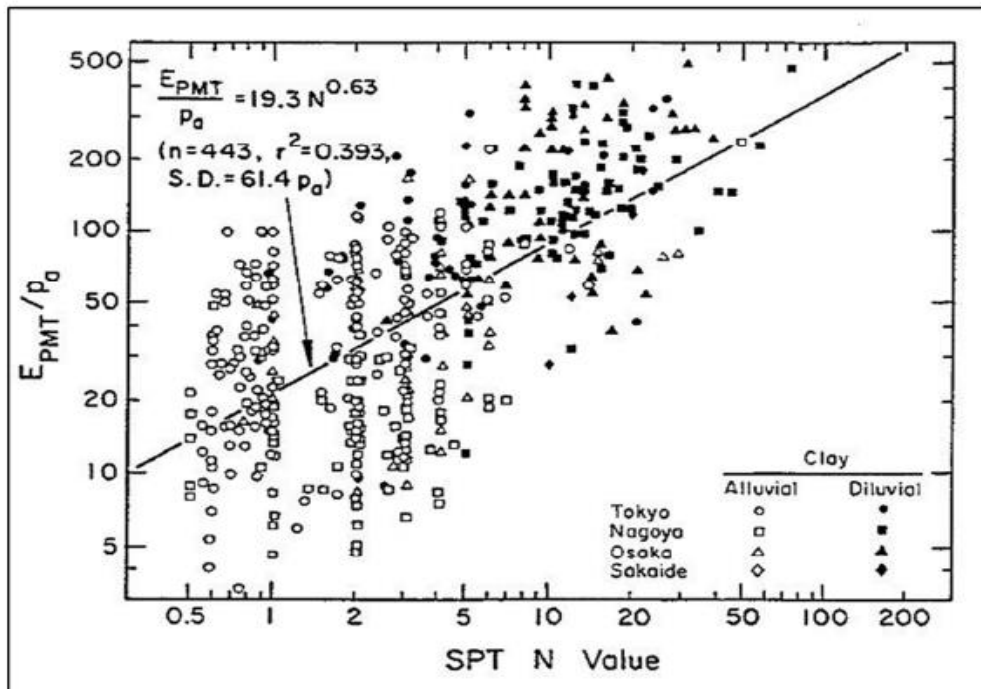


Figure 2.9 Correlation between SPT N and E_{PMT} for clays (Ohya et al. (1982))

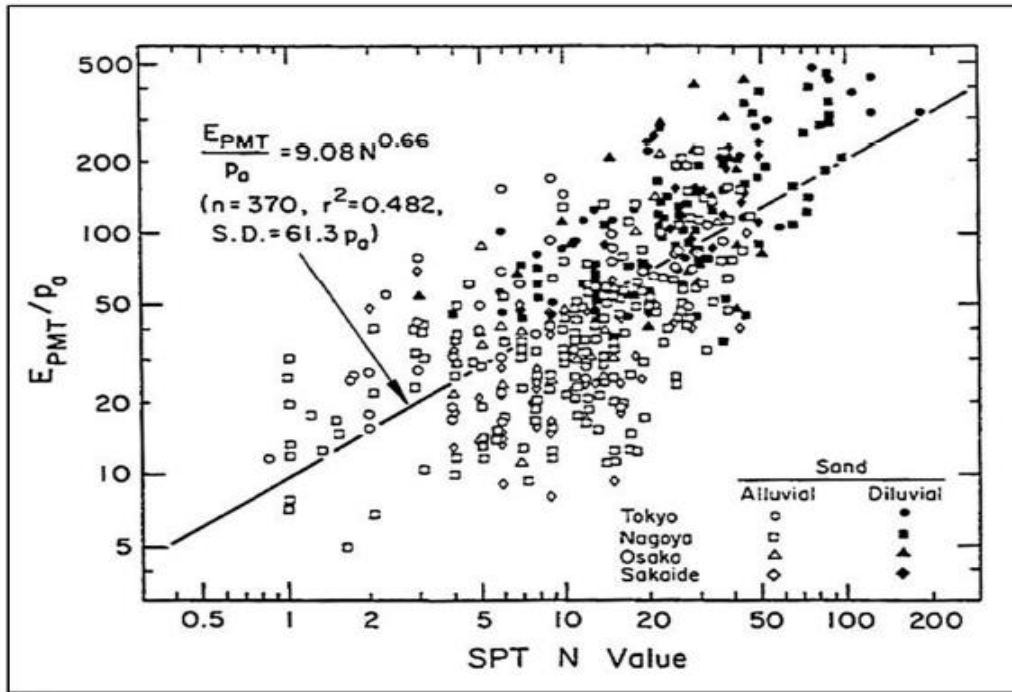


Figure 2.10 Correlation between SPT N and E_{PMT} for sands (Ohya et al. (1982))

Further nonlinear relationships between SPT and both E_{PMT} and P_L for sand and clay were proposed by Bozbey (2010) for data measured during an extensive geotechnical investigation conducted in Istanbul, Turkey. In glacial tills, there is a study conducted by Yagiz (2008), with a linear relationship with an intercept between the corrected SPT-N values (N_{cor}) with both E_{PMT} and P_L in Gumusler country, 10 km north of the city of Denizli, Turkey.

2.3 PREVIOUS RESEARCH ON NUMERICAL SIMULATIONS OF THE PMT

2.3.1 GEOMETRY AND BOUNDARY CONDITION OF THE MODEL

The PMT was simulated by an axisymmetric model in the Schanz et al. (2000), Michel et al. (2000), Jacques (2007), Rita (2008), Levasseur et al. (2009), Malecot et al. (2009), Plaxis 2D (2012), Monnet (2012), Sedran et al. (2013), Fawaz et al. (2014). The geometry sizes, diameter of 1.2 m and height of 1.5 m were used by Schanz et al. (2000), Malecot et al. (2009) and Plaxis

2D (2012). The Levasseur et al. (2009) used a diameter of 6 m and height of 5 m in their geometry model. Jacques (2007) and Monnet (2012) used a geometry model with diameters of 5 and 10 m respectively and 2 m of height above the midpoint of the probe. But both of them did not mention the dimensions below the probe. Fawaz et al. (2014) used 7 m of diameter and 7 m of height below the probe but did not mention the dimensions above the probe. The Michel et al. (2000), Rita (2008) and Sedran et al. (2013) did not define the geometry sizes of their model.

In the boundary conditions, bottom of the model was vertical fixity and both vertical faces of the model were horizontal fixity as used by Schanz et al. (2000) and Plaxis 2D (2012). Bottom of the model was total fixity (both horizontal and vertical) and both vertical faces of the model were horizontal fixity as used by Levasseur et al. (2009), Malecot et al. (2009) and Fawaz et al. (2014). Bottom of the model was vertical fixity and right side of the model was free in both directions (horizontal and vertical) and the left side of the model was horizontal fixity as used by Jacques (2007) and Monnet (2012). The Michel et al. (2000), Rita (2008) and Sedran et al. (2013) once again did not define the boundary conditions of their model.

Each authors used different geometry dimensions and boundary conditions. The geometry models with dimensions and boundary conditions that were available from the literature are shown in Figure 2.11 to Figure 2.13.

To simulate the test at a deeper elevation, a vertical stress was applied at the top of the mesh (load B). The pressuremeter applies a radial stress (load A) at the lower part of the borehole with an imposed stress at each loading steps as stated in the Jacques (2007). But in the Plaxis 2D (2012) and Schanz et al. (2000) load A was applied as a vertical surcharge stress and load B was applied in a radial stress on the probe. In the Levasseur et al. (2009) load B was used for both radial stress and overburden vertical stress.

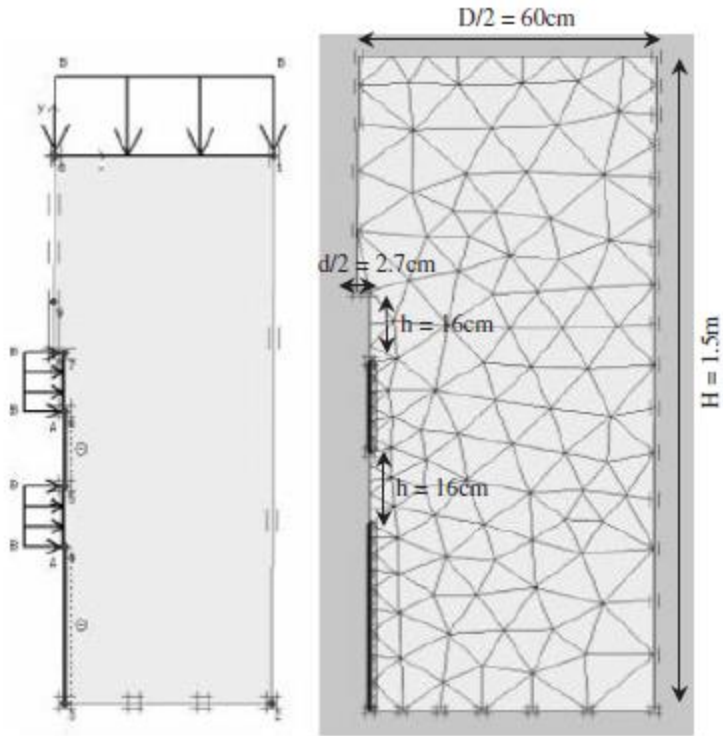


Figure 2.11 The 2D axisymmetric model and associated mesh diagram (Malecot et al. (2009))

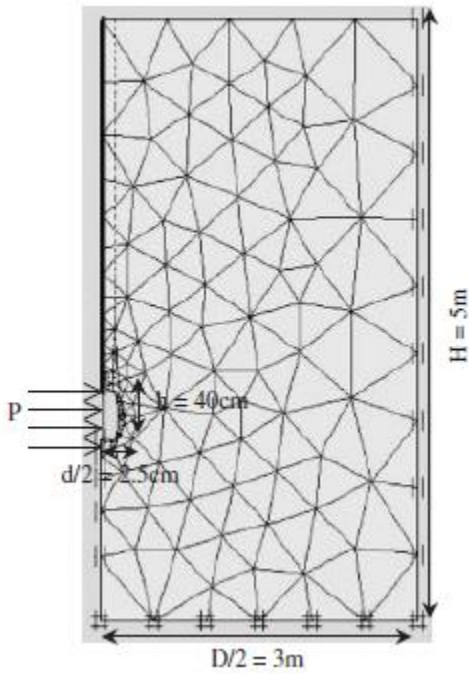


Figure 2.12 The 2D axisymmetric model and associated mesh diagram (Levasseur et al. (2009))

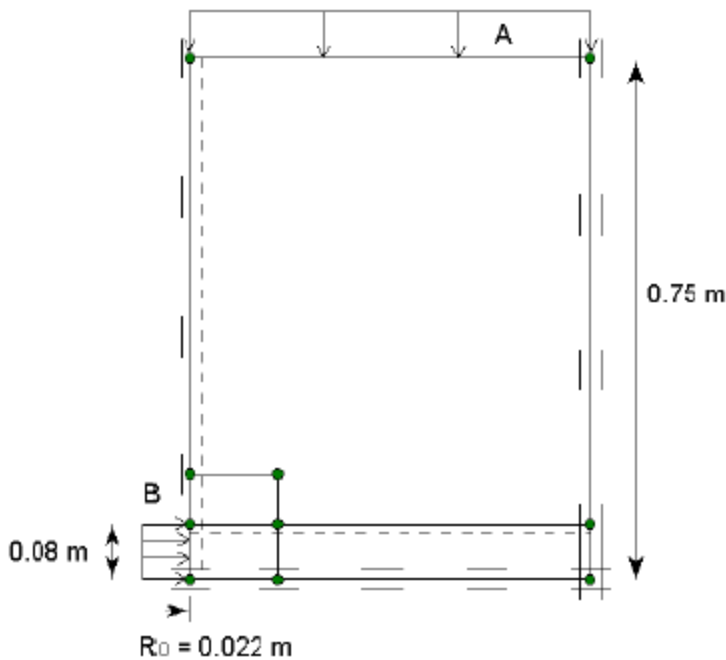


Figure 2.13 Geometry model for PMT (Plaxis 2D (2012))

2.3.2 PROB LENGTH (L) TO DIAMETER (D) RATIO (L/D RATIO)

The PMT was modeled as an axisymmetric problem. In this case, where L/D ratio is higher than 6, the test results were similar to those obtain considering plain strain conditions (Houlsby and Carter (1993)). The L/D ratio used by Waschkowski (1976), Schanz et al. (2000), Jacques (2007), Rita (2008), Levasseur et al. (2009), Plaxis 2D (2012), Monnet (2012) and Sedran et al. (2013) were 6.6, 2.9, 7.5, 6.7, 8, 3.6, 6 and 6.5 respectively. The Michel et al. (2000), Malecot et al. (2009), and Fawaz et al. (2014) did not mention the L/D ratio in their study.

2.3.3 TYPE OF MODEL

A lot of soil constitutive models can be found in the literature that permits to deal with a large variety of geotechnical problems. Nevertheless, these constitutive models have, most of the time, a large number of parameters whose values are not obvious to identify. Classically, the parameters' values are estimated from laboratory tests on small samples or from in- situ tests.

Unfortunately, parameters estimated from laboratory test were difficult because of the weak representative of the soil sample size and the perturbations imposed to the samples during its extraction. Likewise, in-situ tests do not allow the direct identification of the constitutive parameters of the soil layers.

In the literature, a constitutive model was introduced which was formulated in the frame work of classical theory of plasticity. Instead of using Hooke's single stiffness model with linear elasticity in combination with an ideal plasticity according to Mohr-Coulomb (M-C). A new constitutive formulation using a double stiffness model for elasticity in combination with isotropic strain hardening was used. Summarizing the existing double stiffness models the most dominant type of model is the Cam Clay model (Hashiguchi (1985) and Hashiguchi (1993)). To describe the non-linear stress strain behavior of soil, beside the Cam Clay model the pseudo elastic (hypo-elastic) type of model has been developed. There an Hookean relationship was assumed between increments of stress and strain and non-linearity was achieved by means of varying Young's modulus. The Duncan Chang (1970) model known as hyperbolic model captures soil behavior in a very tractable manner on the basis of only two stiffness parameters and it was very much appreciated among consulting geotechnical engineers. The major inconsistency of this type of model which was the reason why it was not accepted by scientists is that, in contrast to the elasto - plastic type of model, a purely hypo elastic model cannot consistently distinguish between loading and unloading. In addition the model was not suitable for collapse load computation in the fully plastic range. These restrictions will be overcome by formulating a model in an elasto - plastic frame work in the constitutive models. The hardening soil model supersedes the Duncan Chang model. Firstly by using the theory of plasticity rather than theory of elasticity and secondly by including soil dilatancy and thirdly by introducing a yield cap.

In case of simulation of PMT, the M-C model was used as a material model by Schanz et al. (2000), Levasseur et al. (2009), Malecot et al. (2009), Monnet (2012) and Fawaz et al. (2014). The hardening soil model (HSM) was used by Michel et al. (2000), Rita (2008), Plaxis 2D (2012) and Sedran et al. (2013). Jacques (2007) used Tresca model as a material model in the simulation study.

2.3.4 DEFORMED MESH AND ANALYSIS

In the PMT analysis, 15 nodes triangular elements were used in the mesh by Jacques (2007) and Rita (2008). The deformed geometry of the PMT after the simulation from Schanz et al. (2000), Rita (2008), Levasseur et al. (2009), Malecot et al. (2009), Plaxis 2D (2012) and Fawaz et al. (2014) are shown in Figure 2.14 to Figure 2.19 respectively.

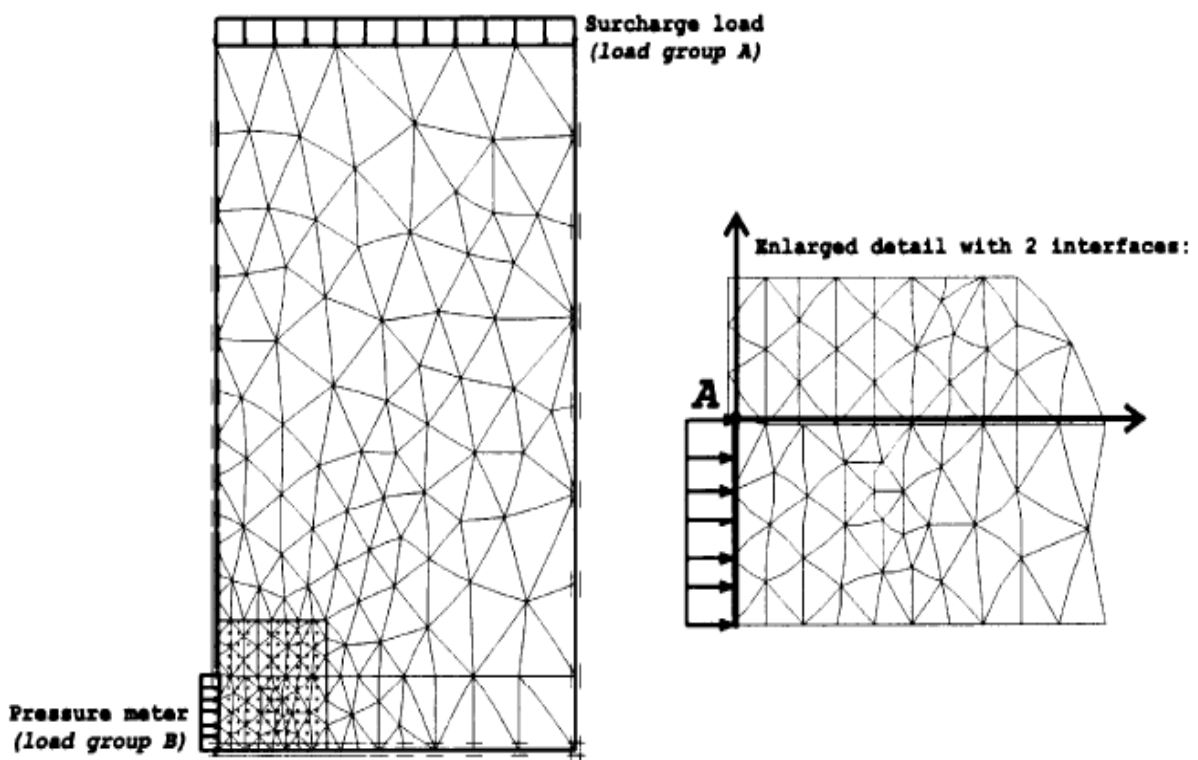


Figure 2.14 FE discretization of the calibration chamber (Schanz et al. (2000))

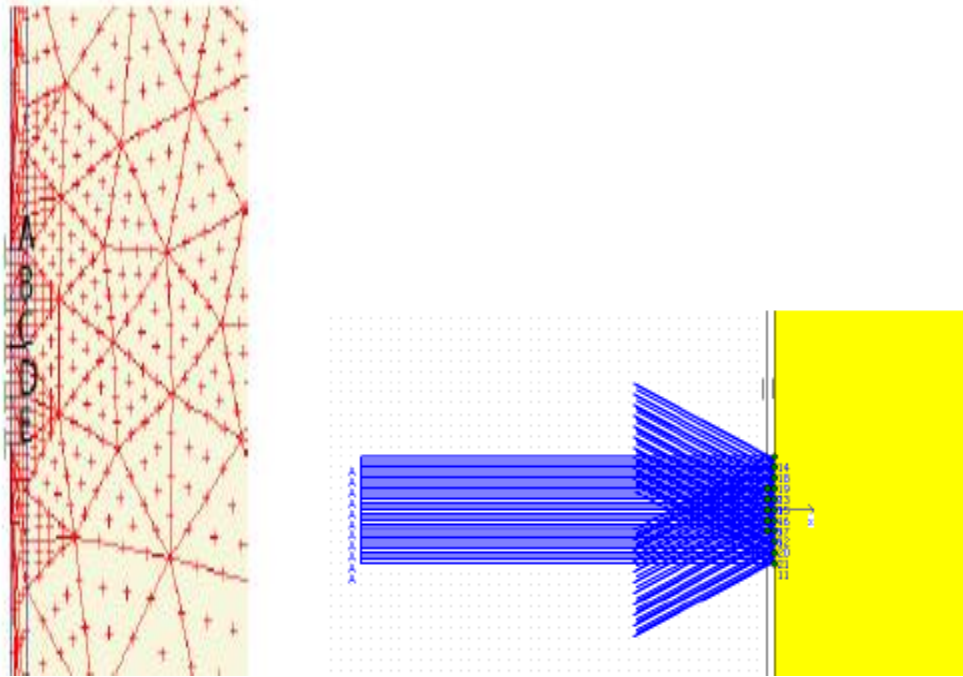


Figure 2.15 Points from which the displacements are read (Rita (2008))

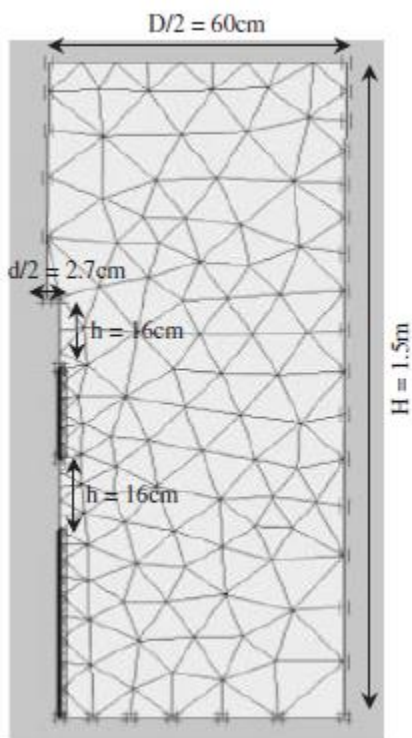


Figure 2.16 The 2D axisymmetric model and associated mesh diagram (Malecot et al. (2009))

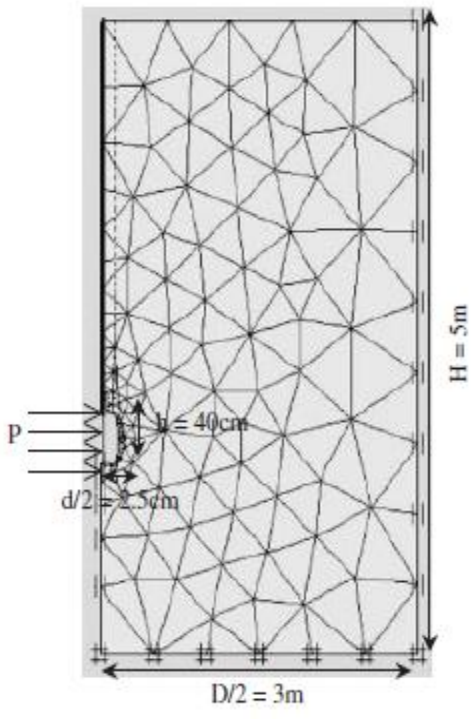


Figure 2.17 The 2D axisymmetric model and associated mesh diagram (Levasseur et al. (2009))

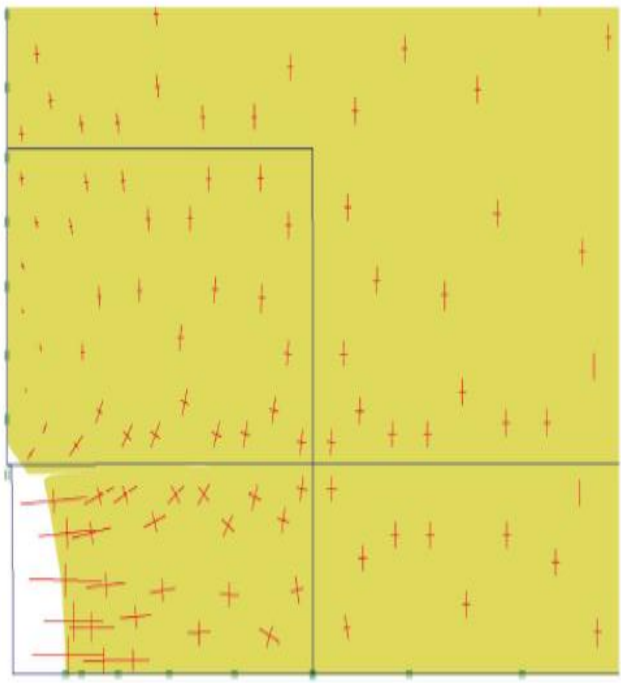


Figure 2.18 Deformed geometry of the PMT (Plaxis (2012))

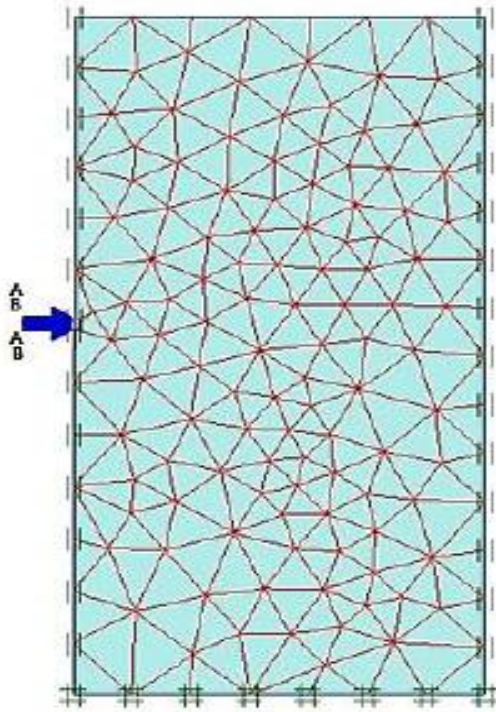


Figure 2.19 Geometry of axisymmetric model (Fawaz (2014))

In this FE analysis of PMT, a vertical interface along the shaft of the PMT borehole and a horizontal interface just above the PM were introduced to allow for a discontinuity in horizontal displacement in the Plaxis 2D (2012). The vertical interface along the borehole face was introduced in the Levasseur et al. (2009) and Malecot et al. (2009).

2.3.5 ANALYSIS RESULTS AND GRAPHS

The numerical results and pressuremeter test data were plotted and compared, which were shown in Figure 2.20 to Figure 2.23 from Schanz et al. (2000), Rita (2008), Plaxis 2D (2012) and Fawaz (2014) respectively. Graphs were drawn for pressure vs volumetric strain. The volumetric strain was calculated from the original radius R_0 and lateral expansion U_x of the PM. The volume change cannot directly be measured from Plaxis and was calculated from Equation 2.15.

$$\frac{\Delta V}{V_0} = \frac{(R_0 + U_x)^2 - (R_0)^2}{(R_0)^2} \quad [2.15]$$

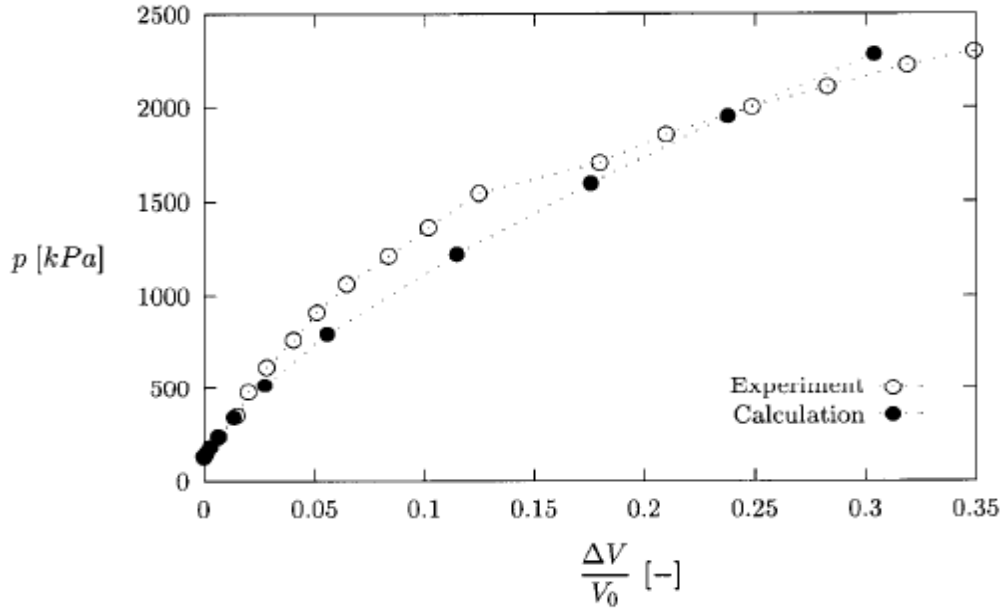


Figure 2.20 Comparison between experimental and numerical results of the PMT (Schanz et al. (2000))

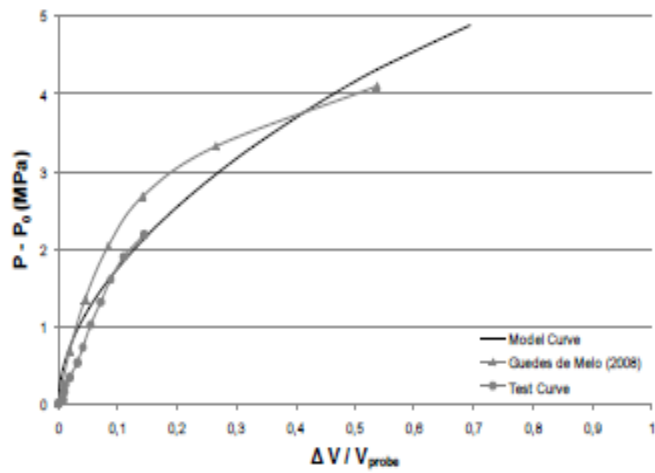


Figure 2.21 Model and test curves at 500kPa of effective vertical stress (Rita (2008))

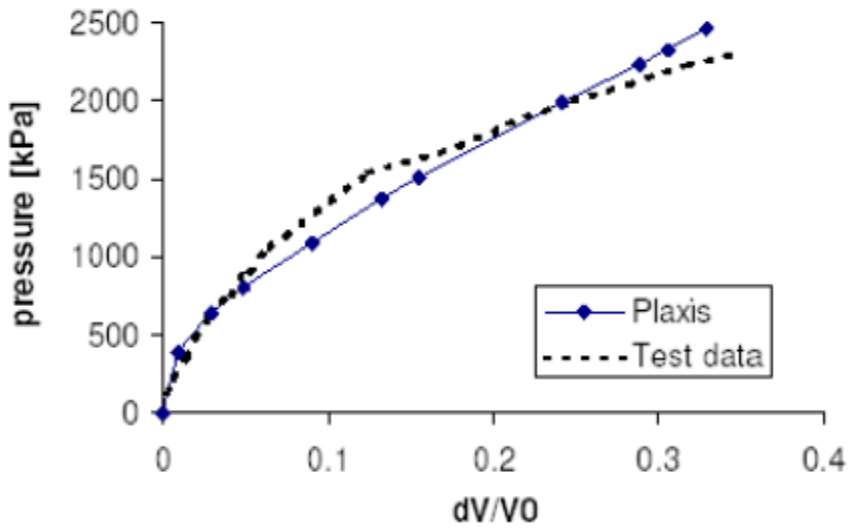


Figure 2.22 Comparison of numerical results and PMT data (Plaxis (2012))

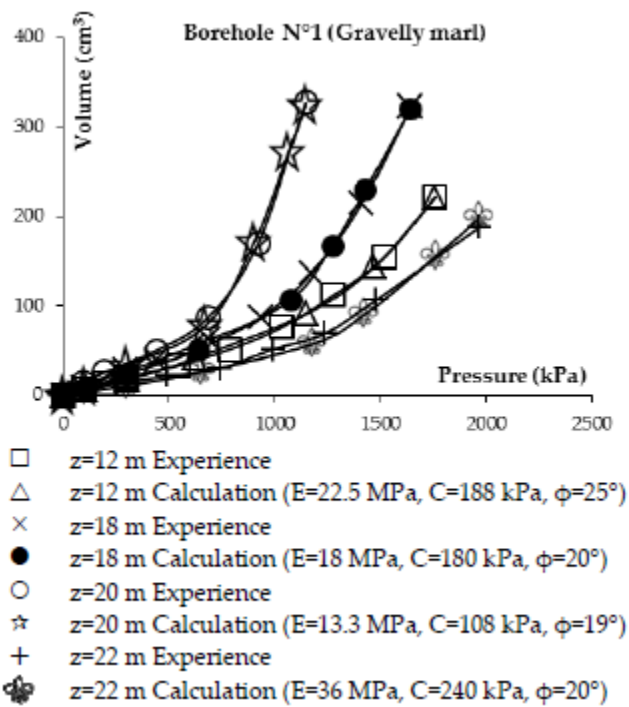


Figure 2.23 Experimental and numerical pressure-volume curves at different depth (Fawaz (2014))

2.3.6 COMPARISON OF PM AND YOUNG MODULUS

The pressuremeter modulus (E_M) and its comparison to the Young modulus (E) of soil were performed by Sedran et al. (2013) and Fawaz et al. (2014). Pressuremeter testing provides stress-strain data for pseudo-elastic and elastic-plastic ranges of soil deformation. The analysis of stress and strain changes in a soil mass due to PMT loading is based in the theory of cavity expansion as it pertains to an infinitely long cylinder expanding into an infinite soil range. Assuming uniform isotropic and linear elastic soil behavior, the elastic property of the soil is represented by the pressuremeter modulus (E_M) (Briaud (1992)), and is calculated with the following expression.

$$E_M = (1 + \nu)(p_2 - p_1) \frac{\left[1 + \left(\frac{\Delta R}{R_0}\right)_2\right]^2 + \left[1 + \left(\frac{\Delta R}{R_0}\right)_1\right]^2}{\left[1 + \left(\frac{\Delta R}{R_0}\right)_2\right]^2 - \left[1 + \left(\frac{\Delta R}{R_0}\right)_1\right]^2} \quad [2.16]$$

Where p and $\frac{\Delta R}{R_0}$ are the pressure and the corresponding radial strain recorded at the beginning (subscript 1) and at the end (subscript 2) of the linear portion of the PMT pressure vs radial strain curve respectively. The Poisson's ratio is given by ν . For soils under drained conditions (ie, zero excess pore pressure) a Poisson's ratio of 0.33 is typically used, in which case the pressuremeter modulus is designated as the Menard's modulus E_M (Baguelin et al. (1978)).

2.3.7 CONVENTIONAL LIMIT PRESSURE

The numerical validation of an elastoplastic formulation of the conventional limit pressure measured with the pressuremeter test in cohesive soil studied by Jacques (2007). An elastoplastic pressuremeter theory was used to determine the conventional limit pressure. Then conventional limit pressure was computed by using Plaxis to check the validity of the theoretical results. In the Plaxis, the Tresca failure model was used to determine the conventional limit pressure. The behavior of cohesive soil around the pressuremeter was studied by Jacques (2007). The influence of the permeability in a linear elastoplastic soil and of the geometry of the probe has been studied

(Nahra and Frank (1986)) by the numerical expansion of a cylindrical cavity. The well-known theory of undrained behavior (Baguelin et al. (1972)) has been used (Prapaharan et al. (1989)) to investigate the pressuremeter expansion as a function of the undrained shear strength which varies with the strain rate. Numerical results with a constitutive model (Cambou and Bahar (1993)) show that the test can be assumed to be an undrained one with permeability lower than 10^{-10} m/s.

The stress strain behavior of the cohesive soil is assumed to follow either a linear elasticity relation (Gibson and Anderson (1961) and Silvestri (2003)) a hyperbolic elastoplastic relation (Silvestri (2004)) or a power law (Bolton and Whittle (1999)).

The theoretical analysis was chosen for its ability to describe the pressuremeter test from beginning to end with only a few parameters, when numerical analysis with sophisticated models needs many mechanical parameters, which cannot be precisely fitted. As a matter of fact, on a pressuremeter curve which is computed with an eight parameters model, only one or two parameters can be fitted, while six or seven other parameters must be assumed (Cambou and Bahar (1993)).

During the PMT, three different areas of soil were considered from the borehole wall to the infinite radius. Plasticity appears in the first zone between the radial stress (σ_r) and the circumferential stress (σ_θ). This first plastic area extends between the radius r_a (borehole wall) and r_b (external radius of the first plastic area). The second plastic area between radii r_b and r_c (external radius of both plastic areas). An elastic area extends beyond radius r_c .

In the horizontal and vertical planes the equilibrium of an element of soil is given by

$$\sigma_r - \sigma_\theta + r \frac{d\sigma_r}{dr} = 0 \quad [2.17]$$

The conventional limit pressure (P_{1M}) was obtained by using the following expression.

$$P_{IM} = \gamma Z + c_u \ln \left[\frac{2G(\sqrt{2}-1)+c_u}{(1-K_0)\gamma Z+c_u} \right] \quad [2.18]$$

This relation is quite different from the Menard experimental correlation proposed by the European Regional Technical Committee (Amar et al. (1991)).

$$P_{IM} = 5.5c_u + K_0\gamma Z \quad \text{if } P_{IM} - K_0\gamma Z < 300\text{Mpa} \quad [2.19]$$

$$P_{IM} = 10(c_u - 25) + K_0\gamma Z \quad \text{if } P_{IM} - K_0\gamma Z > 300\text{Mpa} \quad [2.20]$$

The in-situ pressuremeter tests were carried out for over consolidated plastic clay in Paris. The theoretical pressuremeter curve and experimental one are drawn in one graph and compared. Then they used finite element program Plaxis (Brinkgreve and Vermeer (1998)) with the Tresca model to compute the value of the conventional limit pressure, which was compared to the result of theory. The model used was elastoplastic with a constant shearing modulus and five parameters (Young's modulus, Poisson's ratio, undrained shear strength, no friction and dilatancy angle). The method used for the validation was a variation of only one parameter when the other ones stay constant. Finally influence of the vertical stress, coefficient of pressure at rest (K_0), shearing modulus and shear strength in the conventional limit pressure was discussed.

2.3.8 ANALYTICAL METHOD

Analytical method was used to evaluate soil parameters which were used in the M-C model by Fawaz et al. (2014). Different rheological laws have been developed to describe the behavior of soils around the pressuremeter. The study of Combarieu (1995) based on Pasturel's formula has evolved a theoretical relation between the limit pressure (P_L) and soil parameters E , ν , c and ϕ . In case of cohesive and granular soils (c and ϕ different to 0) that relation is given below.

$$P_L + c \cot\phi = (P_0 + c \cot\phi) (1 + \sin\phi) \left(\frac{E}{2(1+\nu)(P_0 + c \cot\phi)(\sin\phi)} \right)^{\frac{\sin\phi}{1+\sin\phi}} \quad [2.15]$$

This formula was used to calculate the cohesion and the friction angle by using the value of the pressure at rest (P_0) and limit pressure (P_L) determined from the in-situ test and elastic modulus obtained in the numerical analysis.

2.4 SUMMARY

This chapter discussed about the literature review of the statistical correlation between SPT and PMT and numerical simulation of the PMT. In the case of statistical correlation, most of the correlation work done in the past was for sand and clay and only one for tills. There is almost no correlation work on Toronto glacial tills. So far there is no clear explanation on correlation between these two parameters for glacial till especially Toronto glacial tills. The literature has a significant lack of information concerning any glacial till such as cohesive or cohesionless glacial tills.

In the case of numerical simulation of PMT, there is bulk of information available but no one has simulated the model for real soil profile. Every author mentions the geometry of the model with some dimensions but they don't clearly mention the soil layers above and below the test depth. In addition to soil profile, authors did not properly define the geometry size, width of the model from axis of symmetry and depth below the mid-point of the probe. Further literature survey show that commonly used models are HSM and MCM. Each author's used different boundary conditions, geometry size, probe L/D ratio and type of model which are shown in Table 2.7.

Table 2.7 Reviews of the literature survey regards FEM simulation of PMT

Author's name	Type of model	Probe L/D ratio	Model geometry size	Boundary condition
Plaxis 2D manual (2012)	HSM*	2.7	Diameter 1.2m Height 0.75m	Bottom – VF* Vertical both side- HF [∇]
Fawaz et al.(2014)	MCM*	Not mention	Width 7m Height 7m below the probe	Bottom – Both fixity Vertical both side- HF [∇]

Jacques (2007)	Tresca Model	7.5	Diameter 5m Height 2m above the mid of probe	Bottom - VF* Right side vertical – both direction free Left side vertical - HF [√]
Levasseur et al. (2009)	MCM*	Not mention	Diameter 1.20m Height 1.5m	Bottom – Both fixity Vertical both side- HF [√]
Schanz et al. (2000)	MCM*	2.9	Diameter 1.2m Height 1.5m	Bottom – VF* Vertical both side- HF [√]
Malecot et al. (2009)	MCM*	8	Diameter 6m Height 5m	Bottom – Both fixity Right side vertical- HF [√] Left side vertical- HF [√] below probe
Rita (2008)	HSM*	6.7	Not define	Not define
Sedran et al. (2013)	HSM*	6.5	Not define	Not define
Monnet (2012)	MCM*	6	Diameter 10 m Height 2 m above the mid of probe	Bottom –VF* Right side vertical – Free Left side vertical – HF [√] above probe
Michel et al.(2000)	HSM*	Not define	Not define	Not define
Waschkowski (1976)		6.6		

* HSM – Hardening soil model

• MCM – Mohr Coulomb model

* VF – Vertical fixity of the model

√ HF – Horizontal fixity of the model

CHAPTER 3: STATISTICAL CORRELATION BETWEEN SPT-N VALUES WITH PMT PARAMETERS FOR GLACIAL TILLS

3.1 INTRODUCTION

The statistical analysis is carried out in this chapter to investigate the relationship between SPT-N value with both E_{PMT} and P_L . The first step is to collect the pairs of PMT test data and SPT-N value at the same depths in the same boreholes. Secondly selected data are corrected and filtered according to the methodology discussed in the section 3.2. Thirdly the general ranges of SPT-N, E_{PMT} and P_L values are discussed in the section 3.3. Then correlation between SPT-N value with both E_{PMT} and P_L are discussed in the section 3.4 and 3.5 respectively. In addition the comparisons are done between the studied correlation equations with literature equations and values in the section 3.6. And finally the ranges of corrected and filtered SPT-N, E_{PMT} and P_L values and correlation equations are summarized in the section 3.7.

3.2 DATA SELECTION, SPT-N VALUE CORRECTION AND FILTERING

SPTs conducted near the PMTs at similar depths are selected to develop the relationship between SPT-N values and both E_{PMT} and P_L in this chapter for the following stations such as Allen, Avenue, Bathurst, Bayview, Bermondsey, Blackcreek, Birchmount, Caledonia, Don Mills, Kennedy, Lesile, Mount Dennis, Victoria, Warden, West Portal and Wynford. The typical borehole report is attached in Appendix 3.1. The pairs of readings (SPT-N and E_{PMT}) for clayey silt and silty sand till are not available from these stations in this study.

SPT-N correction

The first correction for SPT-N values are performed according to Cao et al. (2015) for field measured SPT-N for penetration depth. This means that some situations, the field SPT hammer are refused while driving, when it reached boulders or cobbles. In this situation hammering is stopped and number of blows is counted before full penetration of 305 mm. Then the field SPT-

N values are corrected according to equation 2.1 in Chapter 2. For example, when the sample tube is driven 175 mm into the ground and the number of blows is 40, then the SPT N-value is 70 ($= \frac{305 \times 40}{175}$). Typical correction calculation sheet is attached in Appendix 3.2.

The second corrections are performed according to the CFEM (2006). Because of the variability in equipment and operating conditions, direct use of SPT-N values for geotechnical design is not recommended. As a result, many corrections shall be done on the field SPT-N values. Those corrections are described in Chapter 2, section 2.2.1.2 based on CFEM (2006). In case of cohesive glacial tills, overburden correction is not accommodated in this study. In these situations, the SPT-N became $SPT-(N)_{60}$. In the case of cohesionless glacial tills, overburden corrections is accommodated. In these situations, the SPT-N became $SPT-(N_1)_{60}$. Typical correction calculation sheets for each station is attached in Appendix 3.2. Based on these corrections, the conclusion is made that after the correction, the SPT-N value became half of the field measured SPT-N value, specifically in the deeper elevation.

Filtering data

The processing of these data is one of the most challenging works in this project. Reliability of an analysis result is mostly defined by the accuracy of selected data rather than the method used for the analysis. Therefore, the selection of the most representative parameters for a site is the key to a successful analysis. With that in mind, in order to evaluate the correlation between SPT-N values and both E_{PMT} and P_L more accurately, the compiled data are filtered by using the following methodology.

- (1) The SPT's often reached refusal, i.e. blow count (N) values are greater than 100 for 300 mm or less increment when the SPT sampler hits a cobble or boulder within the glacial till. As a result the SPT-N values are assigned values of 100 or more than 100. The SPT-N values greater than 100 are disregarded.
- (2) The data situated far from the trend line is discarded by visual inspection compare to other data.

(3) In such cases the same SPT-N value is associated with different values of both E_{PMT} and P_L and this pair of readings are omitted.

Apparently more theoretical study is needed to develop a sound rationale to filter the data.

3.3 GENERAL RANGES OF SPT-N, E_{PMT} AND P_L FOR GLACIAL TILLS

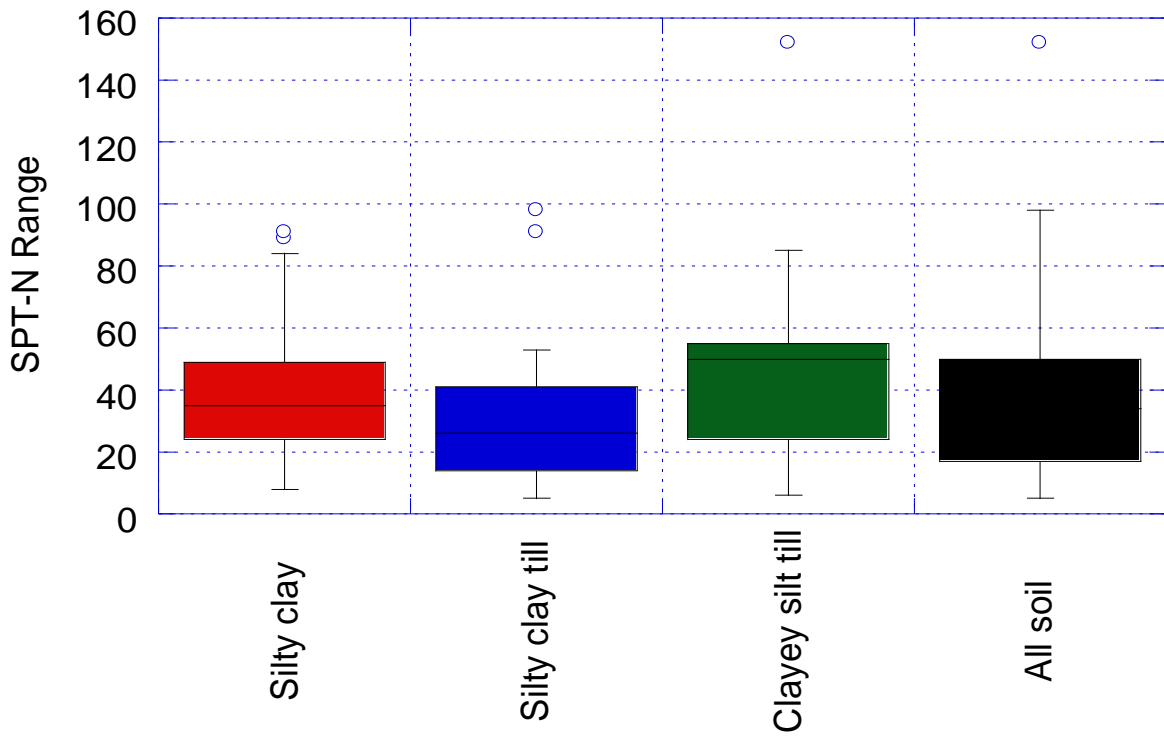
The ranges of SPT-N, E_{PMT} and P_L values are determined for both groups in which all of the data are collected from in-situ tests and in which the data are corrected and filtered.

3.3.1 RANGES OF SPT-N VALUES

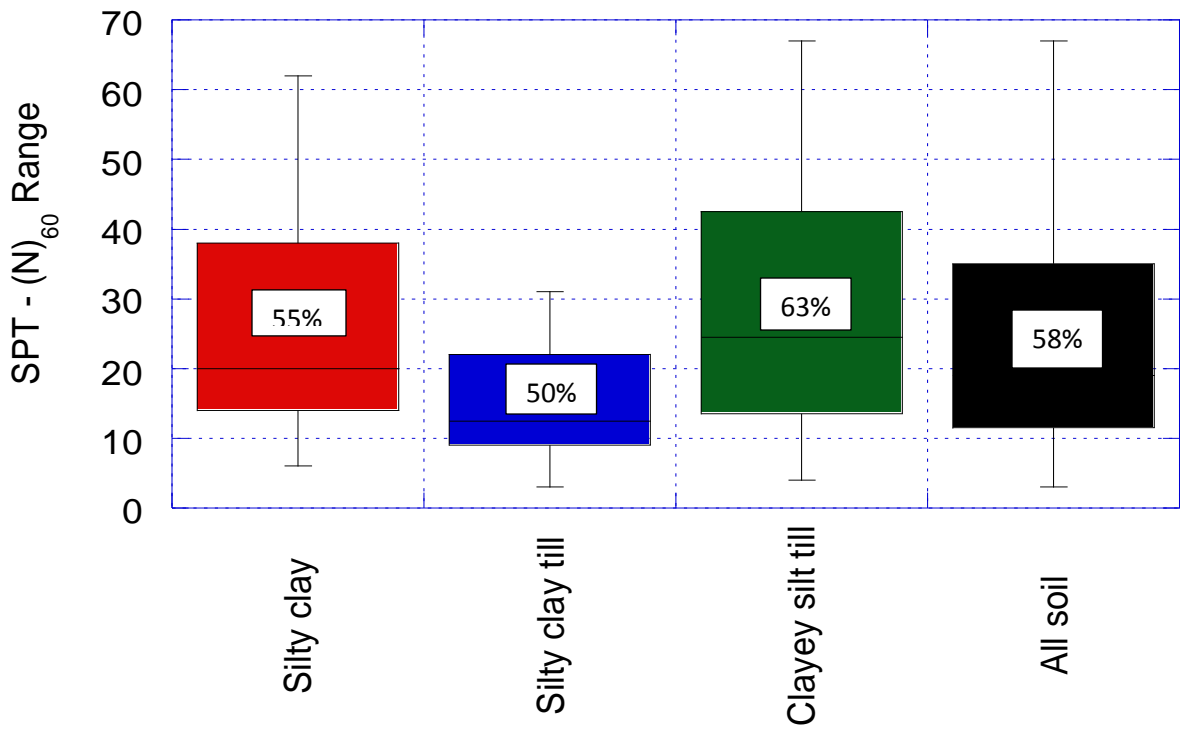
The ranges of SPT-N values of cohesive and cohesionless glacial tills are shown in Figure 3.1 and Figure 3.2 respectively. Further ranges, means and standard deviations of SPT-N values for different types of soil and all soil, for all data as well as corrected and filtered data are shown in Table 3.1. The data that were discarded during the filtering process are shown in Figure 3.1, with small circles in the all data analysis. The percentages (%) marked in Figure 3.2 represents most of the range values that belong to the thick portion of the range diagrams.

Table 3.1 Summary of SPT-N values for different types of soil

Soil type	Ranges of SPT-N values for all data (Corrected & Filtered data)			
	No. of data	Range	Mean	Standard deviation
Cohesive glacial tills				
Silty clay	38 (22)	8-91 (6-62)	38 (26)	23 (16)
Silty clay till	25 (14)	5-98 (3-31)	32 (15)	24 (9)
Clayey silt till	21 (16)	6-152 (4-67)	46 (29)	32 (19)
All soil	84 (52)	5-152 (3-67)	38 (24)	26 (16)
Cohesionless glacial tills				
Sand	23 (18)	21-150 (13-97)	61 (50)	29 (23)
Silt	16 (14)	8-123 (4-98)	66 (46)	33 (30)
Sandy silt	22 (20)	6-86 (4-91)	53 (45)	23 (23)
Silty sand	23 (18)	38-127 (25-76)	63 (49)	21 (18)
Sandy silt till	8 (7)	34-93 (16-80)	58 (60)	20 (25)
All soil	92 (77)	6-150 (4-98)	60 (49)	26 (23)

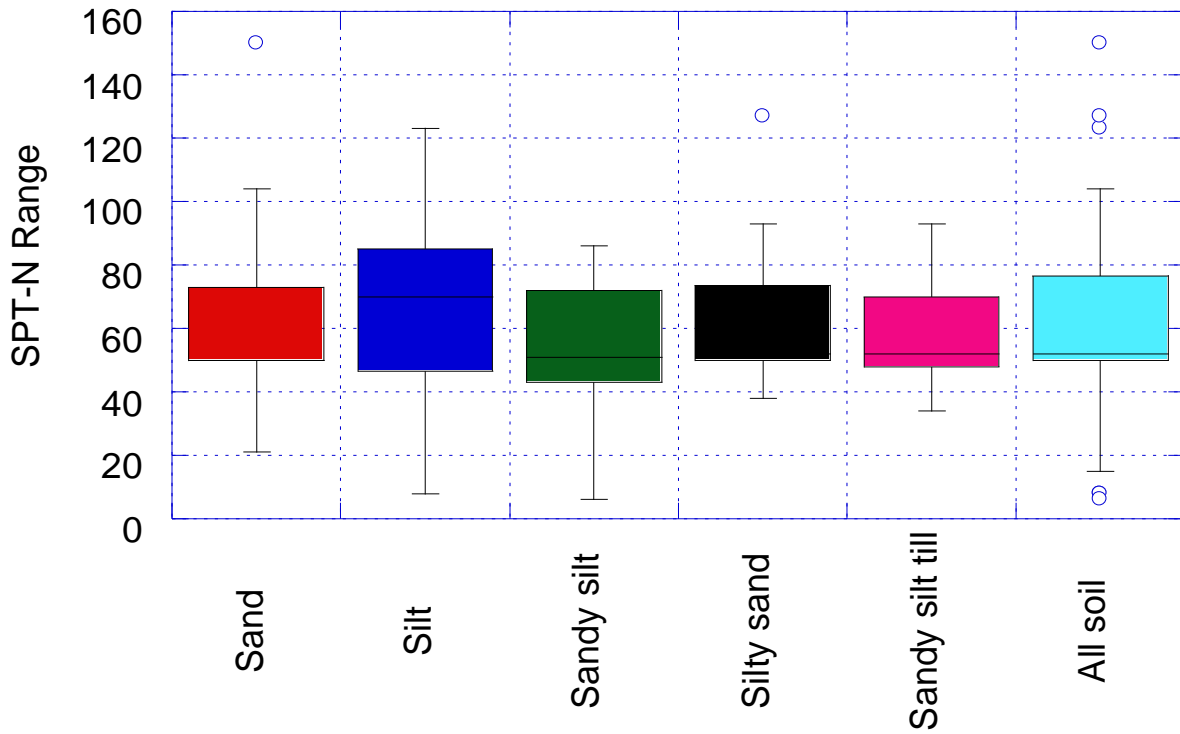


All data

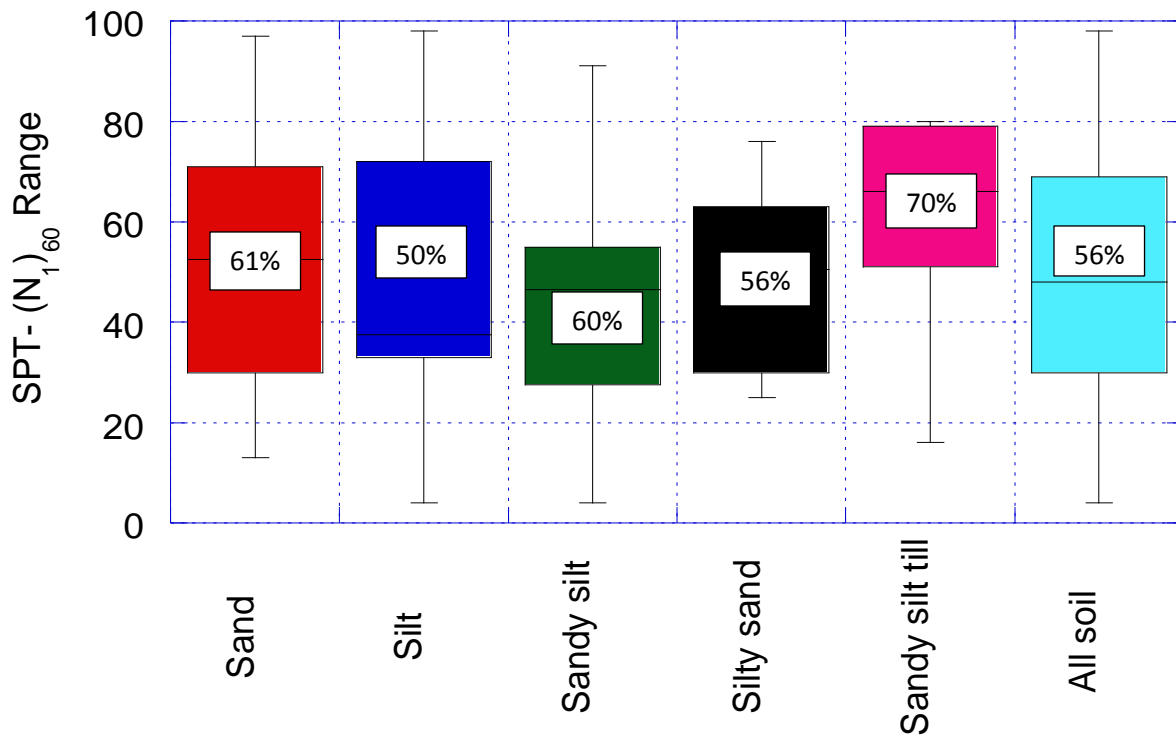


Corrected and filtered data

Figure 3.1 Ranges of SPT-N values for cohesive glacial tills



All data



Corrected and filtered data

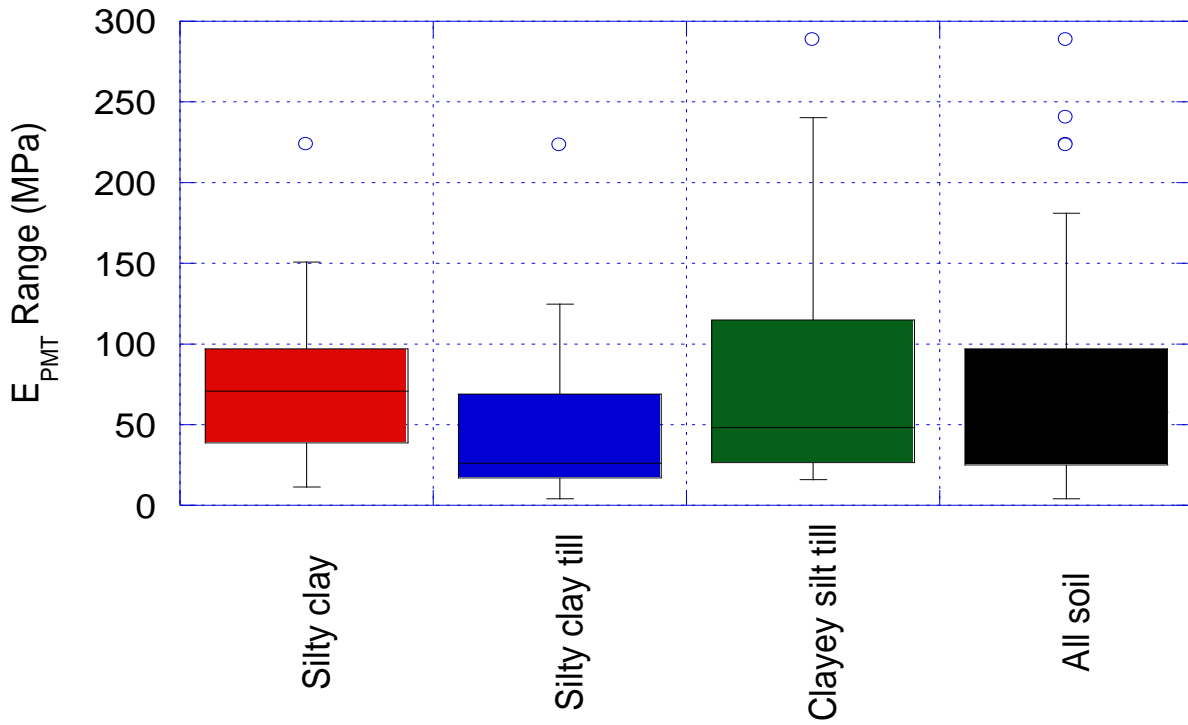
Figure 3.2 Ranges of SPT-N values for cohesionless glacial tills

3.3.2 RANGES OF E_{PMT} VALUES

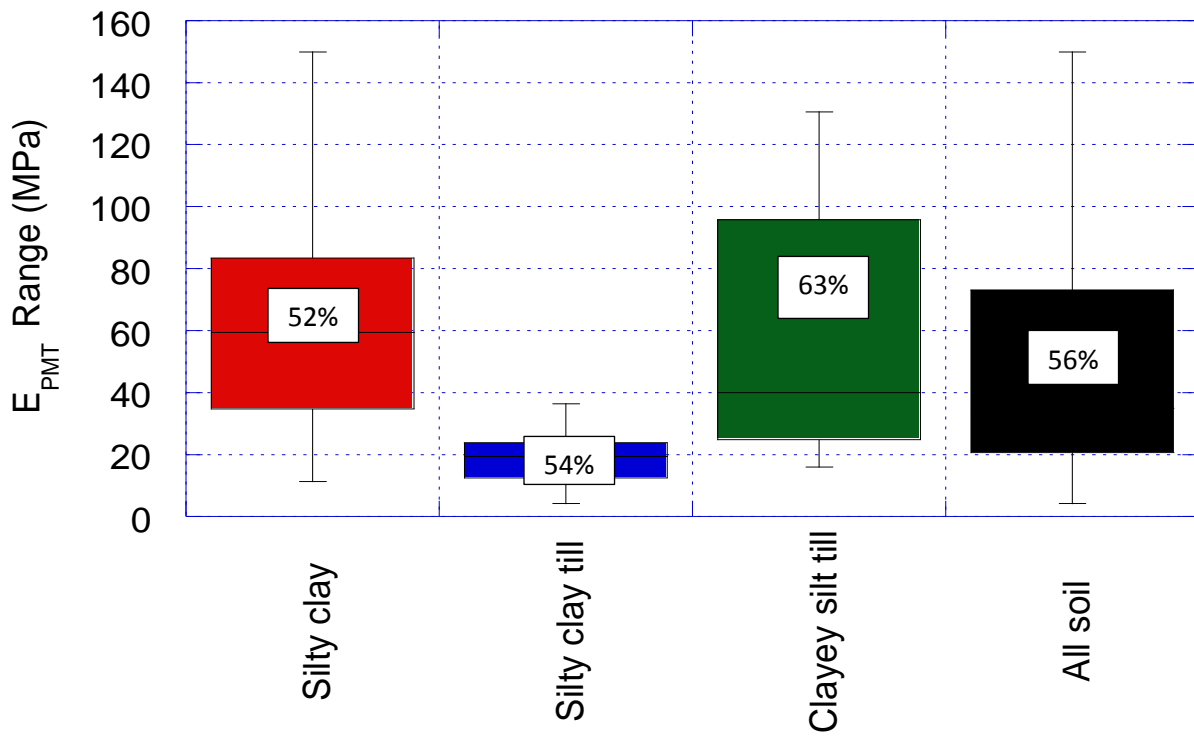
The ranges of E_{PMT} values of cohesive and cohesionless glacial tills are shown in Figure 3.3 and Figure 3.4 respectively. Further ranges, means and standard deviations of E_{PMT} values for different types of soil and all soil, for all data as well as filtered data are shown in Table 3.2. The data that were discarded during the filtering process are shown in Figure 3.3, with small circles in the all data analysis. The percentages (%) marked in Figure 3.4 represents most of the range values that belong to the thick portion of the range diagrams.

Table 3.2 Summary of E_{PMT} values for different types of soil

Soil type	Ranges of E_{PMT} values (MPa) for all data (Filtered data)			
	No. of data	Range	Mean	Standard deviation
Cohesive glacial tills				
Silty clay	38 (23)	11- 224 (11-150)	76 (65)	47 (39)
Silty clay till	25 (13)	4-223 (4-36)	49 (18)	51 (10)
Clayey silt till	21 (16)	16-288 (16-131)	82 (58)	76 (41)
All soil	84 (52)	4 -288 (4-150)	69 (51)	58 (40)
Cohesionless glacial tills				
Sand	22 (14)	26-197 (26-149)	104 (91)	48 (46)
Silt	16 (14)	19-140 (19-140)	84 (82)	32 (33)
Sandy silt	22 (15)	2-163 (28-78)	71 (53)	47 (17)
Silty sand	23 (13)	10-231 (39-96)	105 (69)	58 (18)
Sandy silt till	8 (6)	18-273 (18-134)	112 (76)	79 (39)
All soil	91 (62)	2-273 (18-149)	93 (74)	53 (34)

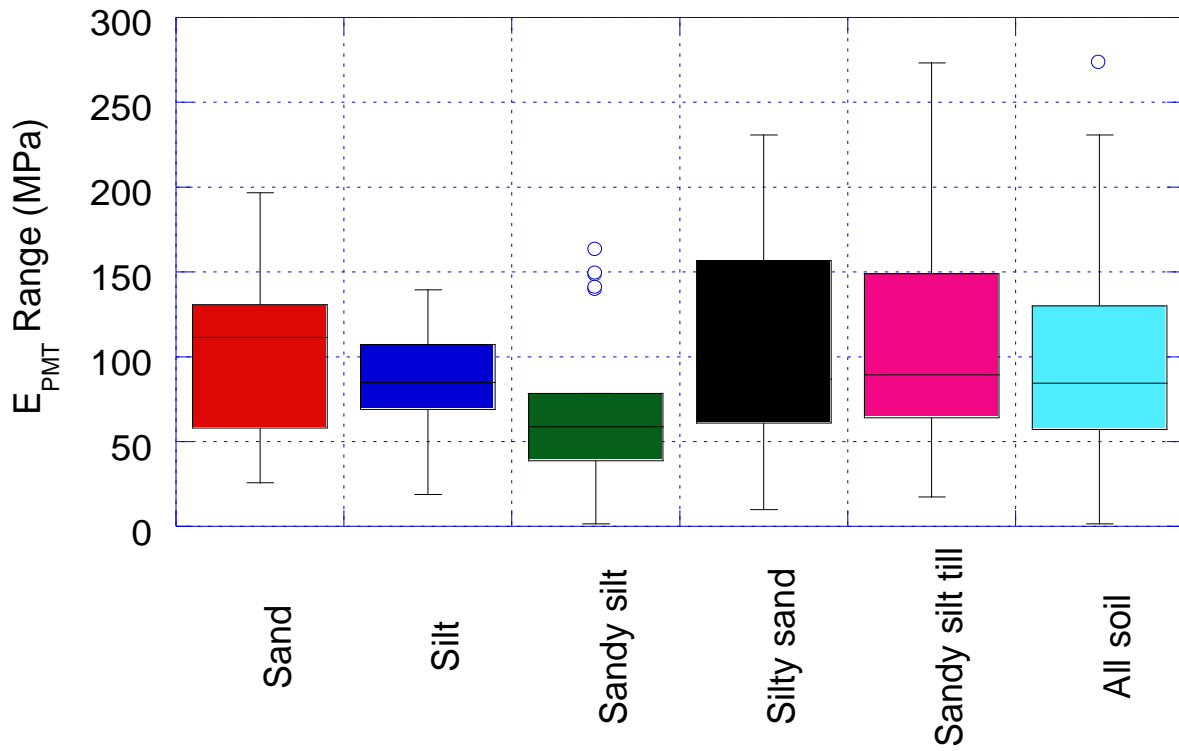


All data

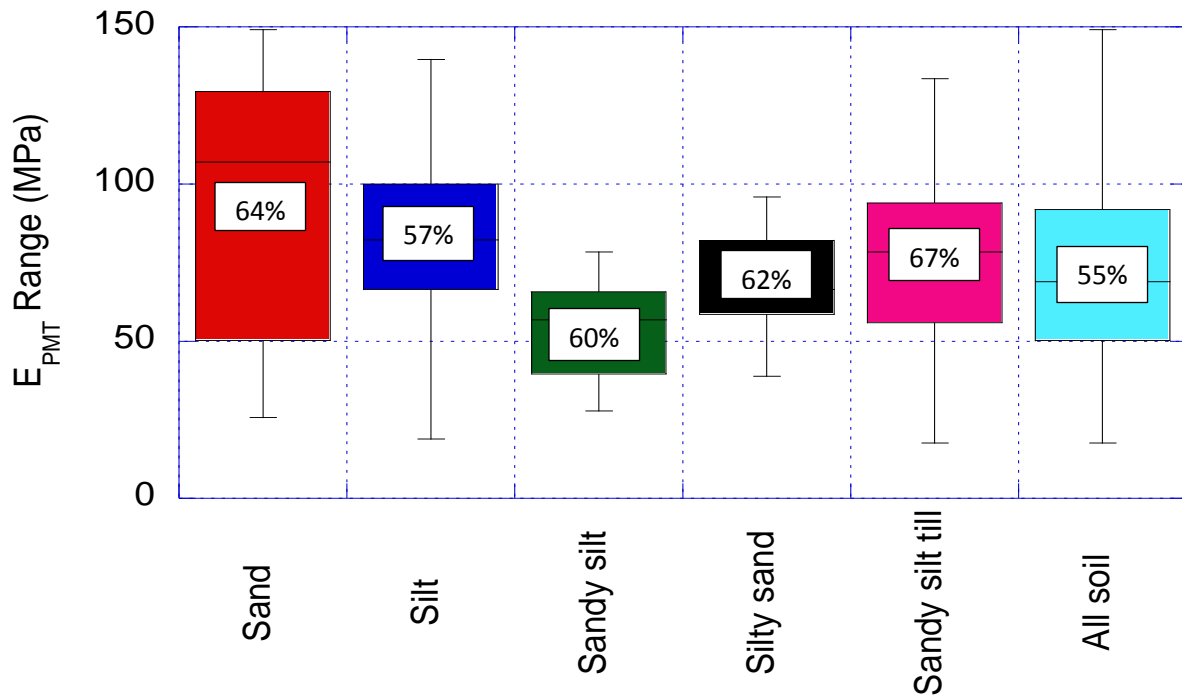


Filtered data

Figure 3.3 Ranges of E_{PMT} values for cohesive glacial tills



All data



Filtered data

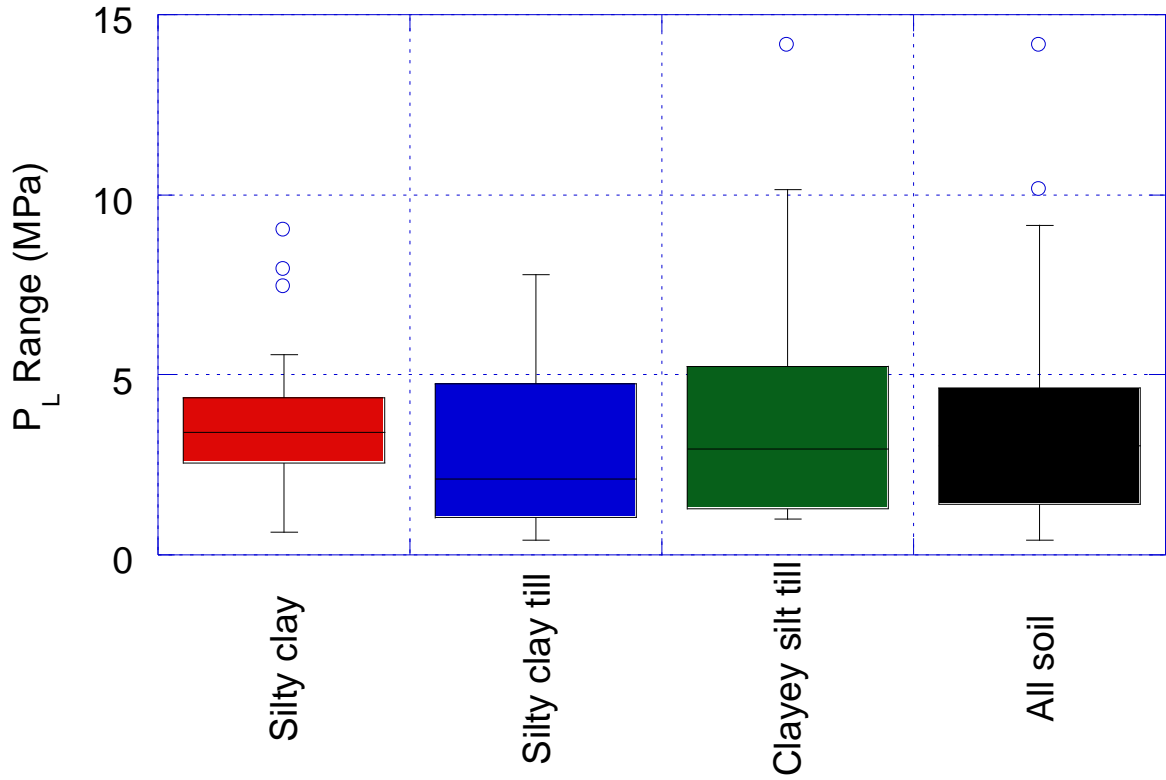
Figure 3.4 Ranges of E_{PMT} values for cohesionless glacial tills

3.3.3 RANGES OF P_L VALUES

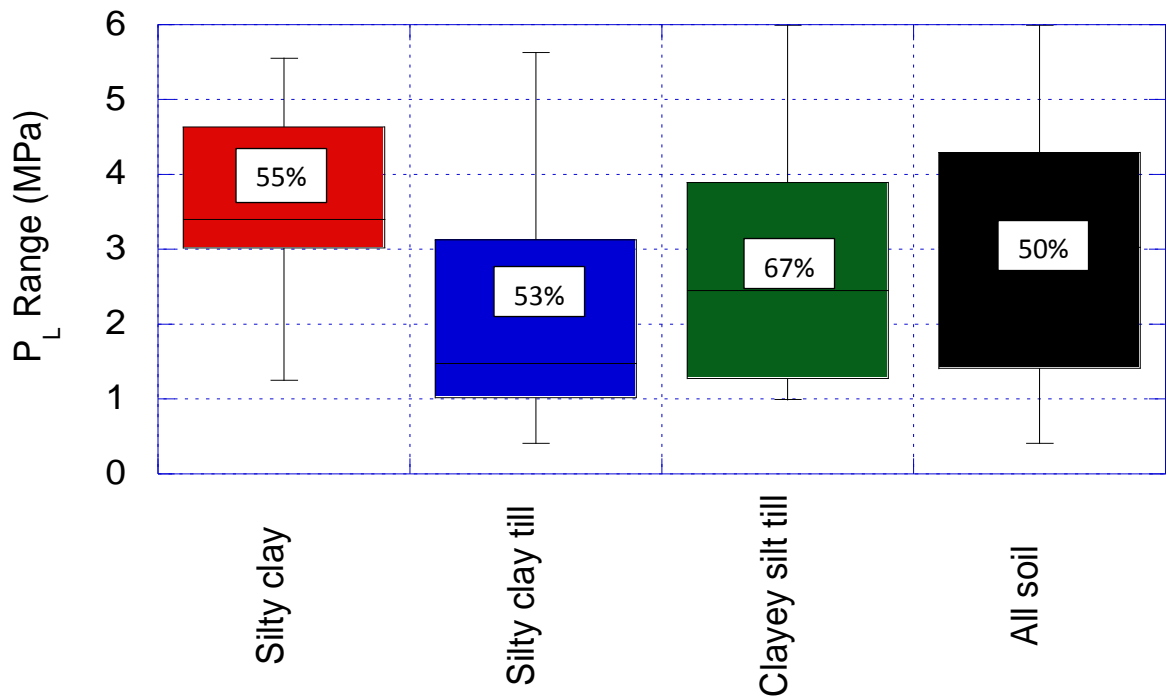
The ranges of P_L values of cohesive and cohesionless glacial tills are shown in Figure 3.5 and Figure 3.6 respectively. Further ranges, means and standard deviations of P_L values for different types of soil and all soil, for all data as well as filtered data are shown in Table 3.3. The data that were discarded during the filtering process are shown in Figure 3.3, with small circles in the all data analysis. The percentages (%) marked in Figure 3.4 represents most of the range values that belong to the thick portion of the range diagrams.

Table 3.3 Summary of P_L values for different types of soil

Soil type	Ranges of P_L values (MPa) for all data (Filtered data)			
	No. of data	Range	Mean	Standard deviation
Cohesive glacial tills				
Silty clay	38 (22)	0.64-9.02 (1.25-5.56)	3.56 (3.62)	1.89 (1.23)
Silty clay till	25 (17)	0.41-7.78 (0.41-5.63)	2.72 (2.35)	2.13 (1.85)
Clayey silt till	20 (15)	1.0 - 14.15 (1.00-6.00)	4.0 (2.79)	3.55 (1.72)
All soil	83 (54)	0.41-14.15 (0.41-6.00)	3.42 (3.00)	2.47 (1.65)
Cohesionless glacial tills				
Sand	23 (17)	0.21-13.32 (2.42-13.32)	7.23 (7.97)	3.55 (3.46)
Silt	16 (12)	0.97-14.57 (3.17-9.08)	7.10 (7.05)	3.04 (1.81)
Sandy silt	22 (18)	0.29-15.79 (1.33-9.03)	5.40 (4.52)	3.65 (2.13)
Silty sand	23 (18)	1.42-14.30 (1.42-13.55)	7.28 (6.37)	3.80 (3.67)
Sandy silt till	8 (4)	1.7-22.49 (6.00-8.04)	9.64 (7.02)	6.83 (0.87)
All soil	92 (69)	0.21- 22.49 (1.33-13.55)	7.00 (6.44)	4.00 (3.09)

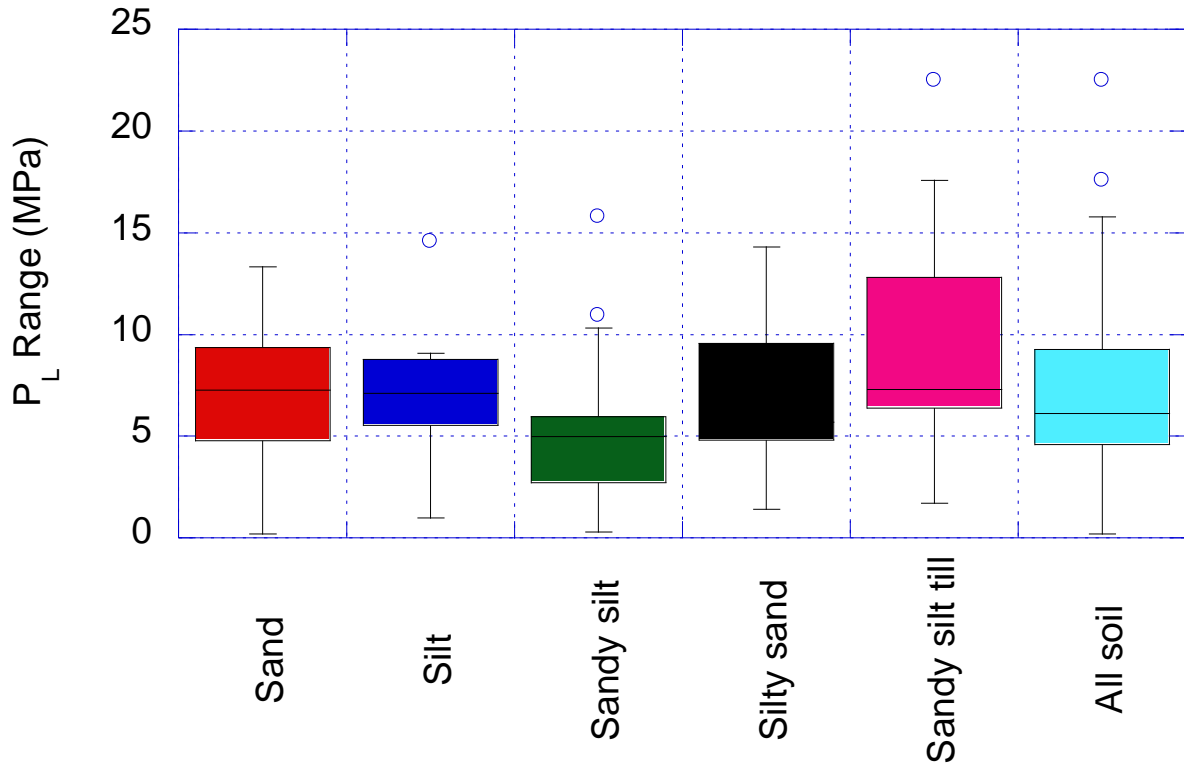


All data

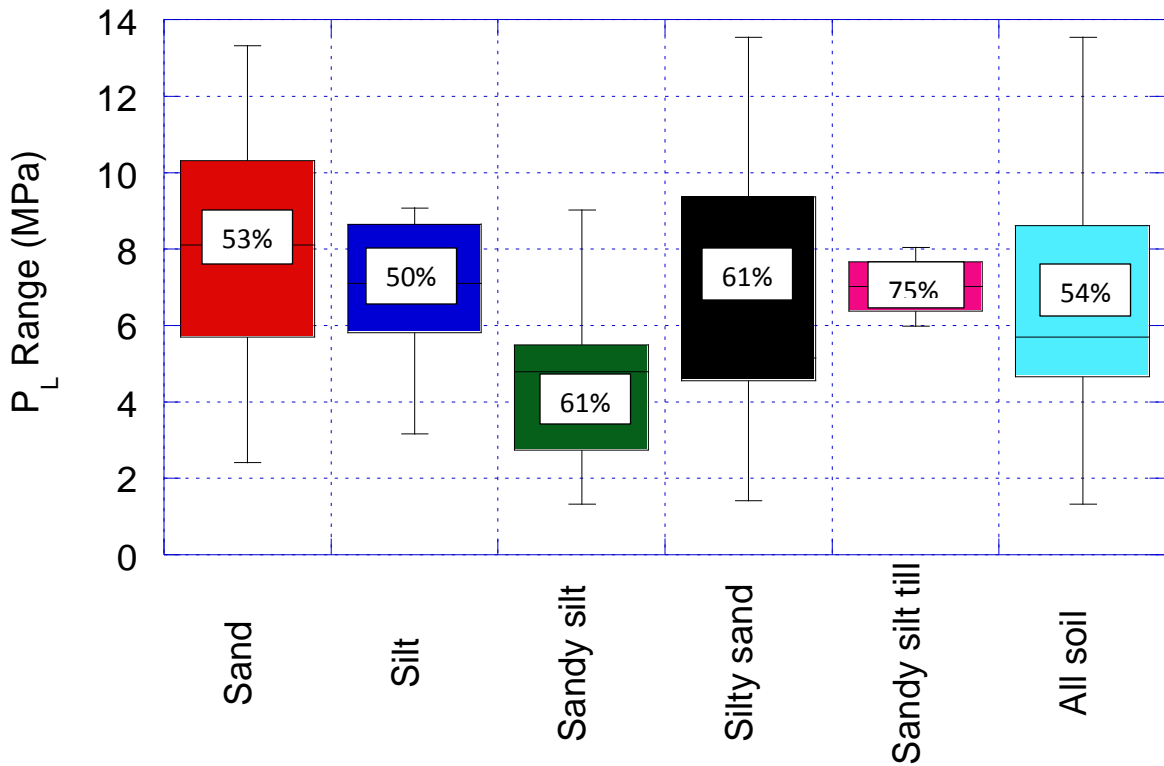


Filtered data

Figure 3.5. Ranges of P_L values for cohesive glacial tills



All data



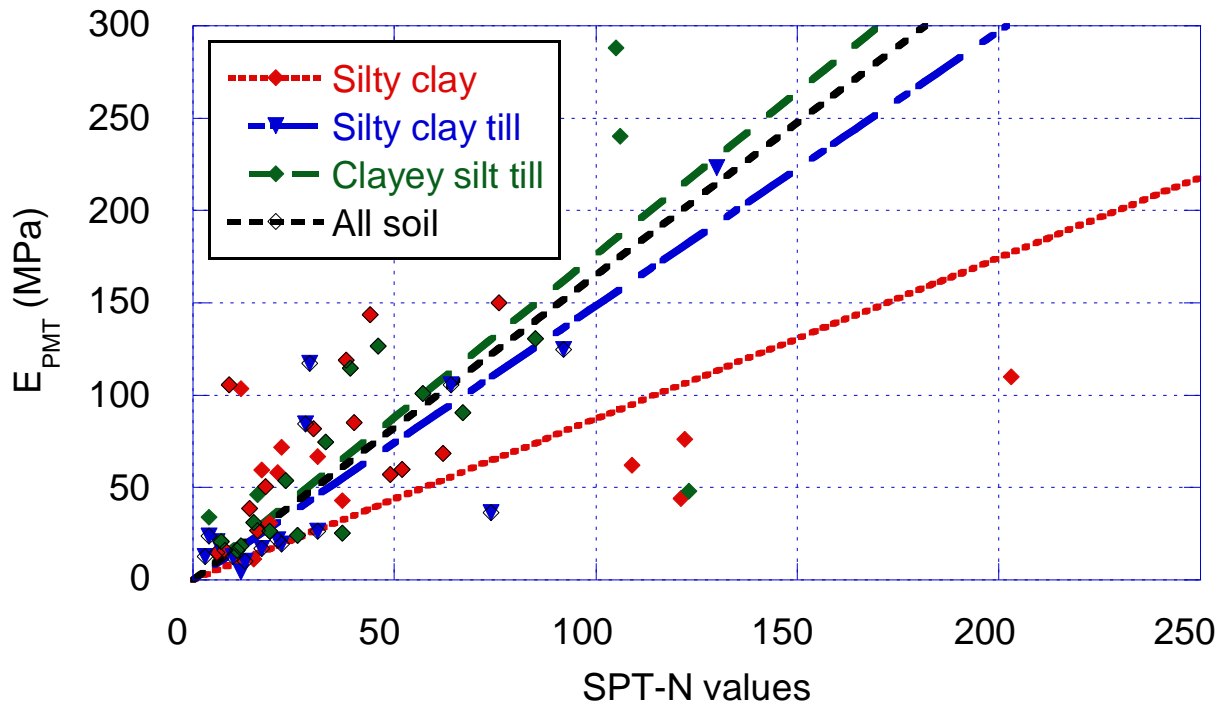
Filtered data

Figure 3.6 Ranges of P_L values for cohesionless glacial tills

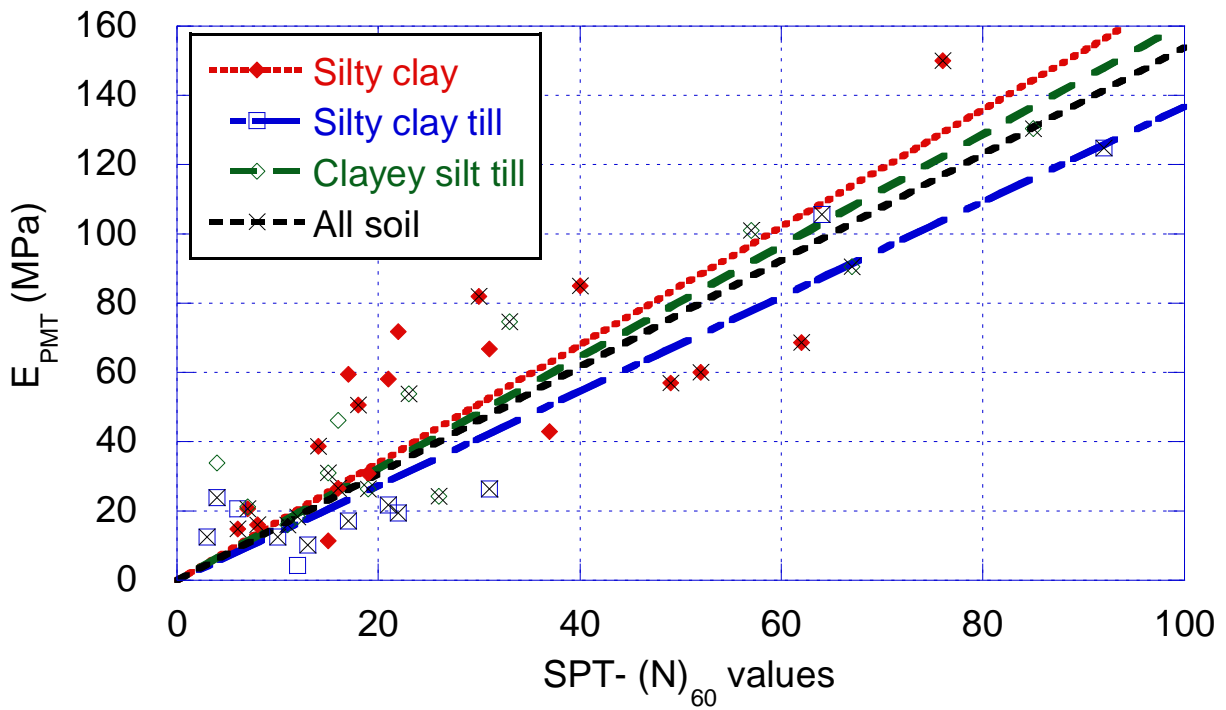
3.4 CORRELATION BETWEEN SPT-N AND E_{PMT} VALUES

(a) Low plasticity cohesive glacial tills

The correlation between SPT-N values and E_{PMT} have been plotted for low plasticity cohesive glacial tills in both original data as well as corrected and filtered data formats, as shown in Figure 3.7. The correlation functions are determined for both cases in which all the data were included and in which the data were corrected and filtered. The correlation functions and coefficients are given in Table 3.4. The corrected and filtered data analysis provides a much improved correlation coefficient compared to all original data analysis.



All data

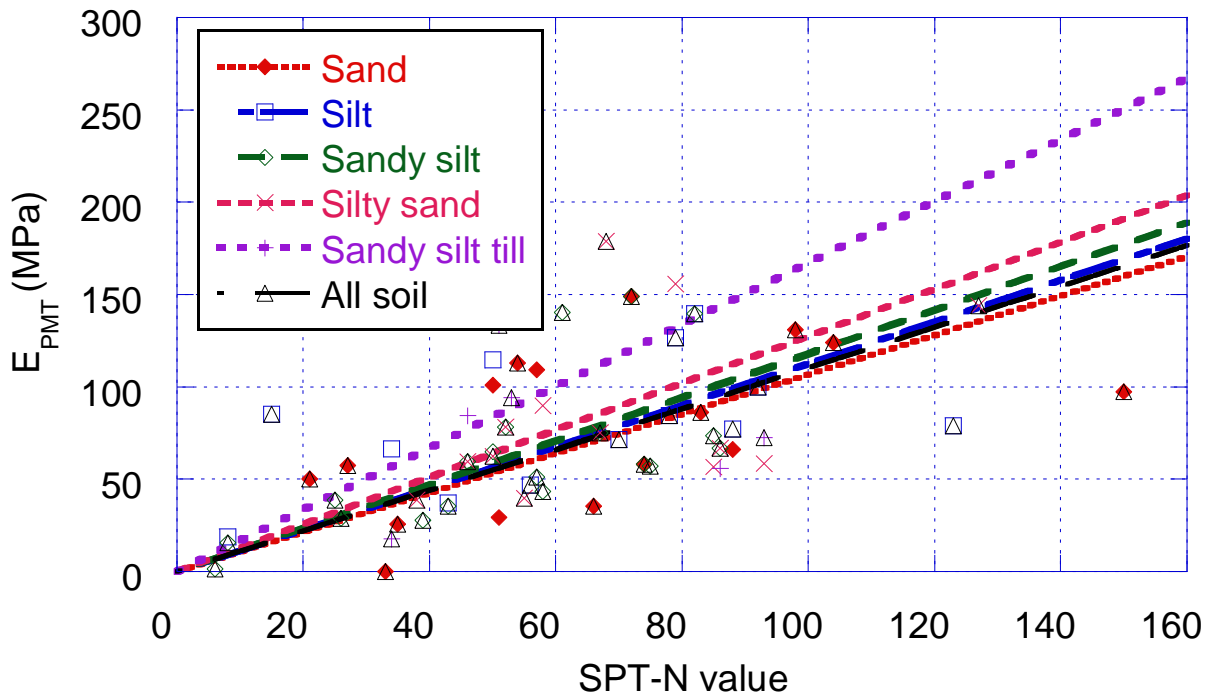


Corrected and filtered data

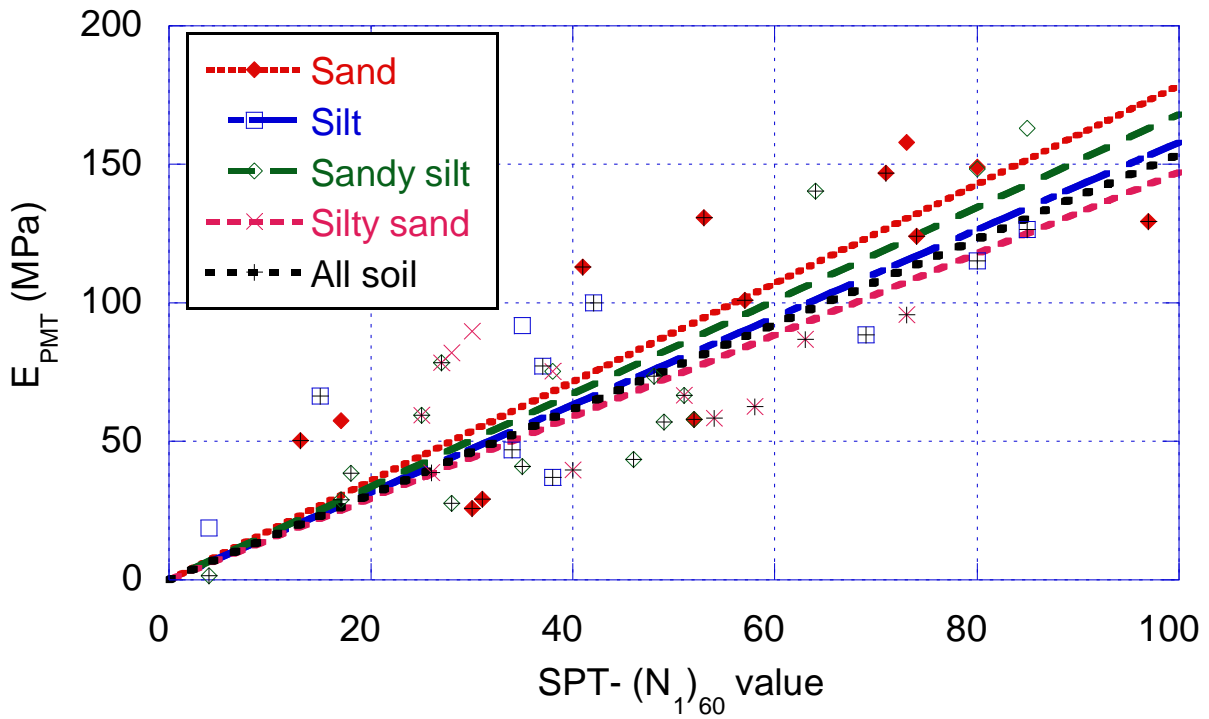
Figure 3.7 Correlations between SPT-N vs E_{PMT} for cohesive glacial tills

(b) Cohesionless glacial tills

The correlation between SPT-N values and E_{PMT} have been plotted for cohesionless glacial tills in both original data as well as corrected and filtered data formats, as shown in Figure 3.8. The correlation functions and coefficients are given in Table 3.4. The corrected and filtered soil data analysis shows that there is a better correlation relationship between SPT-N and E_{PMT} . After corrected and filtered, the sandy silt till does not have enough pairs of data.



All data



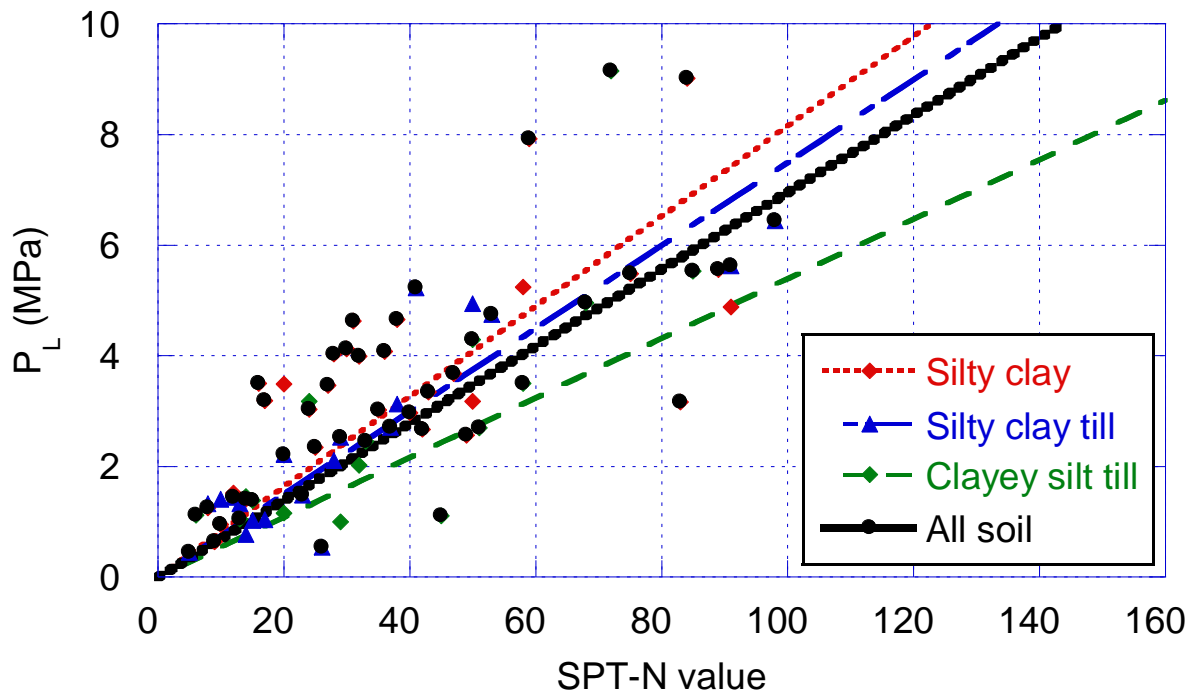
Corrected and filtered data

Figure 3.8 Correlations between SPT-N vs E_{PMT} for cohesionless glacial tills

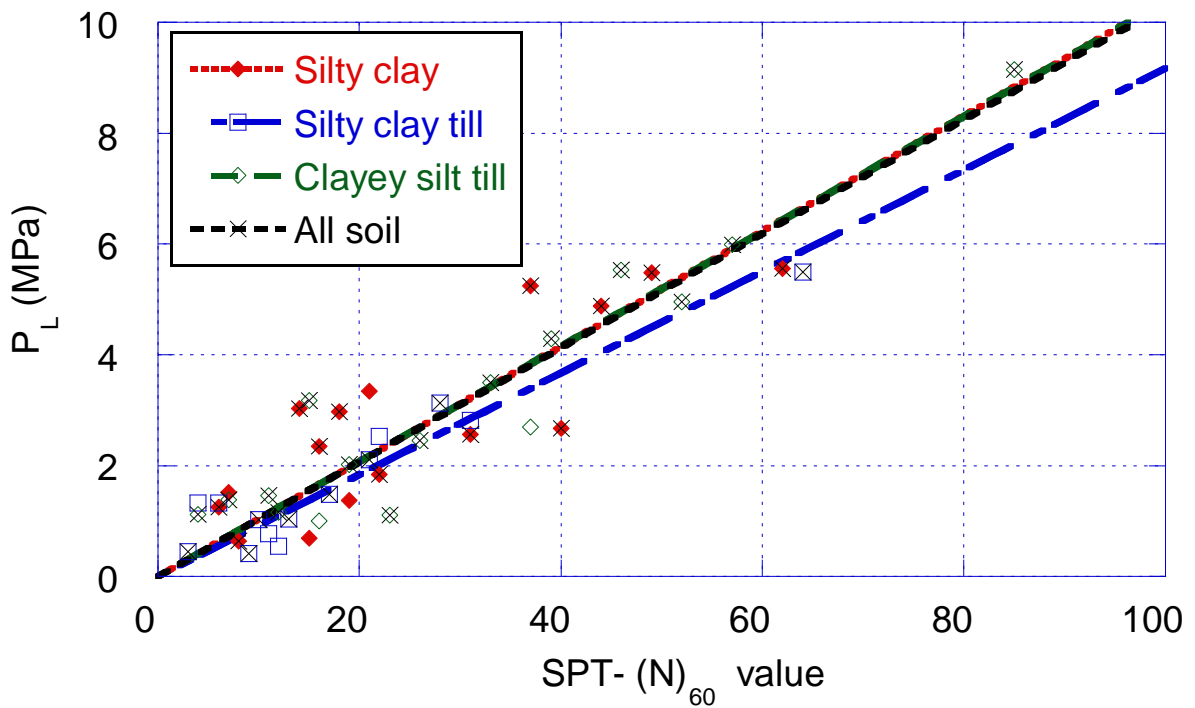
3.5 CORRELATION BETWEEN SPT-N AND P_L VALUES

(a) Low plasticity cohesive glacial tills

The correlation between SPT-N values and P_L have been plotted for low plasticity cohesive glacial tills in both original data as well as corrected and filtered data formats, as shown in Figure 3.9. The correlation functions are determined for both cases in which all the data were included and in which the data were corrected and filtered. The correlation functions and correlation coefficients are given in Table 3.4. The corrected and filtered data analysis provides a much improved correlation coefficient compared to all original data analysis.



All data

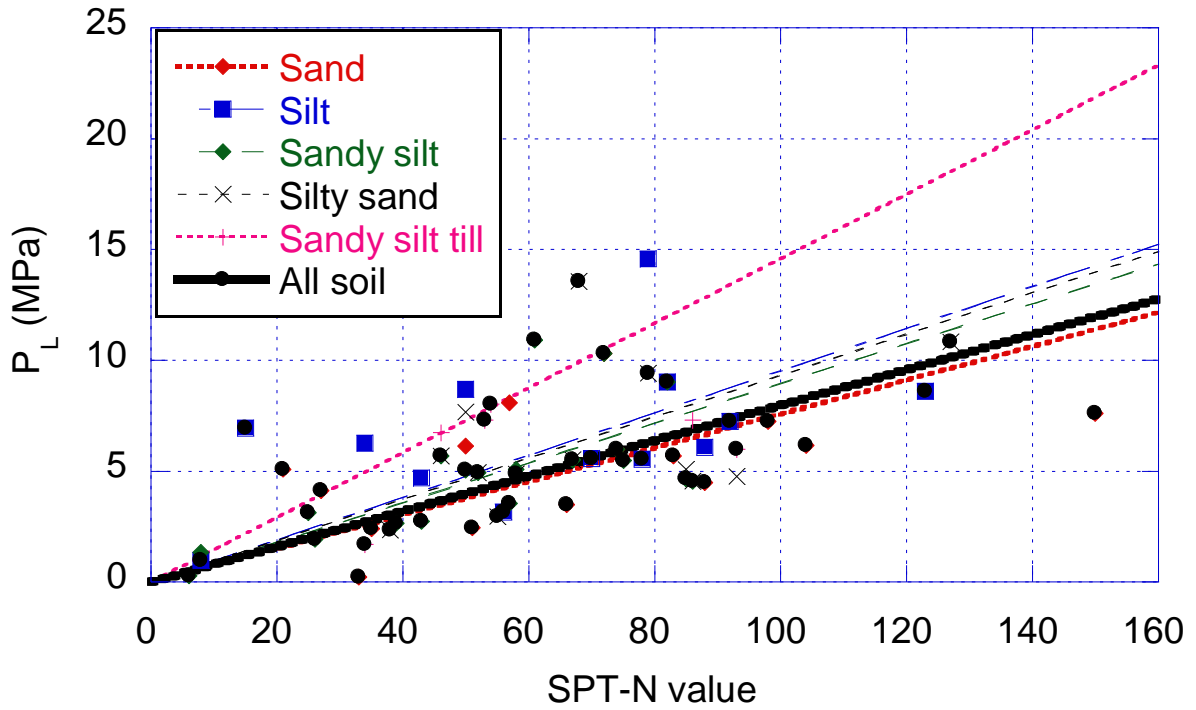


Corrected and filtered data

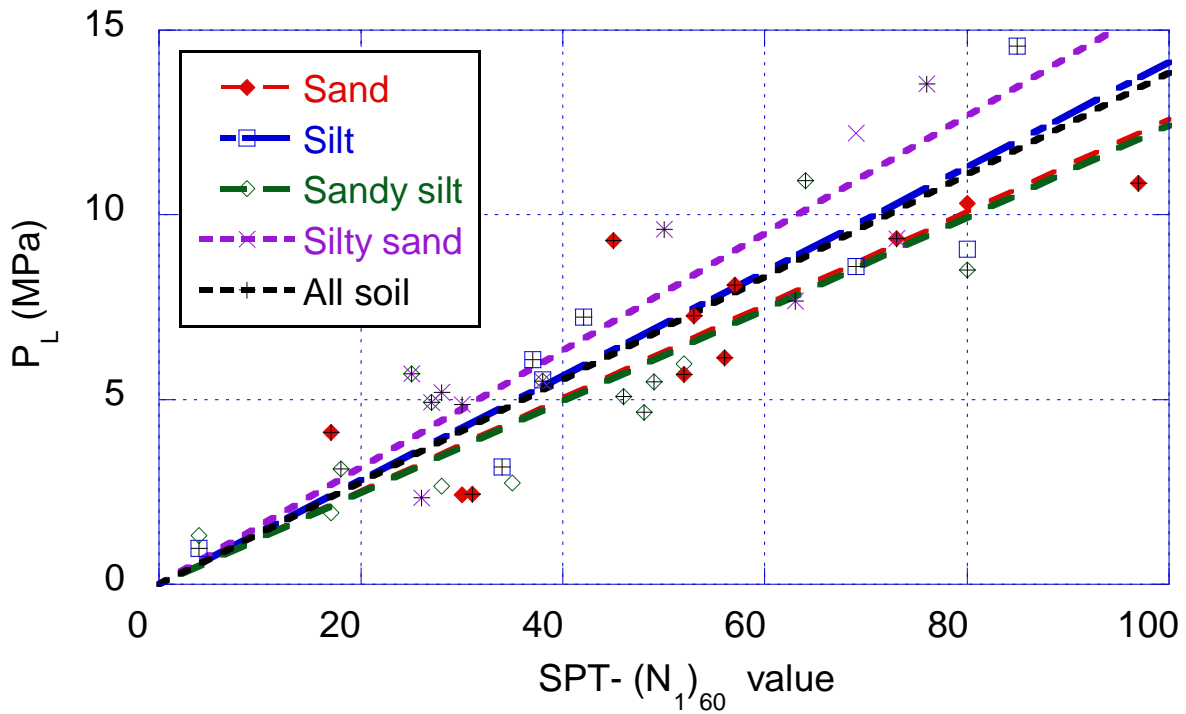
Figure 3.9 Correlations between SPT-N vs P_L for cohesive glacial tills

(b) Cohesionless glacial tills

The correlation between SPT-N values and P_L have been plotted for cohesionless glacial tills in both original data as well as corrected and filtered data formats, as shown in Figure 3.10. The correlation functions and coefficients are given in Table 3.4. The all soil data analysis shows that there is a weak correlation relationship between SPT-N and P_L where the correlation coefficient (R^2) is 0.04 to 0.46. After corrected and filtered, sandy silt till does not have enough pairs of data. The corrected and filtered data analysis provides a much improved correlation coefficient (0.67 to 0.85) compared to all the original data analysis.



All data



Corrected and filtered data

Figure 3.10 Correlations between SPT-N vs P_L for cohesionless glacial tills

Table 3.4 Summary of correlations between SPT-N values with both E_{PMT} and P_L values for different types of soil

Soil type	Correlation equations (E_{PMT}) (MPa) (R^2)		Correlation equations (P_L) (MPa) (R^2)	
	All data	Corrected & Filtered data	All data	Corrected & Filtered data
Cohesive glacial tills				
Silty clay	0.87N (0.23)	1.70(N) ₆₀ (0.55)	0.082N (0.27)	0.104(N) ₆₀ (0.68)
Silty clay till	1.49N (0.72)	1.37(N) ₆₀ (0.91)	0.075N (0.80)	0.092(N) ₆₀ (0.89)
Clayey silt till	1.76N (0.48)	1.61(N) ₆₀ (0.83)	0.054N (0.19)	0.104(N) ₆₀ (0.90)
All soil	1.65N (0.41)	1.54(N) ₆₀ (0.83)	0.070N (0.23)	0.103(N) ₆₀ (0.87)
Cohesionless glacial tills				
Sand	1.07N (0.15)	1.79(N_1) ₆₀ (0.79)	0.076N (0.16)	0.126(N_1) ₆₀ (0.71)
Silt	1.13N (0.20)	1.58(N_1) ₆₀ (0.45)	0.095N (0.04)	0.141(N_1) ₆₀ (0.85)
Sandy silt	1.18N (0.46)	1.68(N_1) ₆₀ (0.77)	0.090N (0.46)	0.124(N_1) ₆₀ (0.67)
Silty sand	1.27N (0.07)	1.47(N_1) ₆₀ (1.0)	0.093N (0.08)	0.158(N_1) ₆₀ (0.80)
Sandy silt till	1.67N (0.37)	No correlation	0.146N (0.32)	No correlation
All soil	1.10N (0.26)	1.54(N_1) ₆₀ (0.58)	0.080N (0.26)	0.139(N_1) ₆₀ (0.71)

3.6 COMPARISONS OF CORRELATIONS BETWEEN SPT- $(N_1)_{60}$ VALUES AND BOTH E_{PMT} AND P_L VALUES

There is a limited information available about the correlation between SPT-N values and both E_{PMT} and P_L for sand and clay, and is particularly sparse for glacial tills. This section presents a study on the correlation between SPT- $(N_1)_{60}$ values and both E_{PMT} and P_L for glacial tills in the city of Toronto. In addition, the comparison is performed between this study and the literature for sand and glacial tills. For the sand there are two types of literature models are available. The developed regression line by using corrected and filtered data is compared with available literature models. Further, another comparison of the data is performed for glacial till within the studied data. In this comparison, a linear correlation with intercept is used due to the available linear literature model.

3.6.1 COMPARISONS OF CORRELATION BETWEEN SPT- $(N_1)_{60}$ VALUES AND E_{PMT} FOR SAND

The approximate correlation between SPT-N and E_{PMT} proposed by Ohya et al. (1982) and Bozbey (2010) are plotted on Figure 3.11(a) with the studied data. In this comparison, a nonlinear power best fit line is plotted for the studied corrected and filtered data due to the available nonlinear literature model. For the preliminary estimation of the E_{PMT} for the sand, the E_{PMT} can be estimated from the SPT- $(N_1)_{60}$ values using the following relationship.

$$E_{PMT} \text{ (MPa)} = 4.992 (N_1)_{60}^{0.74} \quad R^2 = 0.81 \quad [3.1]$$

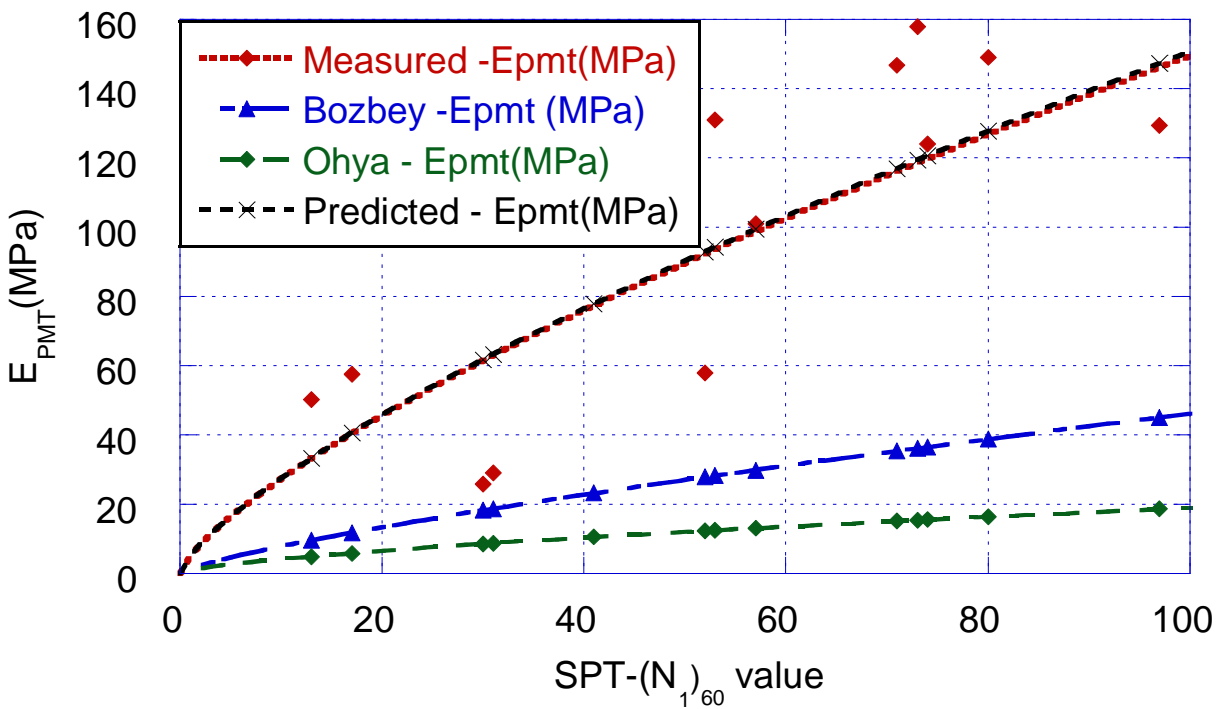
The predicted E_{PMT} values are calculated by using “Eq. 3.1” and the measured and predicted E_{PMT} values are also presented in Figure 3.11(a).

Another comparison of the data is performed with the research conducted by Briaud (1992), as shown in Figure 3.11(b). In this comparison a linear correlation with a zero intercept has been used due to the available linear literature model. For the preliminary estimation of the E_{PMT} for the sand, the E_{PMT} can be estimated from the SPT- $(N_1)_{60}$ values using the following relationship.

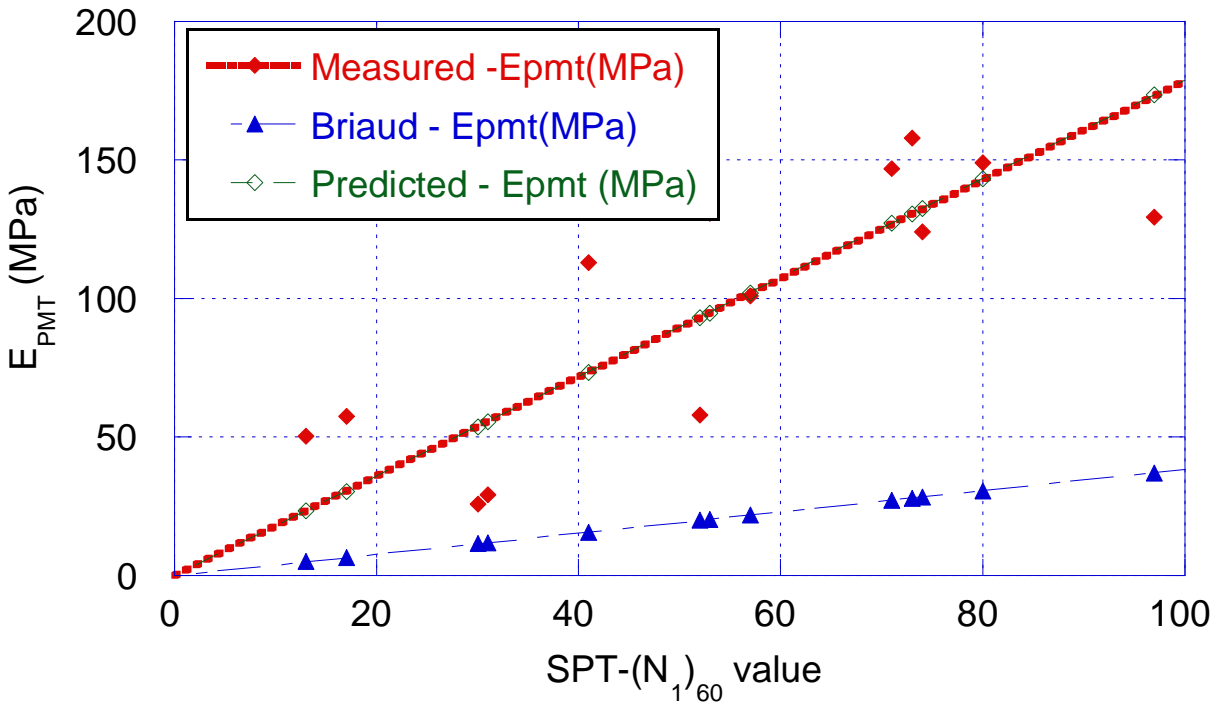
$$E_{PMT}(\text{MPa}) = 1.79 (N_1)_{60} \quad R^2 = 0.79 \quad [3.2]$$

The predicted E_{PMT} values are calculated by using “Eq. 3.2” and the measured and predicted values are also presented in Figure 3.11(b).

Further, a comparison of the E_{PMT} range is performed with the research by Briaud (1992). The E_{PMT} value for dense sand is greater than 22.5 MPa from Briaud (1992). In this study the E_{PMT} range is 26 – 149 MPa. It is higher than Briaud (1992)’s value. This is because the studied sand in this project is dense to very dense with cobbles and boulders. In addition to that comparison, the range of SPT- $(N_1)_{60}$ value is performed with the CFEM (2006). The SPT-N value of dense sand is greater than 50 in the CFEM (2006). The mean value of SPT- $(N_1)_{60}$ is 50 in this study. It shows that the studied SPT- $(N_1)_{60}$ value of dense sand is a good agreement with CFEM (2006).



(a) Non-linear relationship



(b) Linear relationship

Figure 3.11 Comparison of correlation between SPT-(N_1)₆₀ and E_{PMT} for sand

3.6.2 COMPARISON OF CORRELATION BETWEEN SPT-(N_1)₆₀ VALUES AND P_L FOR SAND

An approximate correlation between SPT-N and P_L proposed by Bozbey (2010) is plotted on Figure 3.12(a) with this investigation. In this comparison, a nonlinear power best fit line is plotted for the studied corrected and filtered data due to the nonlinearity nature of the literature model. For the preliminary estimation of the P_L for the sand, the P_L can be estimated from the SPT-(N_1)₆₀ values using the following relationship.

$$P_L (\text{MPa}) = 0.223 (N_1)_{60}^{0.86} \quad R^2 = 0.73 \quad [3.3]$$

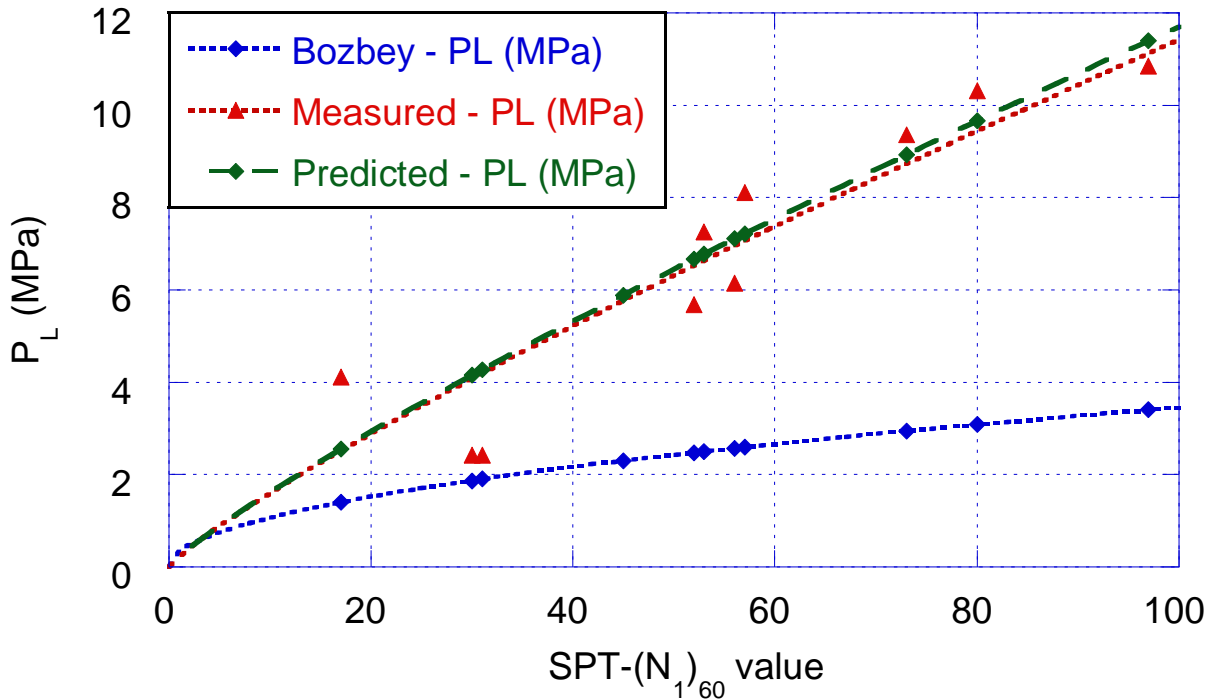
The predicted P_L values are calculated by using “Eq. 3.3” and the measured and predicted values are also presented in Figure 3.12(a).

Another comparison of the corrected and filtered data is performed with the results from Briaud (1992) and is plotted on Figure 3.12(b). In this comparison, a linear correlation with a zero intercept has been used due to the linearity nature of the literature model. For the preliminary estimation of the P_L for the sand, P_L can be estimated from the SPT- $(N_1)_{60}$ value using the following relationship.

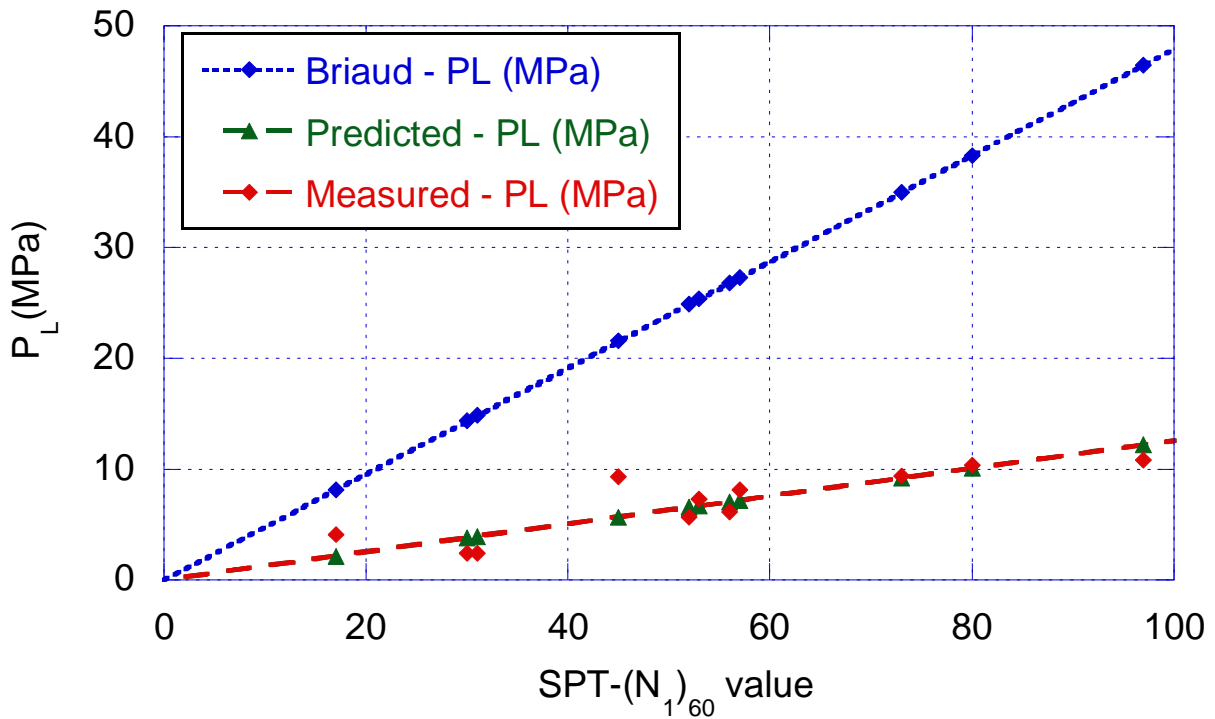
$$P_L \text{ (MPa)} = 0.126 ((N_1)_{60}) \quad R^2 = 0.71 \quad [3.4]$$

The predicted P_L values are calculated by using “Eq. 3.4” and the measured and predicted values are also presented in Figure 3.12(b).

Further, a comparison of range of P_L is performed with Briaud (1992). The P_L value for dense sand is greater than 2.5 MPa from Briaud (1992). In this study the P_L range is from 2.42 MPa – 13.32 MPa. It shows that the lower limit of the range is closer to Briaud’s (1992) value, but the upper limit of the range is much higher than that reported by Briaud (1992).



(a) Non-linear power best fit



(b) Linear relationship

Figure 3.12 Comparison of correlation between SPT-(N_1)₆₀ and P_L for sand

3.6.3 COMPARISONS OF CORRELATION BETWEEN SPT-(N_1)₆₀ VALUES WITH BOTH E_{PMT} AND P_L FOR GLACIAL TILLS

The comparison of the corrected and filtered data is performed for glacial till with Yagiz (2008) as shown in Figure 3.13. In this comparison, a linear correlation with an intercept has been used due to the linearity nature of the literature model. For the preliminary estimation of the E_{PMT} and P_L for the glacial till, E_{PMT} and P_L can be estimated from the SPT-(N_1)₆₀ value using the following relationships.

$$E_{PMT}(\text{MPa}) = 1.492 (N_1)_{60} + 1.635 \quad R^2 = 0.83 \quad [3.5]$$

$$P_L(\text{MPa}) = 0.094 (N_1)_{60} + 0.211 \quad R^2 = 0.84 \quad [3.6]$$

The predicted E_{PMT} and P_L values using “Eq. 3.5” and “Eq. 3.6”, and the measured E_{PMT} and P_L values, are plotted in Figure 3.13(a) and (b) respectively. The comparison shows that measured E_{PMT} and P_L are higher than the literature value. The reason for this is that the Toronto area glacial tills deposit consists of cobbles and boulders (Ng et al. (2011)). The literature model equation shows N_{cor} . The N_{cor} means, either the SPT-N is corrected for whole factors which are mentioned in the CFEM (2006) or only some factors. There are still uncertainties in this regard.

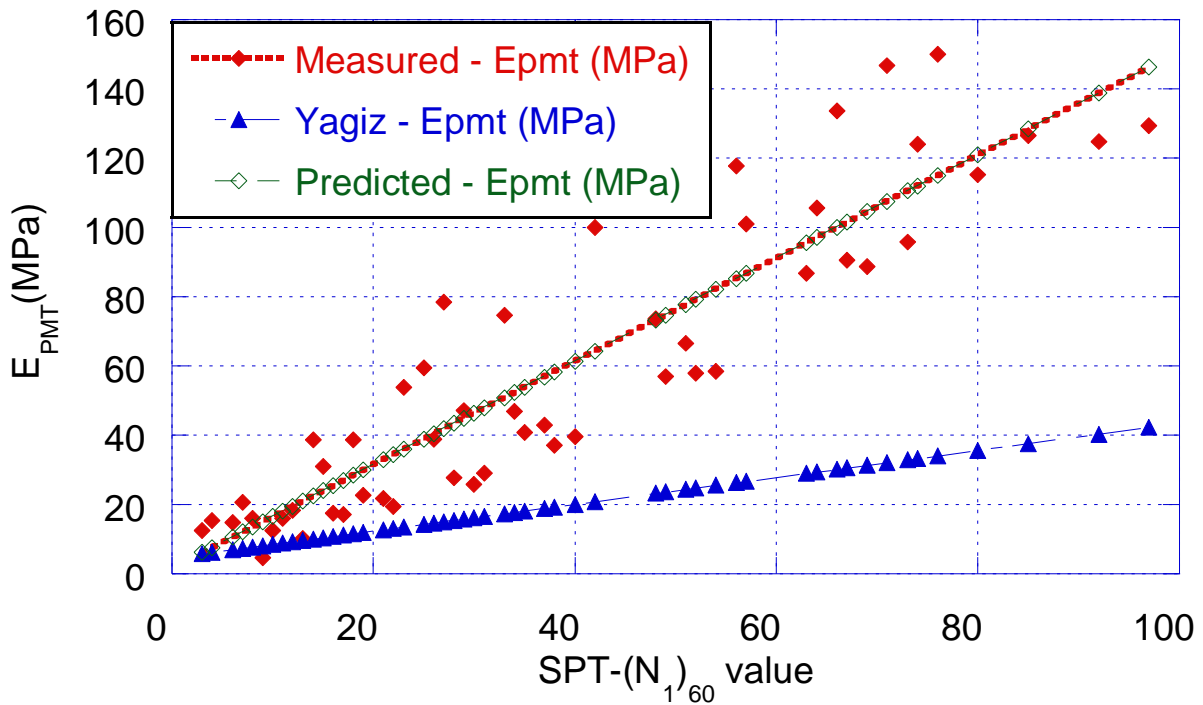


Figure 3.13(a) Comparison of correlation between SPT-(N_1)₆₀ vs E_{PMT} for linear with intercept relationship for glacial tills

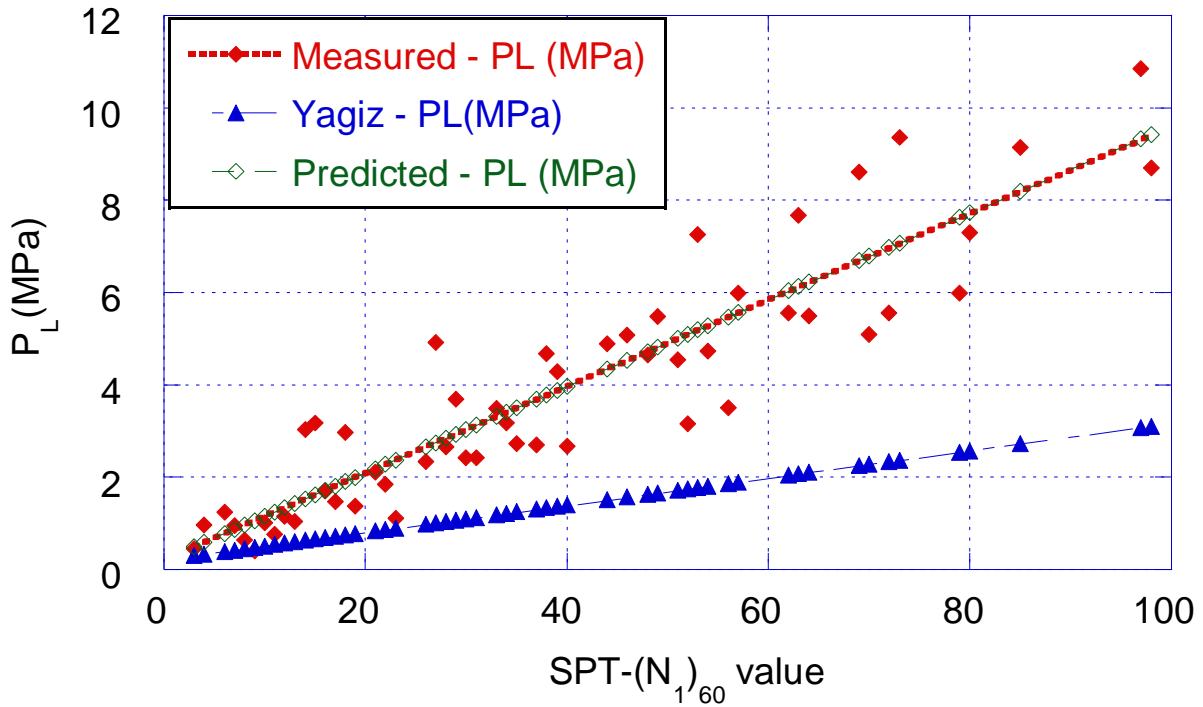


Figure 3.13 (b) Comparison of correlation between SPT- $(N_1)_{60}$ vs P_L for linear with intercept relationship for glacial tills

3.6.4 COMPARISONS OF CORRELATION BETWEEN SPT- $(N_1)_{60}$ VALUES AND E_{PMT}/P_L RATIO FOR SAND

The range of E_{PMT}/P_L ratio for sand is between 9 and 20, with an average of 14 and standard deviation of 4. The E_{PMT}/P_L ratio is compared to the studied by Bozbey (2010). The range in Bozbey's study is from 7 to 12. It shows that lower trend value differs with 2 and upper trend value differs with 8. The studied mean value (14) is closer to the literature upper limit (12). The main reason of the difference is the compactness of the sand. The compactness of sand may vary from very loose, loose, medium, dense to very dense due to the inconsistencies. The CFEM (2006) state that the ration of E_{PMT}/P_L for loose silty sand is 5 and sand and gravel is 7. The E_{PMT}/P_L ratio in this study is higher than the literature value due to the presence of gravel and cobbles in the sand. This was mentioned in the grain size analysis report which was conducted with the selected sample from the proposed ECLRT project.

Figure 3.14 (a) represents the variation of the pressuremeter modulus with pressure limit. It is clear that the E_{PMT} varies linearly with the pressure limit with a relationship of $E_{PMT} = 14P_L$ ($R^2 = 0.83$). Further Figure 3.14 (b) represents the variation of the E_{PMT}/P_L with SPT- $(N_1)_{60}$ values. It shows that the linear relationship with an intercept gives better correlation coefficient ($R^2 = 0.62$) compare to other relationships. The correlation equation between E_{PMT}/P_L ratio with SPT- $(N_1)_{60}$ is given by $E_{PMT}/P_L = 4.964 + 0.192(N_1)_{60}$.

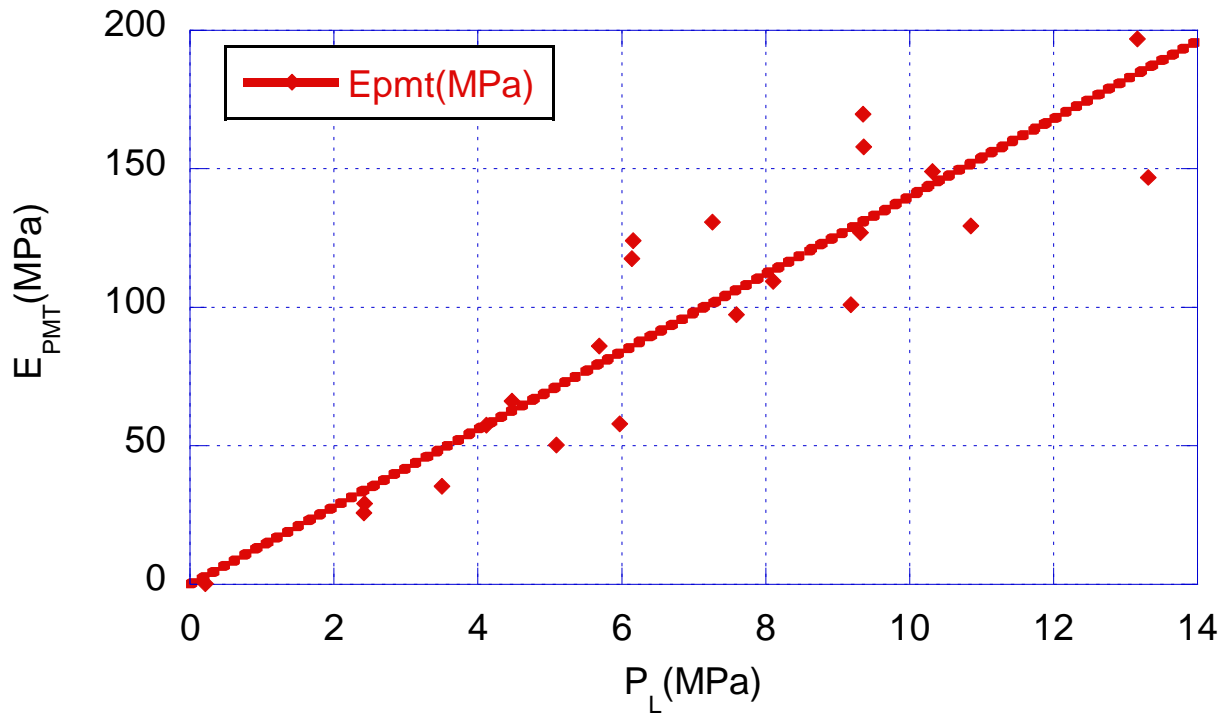


Figure 3.14 (a) Correlation between E_{PMT} vs P_L for sand

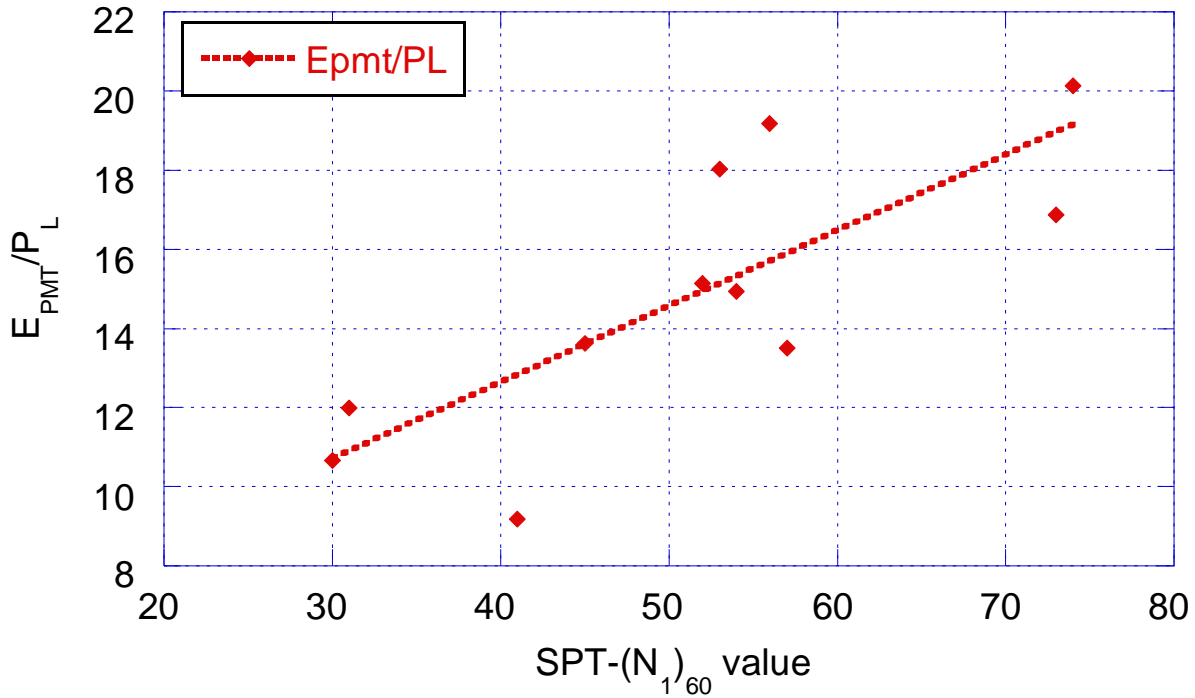


Figure 3.14 (b) Correlation between E_{PMT}/P_L vs SPT- $(N_1)_{60}$ for sand

3.6.5 COMPARISON OF CORRELATION BETWEEN SPT- $(N_1)_{60}$ VALUES AND E_{PMT}/P_L RATIO FOR GLACIAL TILL

In this study, the E_{PMT}/P_L ratio is performed for glacial till in all stations which are mentioned in section 3.2. The range of E_{PMT}/P_L ratio is between 5 and 26, with an average of 14 and standard deviation of 4. The comparison of E_{PMT}/P_L ratio is performed with CFEM (2006) which shows differences with the studied range. It is stated in the literature, the many commonly used correlations in the geotechnical practice to estimate the geotechnical parameters from the in-situ tests, contains a certain amount of inaccuracy. The reasons for this result can easily be related to quality of the in-situ and laboratory tests. Since the database of this study is mainly comprised of contracted construction projects, the quality of the site explorations and testing of the soils are questionable parameters for this type of research. In addition, there is also a more important reason that affects the obtained results which is the heterogeneous nature of the soil.

Figure 3.15 (a) represents the variation of the PMT modulus with pressure limit for glacial till. It is clear that the E_{PMT} varies linearly with the pressure limit with a relationship of $E_{PMT} = 14 P_L$ ($R^2 = 0.77$). Further, Figure 3.15 (b) represents the variation of E_{PMT}/P_L with SPT- $(N_1)_{60}$ values. It shows that the linear relationship with an intercept gives better correlation coefficient ($R^2 = 0.77$). The correlation equation between E_{PMT}/P_L ratio with SPT- $(N_1)_{60}$ is given by $E_{PMT}/P_L = 9.304 + 0.140(N_1)_{60}$.

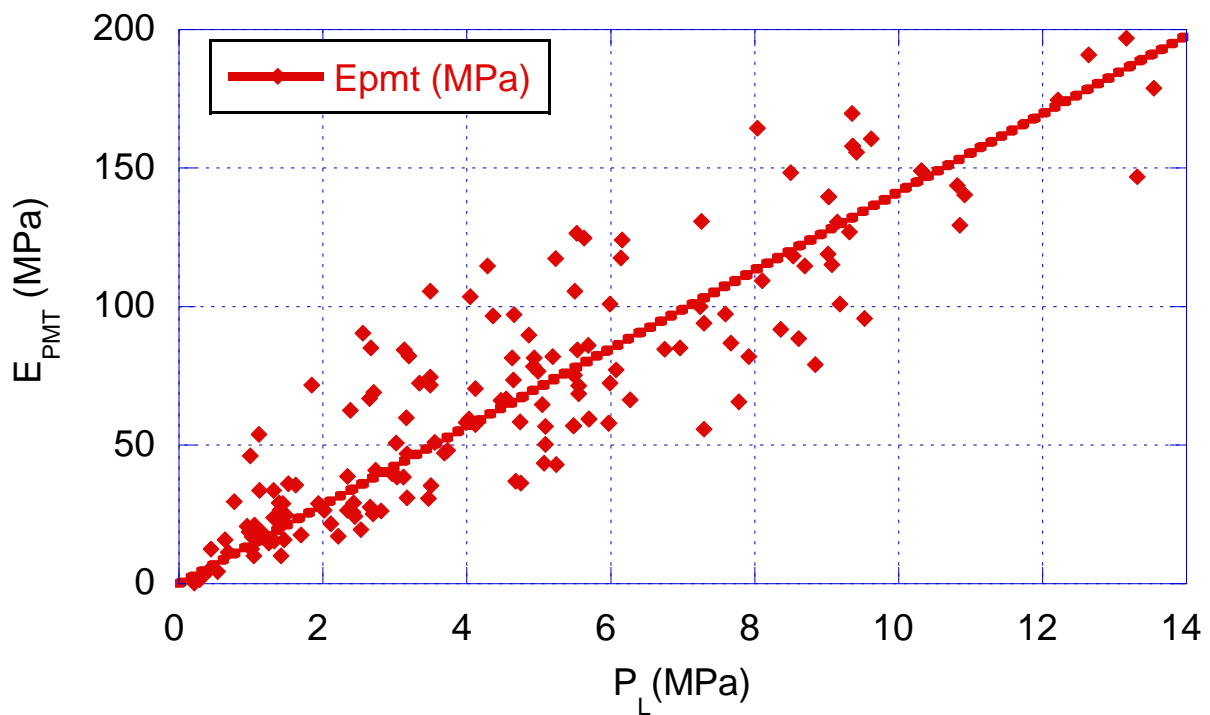


Figure 3.15 (a) Correlation between E_{PMT} vs P_L for glacial till

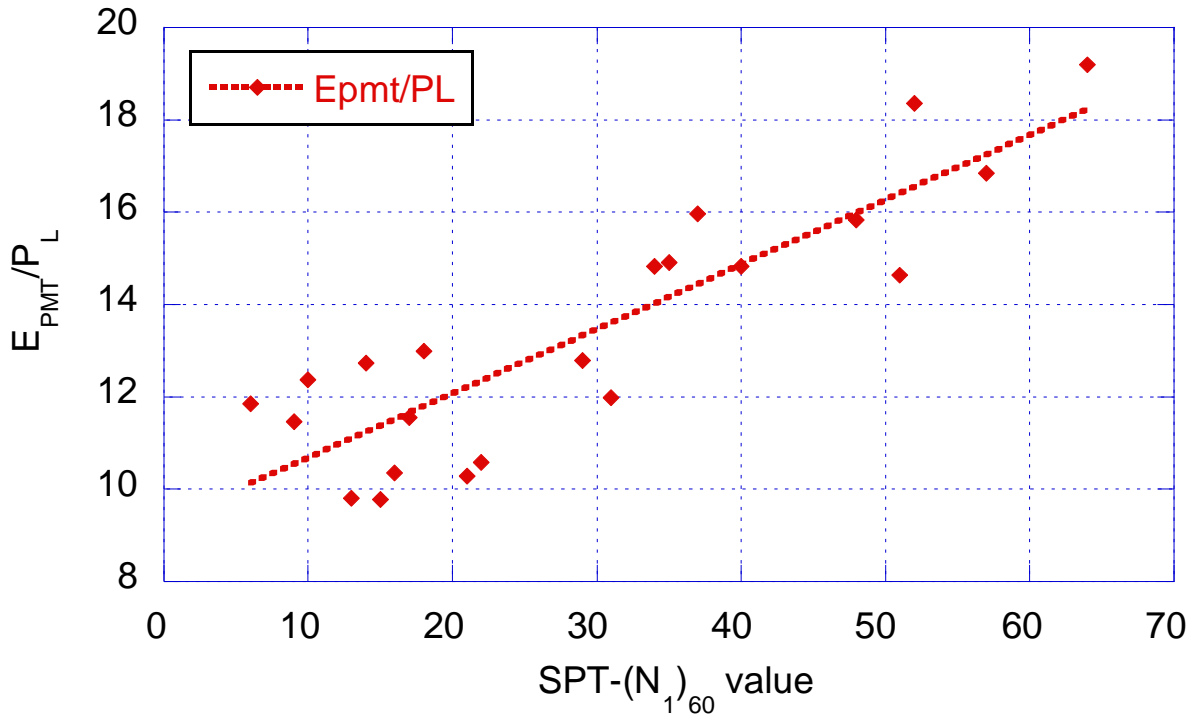


Figure 3.15 (b) Correlation between SPT-(N_1)₆₀ vs E_{PMT}/P_L for glacial till

3.7 SUMMARY

In this chapter, the study is performed based on an intensive site investigation program conducted for the Eglinton Crosstown LRT Project, in the city of Toronto. Data is collected from in-situ tests such as SPT and PMT and analyzed statistically. In this chapter, an attempt is made to develop new relationships between corrected and filtered SPT-N values with both E_{PMT} and P_L for various types of glacial tills. The ranges of SPT-N, E_{PMT} and P_L values are suggested in Table 3.5. The developed new correlation equations are summarized in Table 3.6. The E_{PMT}/P_L ratios also are summarized in Table 3.7. In addition to that the comparison is made with available literatures. There are good agreements with literature values in some extents. The accuracy of the evaluated correlations can be increased by more carefully performed and well controlled in-situ testing, borehole sampling and laboratory testing. In this way, some of the uncertainties can be reduced and the reliability of the correlations would be enhanced.

Table 3.5 Summary of ranges of SPT-N, E_{PMT} and P_L for corrected and filtered data

Cohesive glacial tills						
Soil type	Silty clay	Silty clay till	Clayey silt till	All soil		
SPT- (N) ₆₀	6 -62	3-31	4-67	3-67		
E_{PMT} (MPa)	11- 150	4-36	16-131	4-150		
P_L (MPa)	1.25-5.56	0.41-5.63	1.00 - 6.00	0.41-6.00		
Cohesionless glacial tills						
Soil type	Sand	Silt	Sandy silt	Silty sand	Sandy silt till	All soil
SPT- (N_1) ₆₀	13-97	4-98	4-91	25-76	16-80	4-98
E_{PMT} (MPa)	26-149	19-140	28-78	39-96	18-134	18-149
P_L (MPa)	2.42-13.32	3.17-9.08	1.33-9.03	1.42-13.55	6.0-8.04	1.33-13.55

Table 3.6 Summary of correlation equations for E_{PMT} and P_L

Cohesive glacial tills					
Soil type	Silty clay	Silty clay till	Clayey silt till	All soil	
E_{PMT} (MPa)	$1.70N (N)_{60}$	$1.37 (N)_{60}$	$1.61 (N)_{60}$	$1.54 (N)_{60}$	
P_L (MPa)	$0.104 (N)_{60}$	$0.092 (N)_{60}$	$0.104 (N)_{60}$	$0.103 (N)_{60}$	
Cohesionless glacial tills					
Soil type	Sand	Silt	Sandy silt	Silty sand	All soil
E_{PMT} (MPa)	$1.79 (N_1)_{60}$	$1.58 (N_1)_{60}$	$1.68 (N_1)_{60}$	$1.47 (N_1)_{60}$	$1.54 (N_1)_{60}$
P_L (MPa)	$0.126 (N_1)_{60}$	$0.141 (N_1)_{60}$	$0.124 (N_1)_{60}$	$0.158 (N_1)_{60}$	$0.139 (N_1)_{60}$

Table 3.7 Summary of E_{PMT}/P_L ratio for corrected and filtered data

Soil type	E_{PMT}/P_L Ratio
Sand	9-20
Glacial till	5-26

CHAPTER 4: FINITE ELEMENT SIMULATIONS OF PMTS

4.1 INTRODUCTION

The main aim of this chapter is to back calculate the PMT modulus (E_{PMT}) by using the finite element method (FEM) software, Plaxis 2D. For this purpose Mohr–Coulomb (M-C) model is used. The modelling methods and procedures of using Plaxis 2D are discussed in Section 4.2. The description of the M–C model is discussed in Section 4.3. The Section 4.4 described the 2D - PMT modeling and verification. In this section the PMT model is verified by existing literature model (Levasseur et al. (2009)). There is a good agreement between both models. In Section 4.5, the sensitivity study is performed to investigate the influence of mesh coarseness and boundary conditions. In Section 4.6, the case study is performed based on extensive PMTs are conducted in the Mount Dennis (MD) Station in the ECLRT project in Toronto. In this section, the PMT modulus (E_{PMT}) is calculated for different types of glacial tills according to the borehole # MD 101 with assumed values of Young's modulus. Then the PMT modulus (E_{PMT}) is correlated with the Young's modulus (E) for various types of glacial tills. The Menard's rheological factor (α) is made for each type of glacial tills. Finally the results are summarized in Section 4.7.

4.2 FINITE ELEMENT METHOD

FEM plays a major role in the geotechnical engineering practice because it allows modeling complicated nonlinear soil behavior through constitutive models. It will handle complex problems where analytical solutions are nearly impossible. Nowadays, the FEM has become very popular in the geotechnical engineering design. Even though, before the FEM can be used in design, the accuracy of any proposed solution technique must be proved (Owen and Hinton (1980)). In the FEM, the study object is divided into a number of finite elements, and the interaction between each one of these elements is analyzed for various geometrics with different boundary conditions and interfaces. It can predict the stresses, deformations and pore pressures of a specified soil profile.

4.2.1 CONSTITUTIVE BEHAVIOUR

The constitutive behavior is the stress-strain behavior. The 3D constitutive equations (Eqs. 4.1 – 4.3) can be used to calculate the stresses in a soil mass with neglecting the inertia effects and all body forces except the self-weight γ in x (vertical) direction (Timoshenko and Goodier (1951)). Equilibrium equations (Eqs. 4.1 – 4.3) are in terms of total stresses that must satisfy the boundary conditions. Fig. 4.1 shows the stresses on a typical element. Compressive stresses are considered as positive.

$$\frac{\partial \sigma_x}{\partial X} + \frac{\partial \tau_{yx}}{\partial Y} + \frac{\partial \tau_{zx}}{\partial Z} + \gamma = 0 \quad [4.1]$$

$$\frac{\partial \tau_{xy}}{\partial X} + \frac{\partial \sigma_y}{\partial Y} + \frac{\partial \tau_{zy}}{\partial Z} = 0 \quad [4.2]$$

$$\frac{\partial \tau_{xz}}{\partial X} + \frac{\partial \tau_{yz}}{\partial Y} + \frac{\partial \sigma_z}{\partial Z} = 0 \quad [4.3]$$

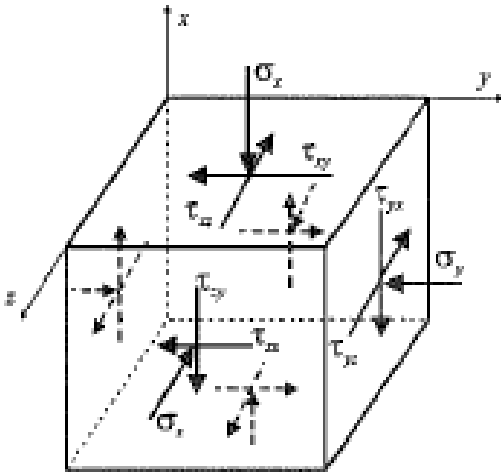


Figure 4.1 Stresses on a typical element

In the equilibrium and compatibility conditions, the constitutive behavior of a soil can be expressed mathematically as Eqs.4.4 or Eqs.4.5.

$$\Delta \sigma = [D] \Delta \varepsilon \quad [4.4]$$

$$\begin{Bmatrix} \Delta\sigma_X \\ \Delta\sigma_Y \\ \Delta\sigma_Z \\ \Delta\tau_{XY} \\ \Delta\tau_{XZ} \\ \Delta\tau_{ZY} \end{Bmatrix} = \begin{bmatrix} D_{11} & D_{12} & D_{13} & D_{14} & D_{15} & D_{16} \\ D_{21} & D_{22} & D_{23} & D_{24} & D_{25} & D_{26} \\ D_{31} & D_{32} & D_{33} & D_{34} & D_{35} & D_{36} \\ D_{41} & D_{42} & D_{43} & D_{44} & D_{45} & D_{46} \\ D_{51} & D_{52} & D_{53} & D_{54} & D_{55} & D_{56} \\ D_{61} & D_{62} & D_{63} & D_{64} & D_{65} & D_{66} \end{bmatrix} \begin{Bmatrix} \Delta\varepsilon_X \\ \Delta\varepsilon_Y \\ \Delta\varepsilon_Z \\ \Delta\gamma_{XY} \\ \Delta\gamma_{XZ} \\ \Delta\gamma_{ZY} \end{Bmatrix} \quad [4.5]$$

For a linear elastic material, the [D] matrix is written as Eqs.4.6.

$$[D] = \frac{E}{(1+\nu)(1-2\nu)} \begin{bmatrix} 1-\nu & \nu & \nu & 0 & 0 & 0 \\ & 1-\nu & \nu & 0 & 0 & 0 \\ & & 1-\nu & 0 & 0 & 0 \\ & & & \frac{1-2\nu}{2} & 0 & 0 \\ & & & & \frac{1-2\nu}{2} & 0 \\ \text{Symmetry} & & & & & \frac{1-2\nu}{2} \end{bmatrix}$$

[4.6]

Where

E - Modulus of elasticity

ν - Poisson's ratio

However, the soil behavior is usually non-linear. Therefore, increments of stress and strain can be more realistically related using the constitutive equation as indicated in Eq. 4.4 (Potts and Zdravkovic (2001)). It is also realistic for the [D] matrix to depend on the current and past history. The constitutive behavior can be stated by means of total or effective stresses. If it is needed to specify the constitutive behavior in terms of effective stress, the principle of effective stress can be used to obtain total stresses required for use with equilibrium equations (Eqs.4.7 – 4.10)

$$\sigma = \sigma' + \sigma_f \quad [4.7]$$

$$\Delta\sigma' = [D']\Delta\varepsilon \quad [4.8]$$

$$\Delta\sigma_f = [D_f] \Delta\varepsilon \quad [4.9]$$

Therefore,

$$\Delta\sigma = ([D'] + [D_f]) \Delta\varepsilon \quad [4.10]$$

Where

σ - Total stress

σ' – Effective stress

σ_f - Pore fluid pressure

D' - Constitutive relationship relating the change in effective stress to the change in strain

D_f - Constitutive relationship relating the change in pore fluid pressure to the change in strain

Plain strain condition

The constitutive relationship Eq 4.5 can be reduced to Eq 4.11 as follows for plain strain conditions.

$$\begin{Bmatrix} \Delta\sigma_x \\ \Delta\sigma_y \\ \Delta\sigma_z \\ \Delta\tau_{xy} \\ \Delta\tau_{yz} \\ \Delta\tau_{xy} \end{Bmatrix} = \begin{bmatrix} D_{11} & D_{12} & D_{14} \\ D_{21} & D_{22} & D_{24} \\ D_{31} & D_{32} & D_{34} \\ D_{41} & D_{42} & D_{44} \\ D_{51} & D_{52} & D_{54} \\ D_{61} & D_{62} & D_{64} \end{bmatrix} \begin{Bmatrix} \Delta\varepsilon_x \\ \Delta\varepsilon_y \\ \Delta\gamma_{xy} \end{Bmatrix} \quad [4.11]$$

Axisymmetric condition

In the case of axisymmetric problems, it is usual to carry out analyses using cylindrical coordinates as shown in Figure 4.2, r (radial direction), z (vertical direction) and θ (circumference direction). Due to the symmetry, there is no displacement in the θ direction and the displacement in the r and z directions are independent of θ and therefore the strains reduce to Eq 4.12 (Timoshenko and Goodier (1951)).

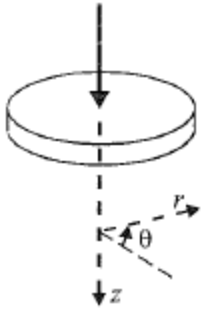


Fig 4.2 Example of axisymmetric co-ordinate axis

$$\epsilon_r = -\frac{\partial u}{\partial r} ; \epsilon_z = -\frac{\partial v}{\partial z} ; \epsilon_\theta = -\frac{u}{r} ; \gamma_{rz} = -\frac{\partial v}{\partial r} - \frac{\partial u}{\partial z} ; \gamma_{r\theta} = \gamma_{z\theta} = 0 \quad [4.12]$$

Where u and v are the displacements in the r and z direction respectively.

Stresses in the axisymmetric element are shown in Figure 4.3 and the [D] matrix is similar to plain strain situation as shown in the Eq 4.11.

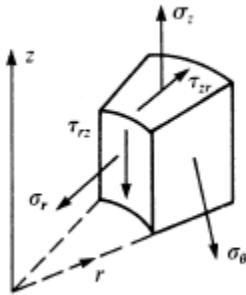


Fig 4.3 Stresses in the axisymmetric element

4.2.2 STEPS INVOLVED IN THE FEM

The following steps are involved in the FEM (Potts and Zdravkovic (2001)).

Step 1: Element discretization

In this process, the geometry of the problem is modelled by an assembly of small regions termed as finite elements, which have nodes defined on the element boundaries, or within the element.

Step 2: Primary variable approximation

Primary variables such as displacements, stresses, etc., must be selected. The rules with regard to how these variables have to vary over a finite element are established. Nodal values are used to express the variations. Displacements are usually adopted as a primary variable in geotechnical engineering.

Step 3: Element equations

The elemental equations (Eq. 4.13) are derived using an appropriate variational principle (e.g., the minimum potential energy).

$$[K_E]\{\Delta d_E\} = \{\Delta R_E\} \quad [4.13]$$

Where

$[K_E]$ - Element stiffness matrix

$\{\Delta d_E\}$ - Vector of incremental element nodal displacements

$\{\Delta R_E\}$ - Vector of incremental element nodal forces

Step 4: Global equations

The element equations are combined to form global equations (Eq. 4.14).

$$[K_G]\{\Delta d_G\} = \{\Delta R_G\} \quad [4.14]$$

Where

$[K_G]$ - Global stiffness matrix

$\{\Delta d_G\}$ - Vector of all incremental global nodal displacements

$\{\Delta R_G\}$ - Vector of all incremental global nodal forces

Step 5: Boundary conditions

The global equations are modified by formulating boundary conditions. Loadings such as line and point loads, pressures, body forces, etc. affect $\{\Delta R_G\}$, and the displacements affect $\{\Delta d_G\}$.

Step 6: Solve the global equations

The displacements $\{\Delta d_G\}$ at all the nodes can be obtained by solving the global equations. These nodal displacements are used to evaluate stresses and strains.

4.3 MOHR-COULOMB MATERIAL MODEL

In this research, the Mohr-Coulomb (M-C) elastoplastic constitutive model is used as a material model for soils. The basic parameters used in this model with their standard units are listed below.

E	: Young's modulus	$[kN/m^2]$
ν	: Poisson's ratio	$[-]$
c	: Cohesion	$[kN/m^2]$
φ	: Friction angle	$[^\circ]$
ψ	: Dilatancy angle	$[^\circ]$

As shown in Fig. 4.4, the Mohr circles of stress at failure are obtained by plotting the results of the laboratory tests in term of effective stresses. The tangent line to the failure circles from several tests, performed with different initial effective stresses, is called the Coulomb failure criterion (Eqs. 4.15 – 4.17).

$$\tau_f = c' + \sigma'_{nf} \tan \varphi' \quad [4.15]$$

Where

τ_f - Shear stress on the failure plane

σ'_{nf} -Normal effective stress on the failure plane

c' -Cohesion

φ' -Angle of shearing resistance

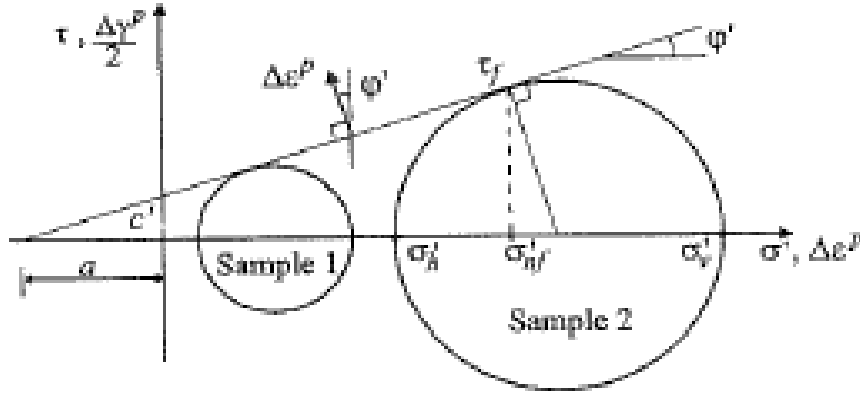


Figure 4.4 Mohr's circles of effective stress (Ports and Zdravkovic (2001))

The M-C failure criterion is defined as:

$$\sigma'_1 - \sigma'_3 = 2c' \cos \varphi' + (\sigma'_1 + \sigma'_3) \sin \varphi' \quad [4.16]$$

$$\sigma'_1 = \sigma'_v, \text{ and } \sigma'_3 = \sigma'_h$$

Therefore, the yield function is given below

$$F(\{\sigma'_1\}, \{k\}) = \sigma'_1 - \sigma'_3 - 2c' \cos \varphi' - (\sigma'_1 + \sigma'_3) \sin \varphi' \quad [4.17]$$

This equation can be more conveniently written in terms of stress invariants p' , J , and θ (Eqs. 4.18 – 4.19).

$$F(\{\sigma'_1\}, \{k\}) = J - \left[\left(\frac{c'}{\tan \varphi'} \right) + p' \right] g(\theta) = 0 \quad [4.18]$$

$$g(\theta) = \frac{\sin \phi'}{\cos \theta + \left(\frac{\sin \theta \sin \phi'}{\sqrt{3}} \right)} \quad [4.19]$$

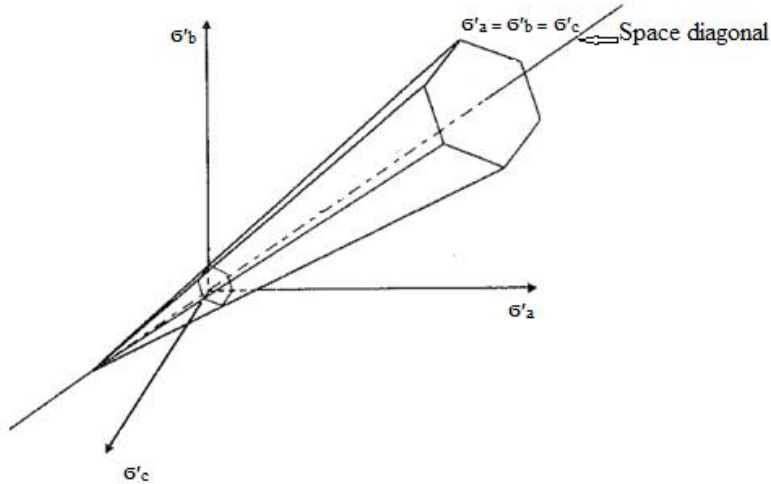


Figure 4.5 Mohr-Coulomb yield surfaces in principal stress space (Ports and Zdravkovic (2001))

As shown in Figure 4.5, an irregular hexagonal cone is plotted by the yield function in principal effective stress space.

4.4 2D PMT MODELLING AND VERIFICATION

4.4.1 2D PMT MODELLING

For the 2D PMT modeling, the FEM software, PLAXIS 2D, is used. PLAXIS name was derived from PLasticity AXISymmetry, a computer program developed to solve the cone penetrometer problem by Pieter Vermeer and De borst. According to (Burd (1999)), the initiation of this program was held at Delft University of Technology Netherland by Pieter Vermeer in 1974. Earlier version of PLAXIS was in DOS interface. In 1998, the first PLAXIS 2D for Windows was released. The new versions and modifications were carried out for the analysis of soil behavior for geotechnical engineers. In this study Plaxis 2D version 2012 is used.

4.4.2 VERIFICATION OF THE MODEL

The 2D FEM model is validated by using a published case study on PMT, which was performed by Levasseur et al. (2009) for Hostun sand. The geometry of the model is shown in Figure 4.6. The PMT test depth is 3 m. In this analysis, an axisymmetric FEM is used which is the same as the way used by Levasseur et al. (2009). In this model, the soil is represented by an M-C model whose parameters are shown in Table 4.1. To validate the model same soil parameters are used with same soil model as M-C by using Plaxis 2D in this verification study. The geometry of the model has shown in Figure 4.7. The deformed mesh diagram and the zoomed view of the diagram are shown in Figure 4.8 and Figure 4.9 respectively. The horizontal displacement diagram and the zoomed view of the diagram are also shown in Figure 4.10 to Figure 4.11 individually. The pressure (P) vs volumetric strain ($\frac{\Delta v}{V}$) curve is plotted with the curve from the literature. There is a good agreement between the two curves, as shown in Figure 4.12.

Table 4.1 Parameters used in the M-C model for dense Hostun sand

Parameter	Levasseur et al. (2009) value
Shear modulus (G_{ref}) (kPa)	22250
Poisson's coefficient (ν)	0.25
Cohesion (c) (kPa)	0
Friction angle (ϕ) ($^{\circ}$)	35
Dilatancy angle (ψ) ($^{\circ}$)	5
Initial stress field coefficient (K_0)	0.4265

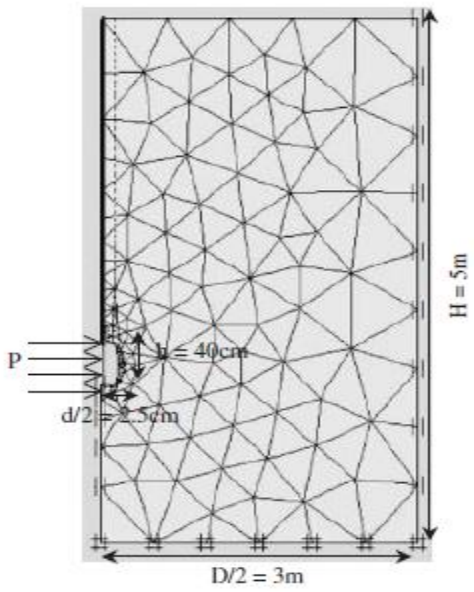


Figure 4.6 2D axisymmetric model and associated mesh (Levasseur et al. (2009))

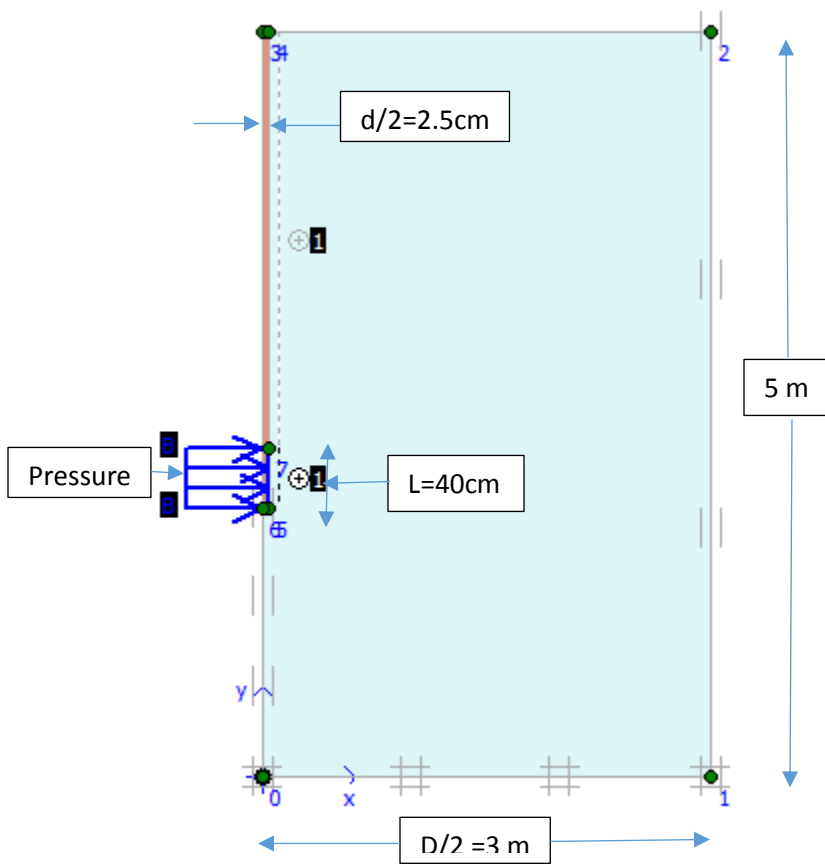


Figure 4.7 Geometry of the PMT model

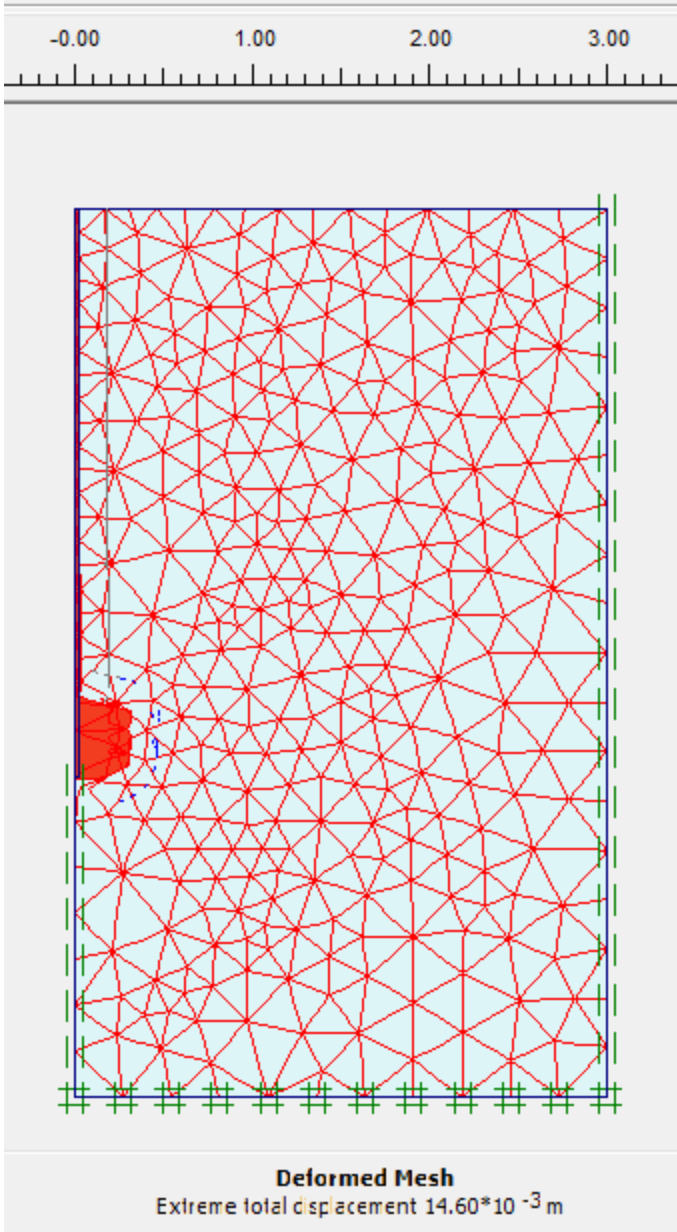


Figure 4.8 Deformed mesh diagram

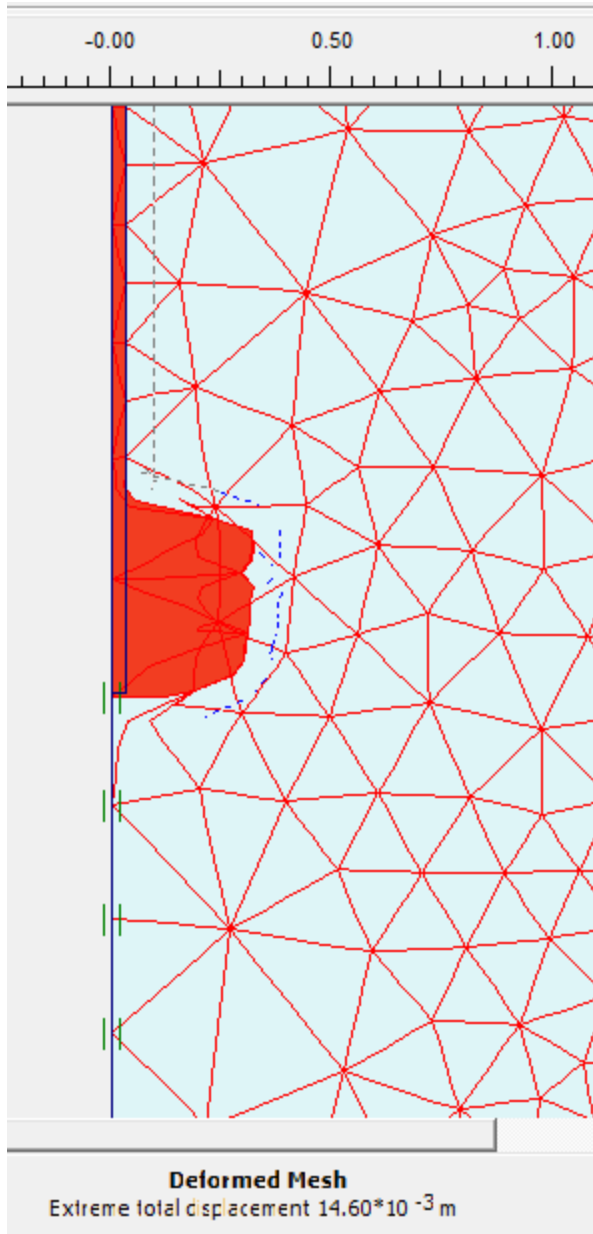


Figure 4.9 Zoomed view of the deformed mesh diagram

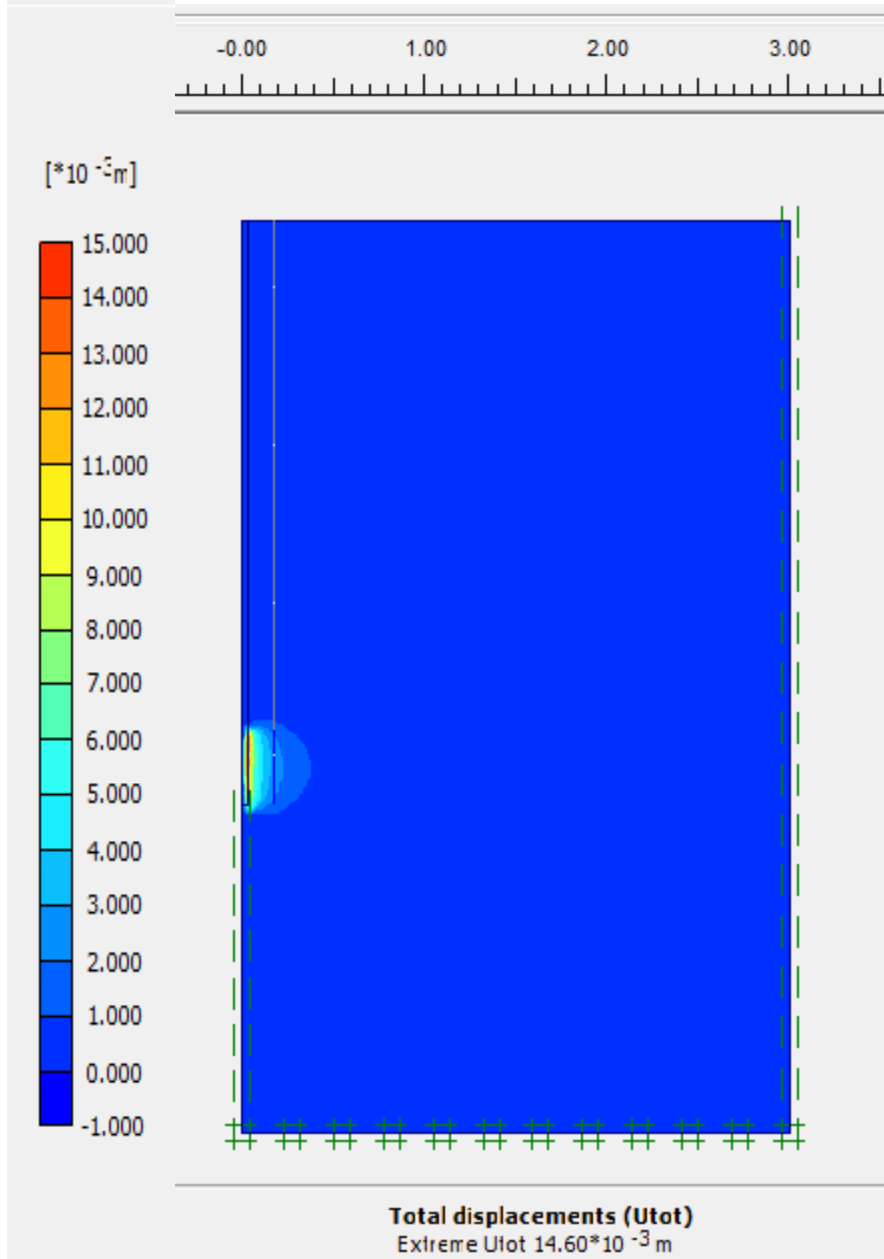


Figure 4.10 Horizontal displacement diagram

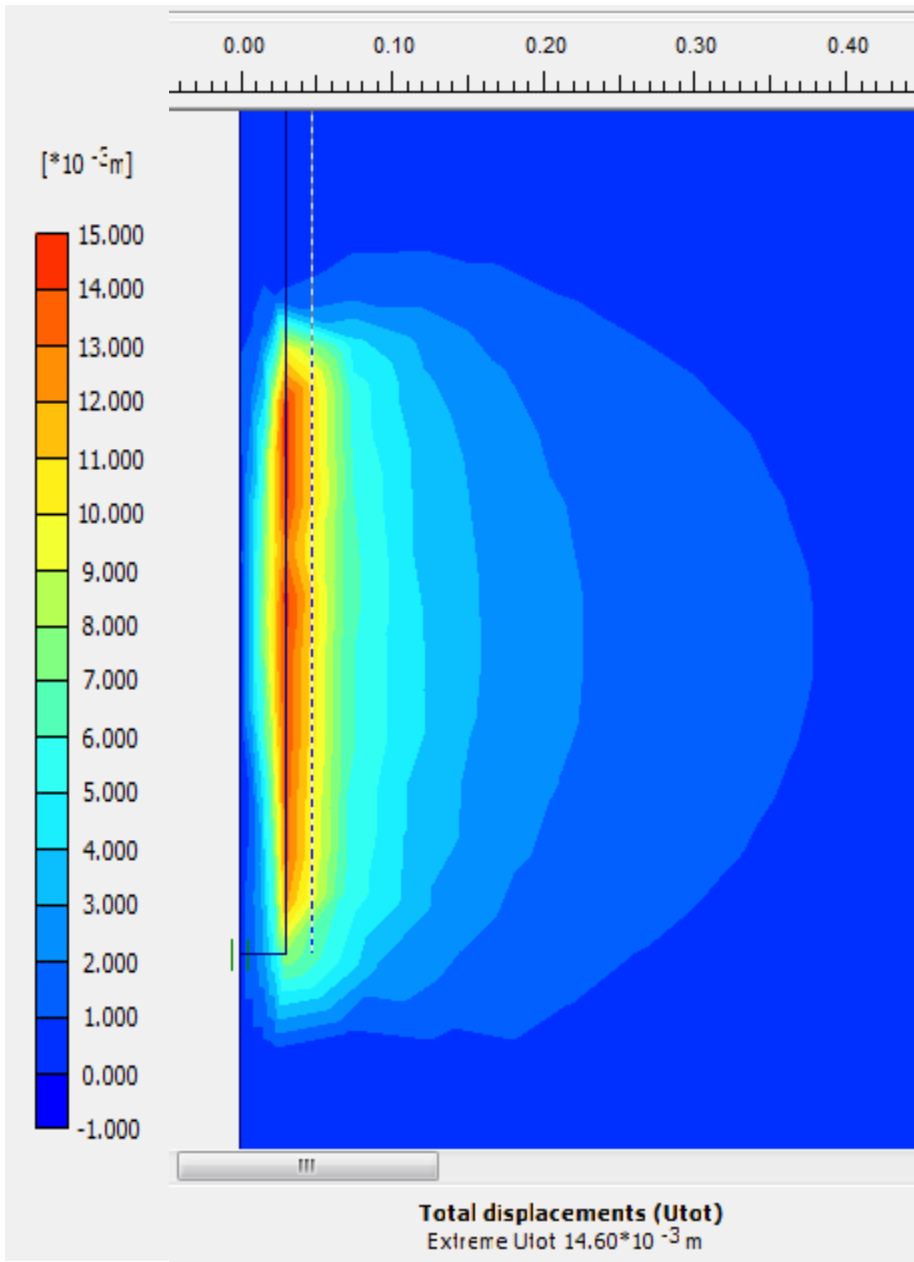


Figure 4.11 Zoomed view of the horizontal displacement diagram

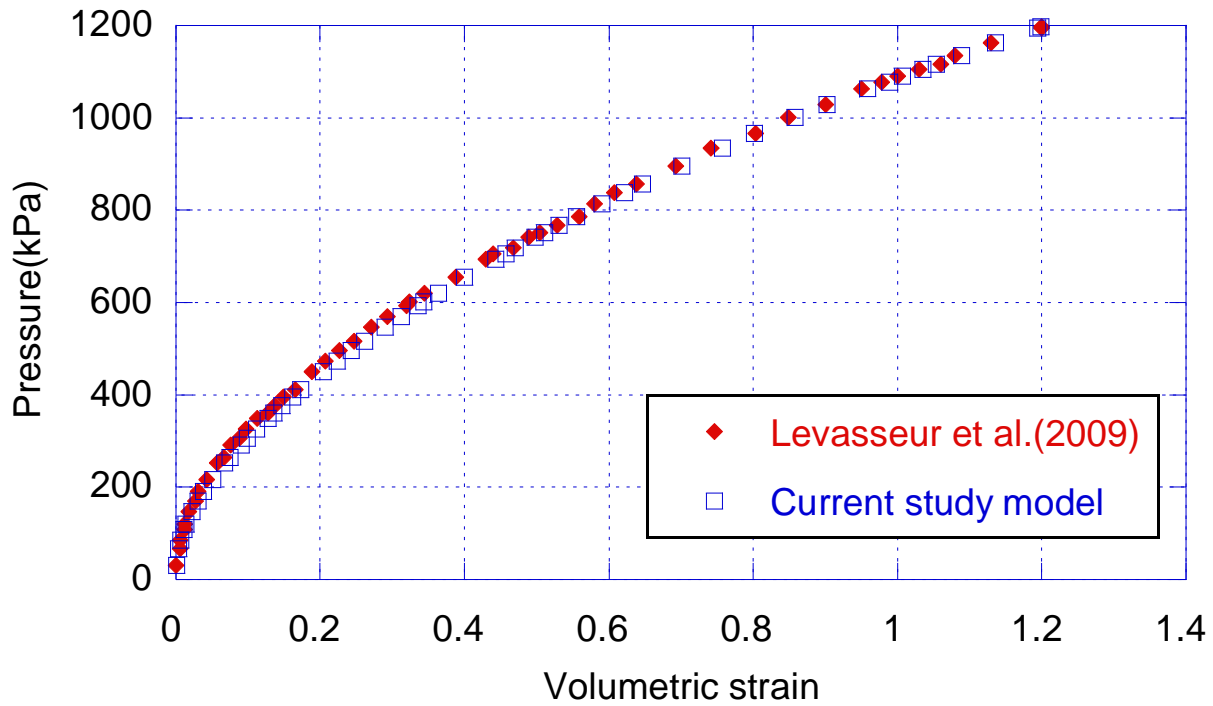


Figure 4.12 Pressure (p) vs volumetric strain ($\frac{\Delta v}{v}$) curves for verification of the model

4.5 SENSITIVITY STUDY

This study is performed to investigate the influence of mesh coarseness, horizontal and vertical boundary conditions in the PMT model. Each case is elaborated below.

4.5.1 MESH COARSENESS

A mesh is a composition of finite elements that can be created in mesh mode in Plaxis 2D. In Plaxis, the mesh coarseness provides a significant influence on the calculation results. The model is implemented with five types of mesh coarseness such as very coarse, coarse, medium, fine and very fine mesh.

In order to evaluate the mesh influence in the Plaxis model, the Levasseur et al. (2009) is used as a bench mark problem to develop the horizontal displacements at the midpoint of the probe for different types of mesh coarseness with some applied pressures which are shown in Table 4.2.

The difference in the horizontal displacement is about 1.27 times higher when the mesh changes from “*very course*” into “*very fine*”. It shows that the very fine mesh gives more accurate results compare to other mesh coarseness, but it consumes more time during the simulation process. Due to that, fine mesh coarseness is adopted in this study. Mean time the differences between very fine to fine mesh coarseness is very small, nearly 0.85% different from very fine to fine.

Table 4.2 Comparison of horizontal displacement related to mesh coarseness

Pressure (kPa)	Horizontal displacement x 10 ⁻³ (m) for mesh coarseness				
	Very fine	Fine	Medium	Course	Very course
500	3.53	3.50	3.49	3.37	2.78
1000	10.98	10.90	10.85	10.83	8.78
1500	21.90	21.41	20.67	20.78	16.81
2000	37.18	35.76	33.87	33.63	26.42

4.5.2 HORIZONTAL BOUNDARY CONDITIONS

The influence of horizontal distance from probe is investigated in this study. The right side boundary from the probe is not clearly stated in the literature. In order to evaluate the horizontal distance’s influence in the Plaxis model, the Levasseur et al. (2009) is used as a bench mark problem to develop the pressure vs volumetric strain curves for different distances from the center of probe. The developed volumetric strain curves are shown in Figure 4.13 with the Levasseur et al. (2009) curve. The values of the volumetric strains with relation to the horizontal distances are shown in Table 4.3 with the Levasseur et al. (2009) value. Concluded from this study, the horizontal distances have no significant influence on the volumetric strain curves other than the 1 m distances.

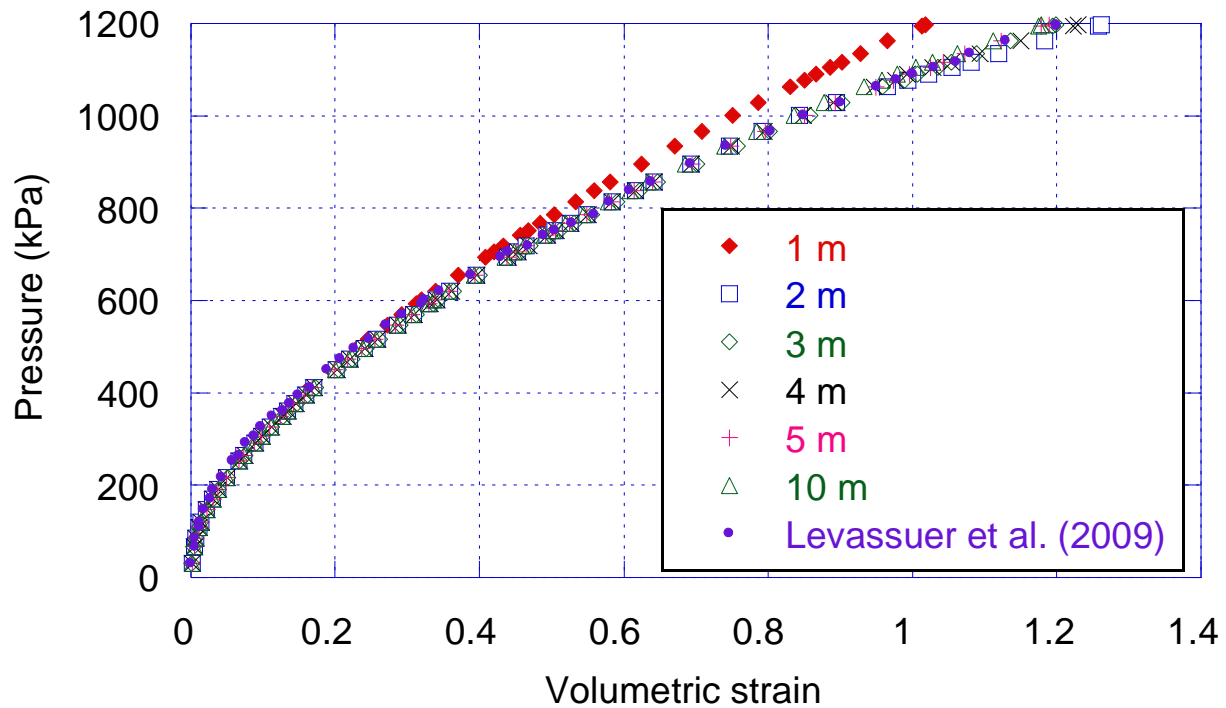


Figure 4.13 Pressure (p) vs volumetric strain ($\frac{\Delta v}{v}$) curves for horizontal boundary conditions

Table 4.3 The values of volumetric strain related to horizontal distances

Horizontal boundary condition (m)	Volumetric strain ($\frac{\Delta v}{v}$)
1	1.0183
2	1.2620
3	1.1943
4	1.2290
5	1.1894
10	1.1785
Levassuer et al. (2009)	1.2000

4.5.3 VERTICAL BOUNDARY CONDITIONS

The influence of vertical distance below the bottom of the probe is investigated in this study. The vertical distance from bottom of the probe is not clearly stated in the literature. In order to

evaluate the vertical distance's influence in the Plaxis model, the Levasseur et al. (2009) is used as a bench mark problem to develop the pressure vs volumetric strain curves for different distances from the bottom of the probe. The developed volumetric strain curves are shown in Figure 4.14 with the Levasseur et al. (2009) curve. The values of the volumetric strain with relation to the vertical boundary conditions are shown in Table 4.4 with the Levasseur et al. (2009) value. Concluded from this study, the vertical boundaries have no significant influence on the volumetric strain curves other than the 0 m distance.

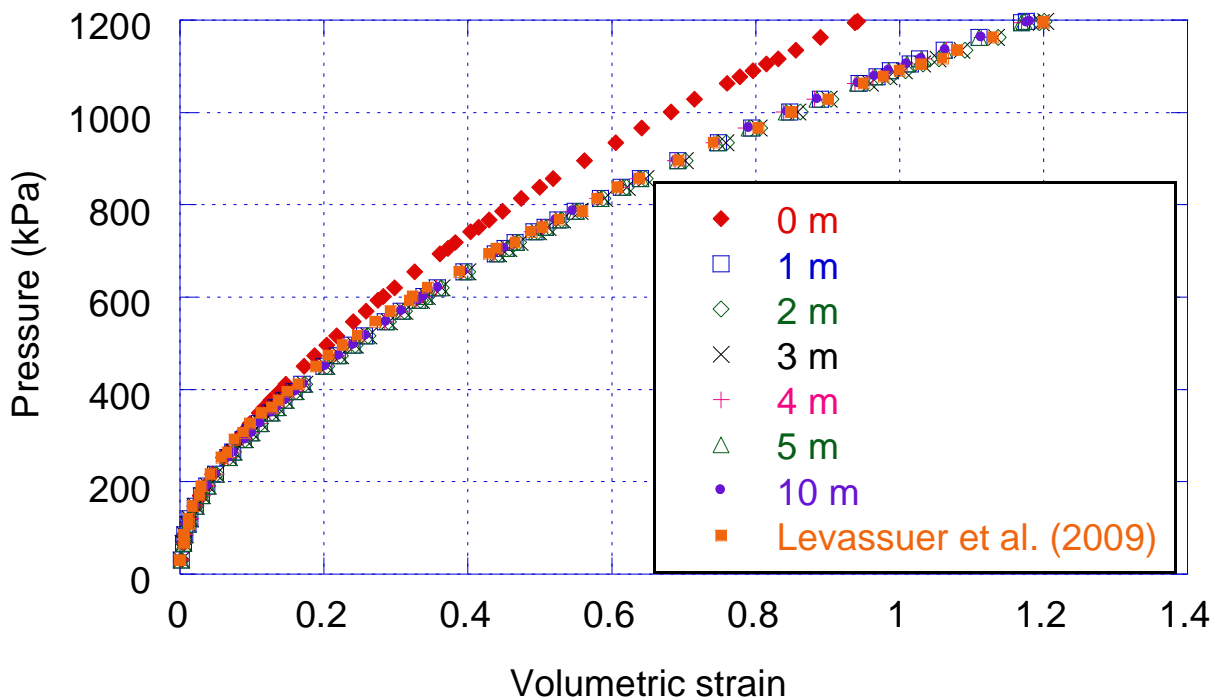


Figure 4.14 Pressure (p) vs volumetric strain ($\frac{\Delta v}{v}$) curves for vertical boundary conditions

Table 4.4 The values of volumetric strain related to vertical boundary conditions

Vertical distance below the bottom of the probe (m)	Volumetric strain ($\frac{\Delta v}{v}$)
0	0.9414
1	1.1756
2	1.2013
3	1.2033

4	1.1776
5	1.1737
10	1.1815
Levassuer et al.(2009)	1.2000

4.6 CASE STUDY AT MOUNT DENNIS STATION

The main goal of this study is to back calculate the Young's modulus (E) of different types of glacial tills from PMT results using FEM. It was made from an extensive research on PMT results conducted in MD station in the ECLRT project in Toronto. It was analyzed from eleven (11) PMT results. The PM tests depth varies from 3.8 m to 35 m. It was concluded, with TTC geotechnical standard (2014), most of the PMT results were from sand to sandy silt from 3 m to 21.3 m and clayey silt till deposited interbedded between silty clay in the depth which varies from 24.5 m to 35 m. These types of materials are very heterogeneous and mixture of gravel, sand, silt and clay size particle in varying proportions (Ng and Xue (2011)). The water table is observed a depth of 4.6 m below the ground surface. The processes of back calculating the E for different types of glacial tills are very complex and arduous task. Therefore in this study, back calculating E_{PMT} for different types of glacial tills with knowing values of E with other soil parameters (c , ϕ , ψ and ν) are keeping constant. The E_{PMT} values are computed from the quasi-linear portion of the pressure vs radial strain curves. The E_{PMT} is correlated with E value for various types of glacial tills. Then the linear correlation equations between E_{PMT} and E are established for different types of glacial tills. The E values are predicted to the field measured E_{PMT} using the established correlation equations. The predicted E values are used as an input values in the simulation and again the E_{PMT} values are calculated from the quasi-linear portion of the pressure vs radial strain curves. The calculated E_{PMT} values have good agreement with field measured E_{PMT} . The Menard " α " factors are developed for various types of glacial tills.

4.6.1 FINITE ELEMENT ANALYSES

The FEM model geometry is created according to soil profile in the MD Station borehole number 101C3. The borehole report and PMT results are attached in Appendix 4.1 and 4.2 respectively. The soil profile has many layers which are shown in Figure 4.15. The width(x axis) and depth (y axis) of the soil profiles are pre-defined in the model tab on the project properties window. The limit of the soil contour is defined as the $x_{\min} = 0$, $x_{\max} = 40$ m and $y_{\min} = -40$ m, $y_{\max} = 0$. The top boundary of the soil layer is at $y = 0$ at grade level and the bottom boundary of the soil layer is $y = -40$ m at bed rock. Once the soil layers are drawn, the soil properties can be assigned according to values shown in Table 4.5. These parameters are grasped from ECLRT geoengineering factual data reports for different type's glacial tills. (cohesionless glacial tills such as sand and sandy silt, cohesive glacial tills such as silty clay and clayey silt till). In addition, a small amount of cohesion ($c = 0.1$ kPa) is assigned for sand to prevent soil failure upon unloading, which the soil may experience near the borehole wall during drilling or pre-boring (Sedran et al. (2013)). A small value of cohesion (c) is adopted to avoid complication while performing the simulation (Plaxis (2012)).

Table 4.5 Summary of soil parameters used in the FEM analysis

Soil type	Depth (m)	Plaxis 2D (MCM)						
		$\gamma_{\text{Unsaturated}}$ (kg/m ³)	$\gamma_{\text{Saturated}}$ (kg/m ³)	c (kN/m ²)	ϕ (⁰)	Ψ (⁰)	ν	Initial E (kN/m ²)
Fill	0.41	14	16	15	0	0	0.25	10000
Sand	3.8	17	21	0.1	41	11	0.33	25000
Sand	6.0	19	22	0.1	42	12	0.33	25000
Sandy silt	9.4	17	20.4	10	43	13	0.33	25000
Sandy silt	13.9	17	20.4	10	39	9	0.33	25000
Sandy silt	15.2	17	20.4	10	42.5	12.5	0.33	25000
Sandy silt	18.3	17	20.4	10	39	9	0.33	25000
Sand	21.3	19	22	0.1	45	15	0.33	25000
Silty clay	24.5	17	20.4	100	32	2	0.33	20000
Clayey silt till	27.3	17	21.8	50	35	5	0.33	20000
Clayey silt till	30.4	17	22.1	50	35	5	0.33	20000
Silty clay	35.0	17	20.4	100	32	2	0.33	20000
Bentonite		12	14	10	0	0	0.10	6000

The soil is modelled with the M-C model since its limited number of input parameters and its popularity in the practice. Due to the granular nature of the soils such as sand and sandy silt, all calculations are made in drained condition. For the silty clay and clayey silt till soils, all calculations are made in undrained (A) condition according to Plaxis 2D material model (2012). The analysis is performed as an axisymmetric and the mesh elements are 15 nodes triangles. The standard fixity boundary condition is applied for the soil profile. As a result Plaxis will automatically generate full fixity at the base of the geometry and roller boundaries at the vertical sides ($U_x=0$; $U_y= \text{free}$). The soil is free on the vertical walls of drilling and vertical movement is possible on the two vertical borders of the soil profile (Houari and Abdeldjalil (2015)). The boundary conditions of the MD Station soil profile are shown in Figure 4.15.

The PMT geometry is discretized using a 2D axisymmetric configuration for PMT probe with a length (460mm)-to-diameter (76mm) ratio of 6.05, typical of the RocTest NX-sized PMT probe.

The recommended length to diameter ratio is 6 or more (Briaud (1992)). Positive interface is introduced on the probe and vertical surface of the PMT borehole. A “Type B” loading is applied on the probe as shown in Figure 4.15 at the test depth during the simulation stages. This loading is applied radially on a length equal to the length of the probe, in downhole (Husein (2001)). The loading condition is shown in Figure 4.15.

Once the geometry modelling process is complete, calculations are proceeded which consists of the generation of meshes and definition of the construction stages. The defined geometry has to be divided into finite elements in order to perform a FEM calculation. A mesh is a composition of finite elements that can be created in mesh mode in Plaxis 2D. In Plaxis, the mesh coarseness provides a significant influence on the calculation results. The model is implemented with five types of mesh coarseness such as very coarse, coarse, medium, fine and very fine mesh.

At the end of the analysis is performed in the section 4.5.1, the fine mesh density is selected due to its accuracy and speed of calculations. A fine mesh is used for the Plaxis 2D models analysis (Khanal (2013)). In addition to that extra geometry lines are created around the probe to locally generate a finer mesh. A typical FE mesh of MD Station is shown in Figure 4.16.

The PMT is simulated in the following three stages.

- (i) Generation of in-situ initial stress condition by imposed by K_0 value as shown in Figure 4.17.
- (ii) Borehole drilling and filled the borehole with mud(bentonite)
- (iii) Applied pressure at the probe borehole interface incrementally.

During the above procedures the probe's volume increases due to the pressure applied to the probe and therefore the soil around it will deform. Then the horizontal displacement is recorded from Plaxis output to calculate the radial strain. The pressure vs radial strain curve is plotted for each Young's modulus (E) in each depth to calculate the PMT modulus (E_{PMT}). In this calculation a special attention is paid to that the two slopes of the experimental and numerical curves in the elastic phase should be similar.

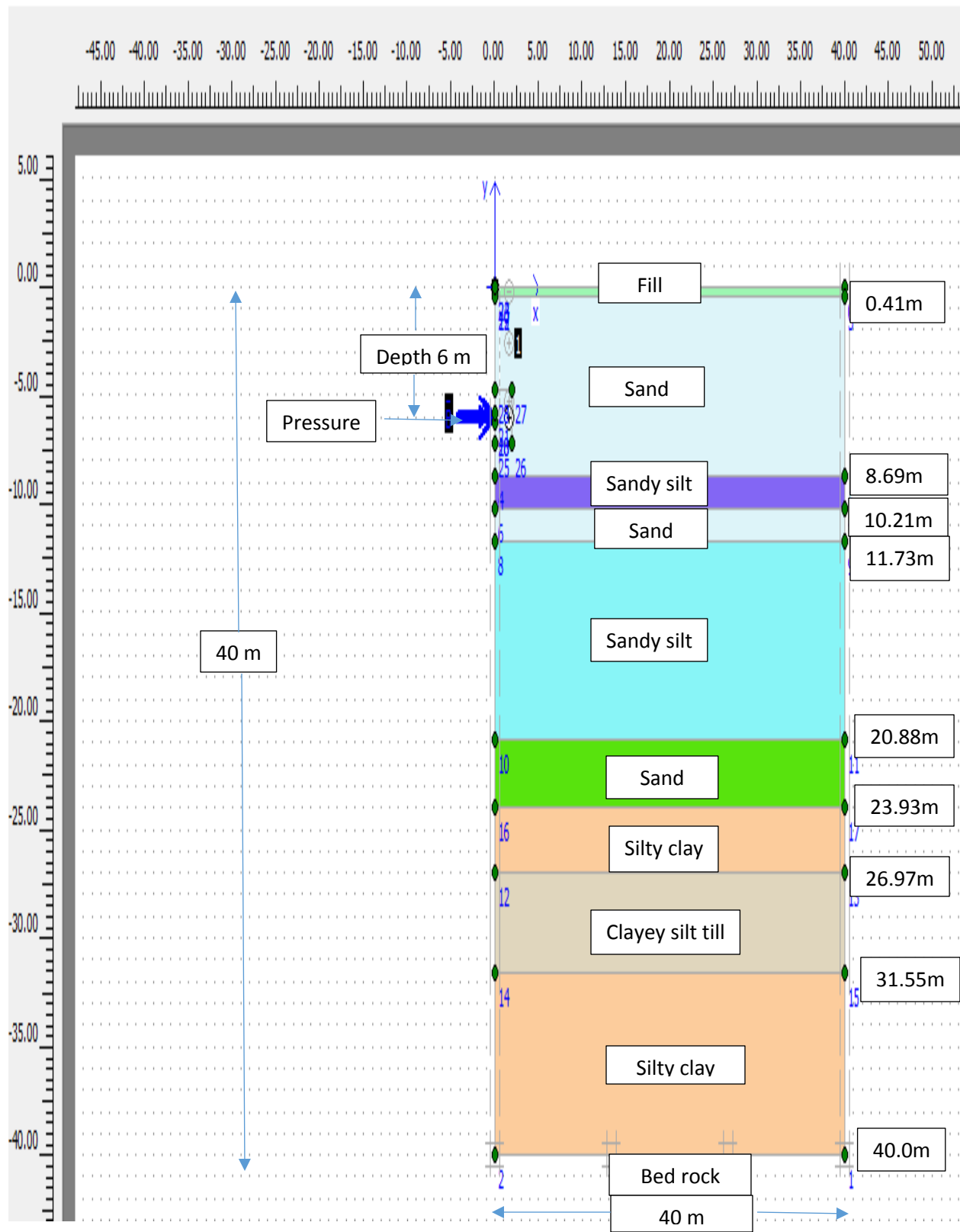


Figure 4.15 10 Soil profile at Mount Dennis Station according to borehole MD101-PMT and test @ 6.0m depth

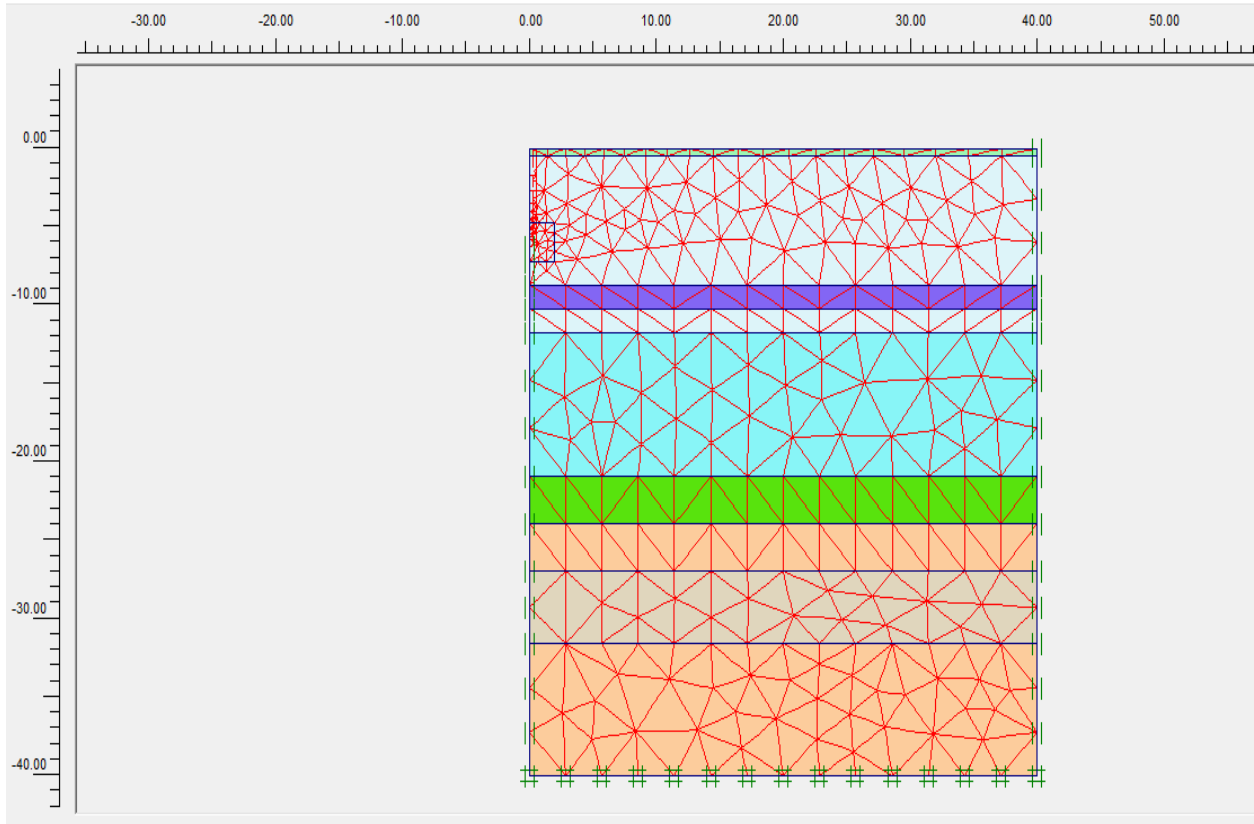


Figure 4.16 Typical FE mesh for numerical simulation at MD Station

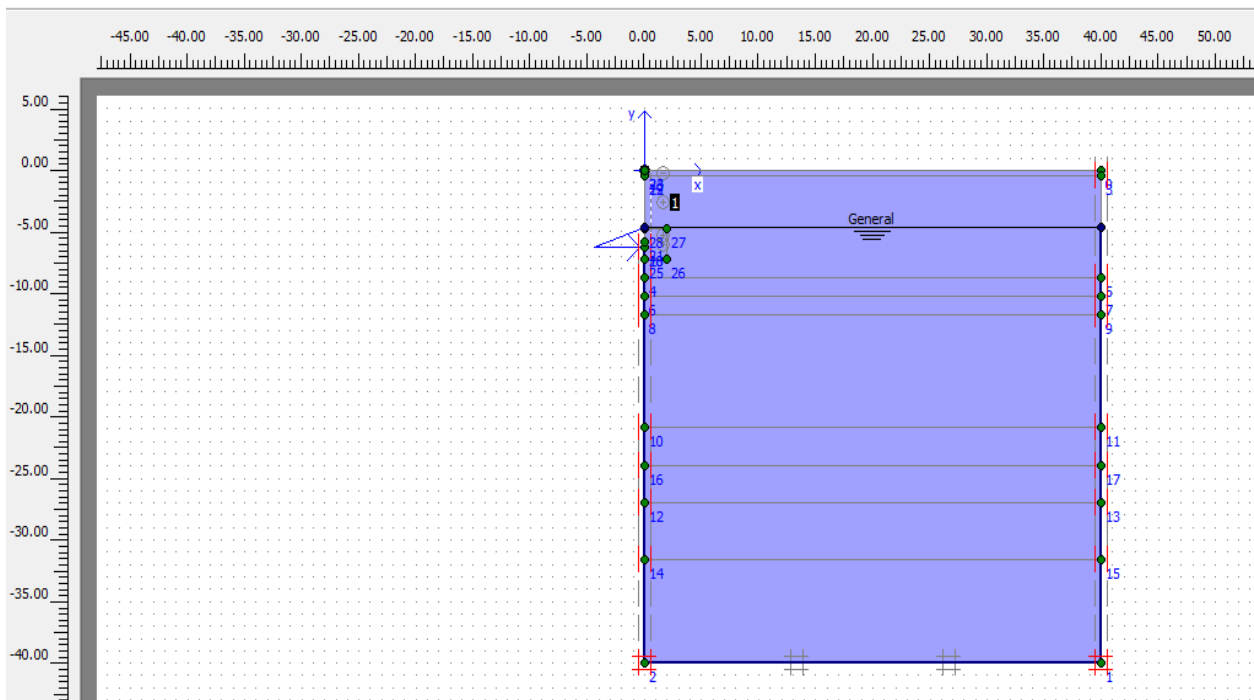


Figure 4.17 Water table diagram for soil profile at MD Station @ test depth 6m after generate the in-situ initial stress condition.

4.6.2 2D FINITE ELEMENT RESULTS AND ANALYSIS

The numerical simulation is performed at different depths from 3.8 m to 35 m according to MD Station borehole MD101-PMT. A range of simulations are completed for different values of Young's modulus in each depth. The pressures are applied on the probe incrementally during the simulation. The displacements are measured at the mid-point of the probe for each pressure increments. The results can be viewed in the output mode and the most notable results are the deformed mesh, total displacement, lateral (horizontal) displacement and cross section of the lateral displacement (U_x).

The typical deformed mesh with the total displacement diagram at 6 m depth is shown in Figure 4.18. The zoomed view of the deformed mesh diagram is shown in Figure 4.19. The x direction (horizontal) displacement at the mid-point of the probe after FEM analysis is shown in Figure 4.20. The zoomed view of the horizontal displacement at the mid-point of the probe is shown in Figure 4.21. The horizontal displacement shaded diagram and the zoomed view of the shaded diagram are shown in Figure 4.22 and Figure 4.23 respectively. A typical cross section of horizontal displacement diagram is shown in Figure 4.24. The zoomed view of the cross section of horizontal displacement diagram is shown in Figure 4.25.

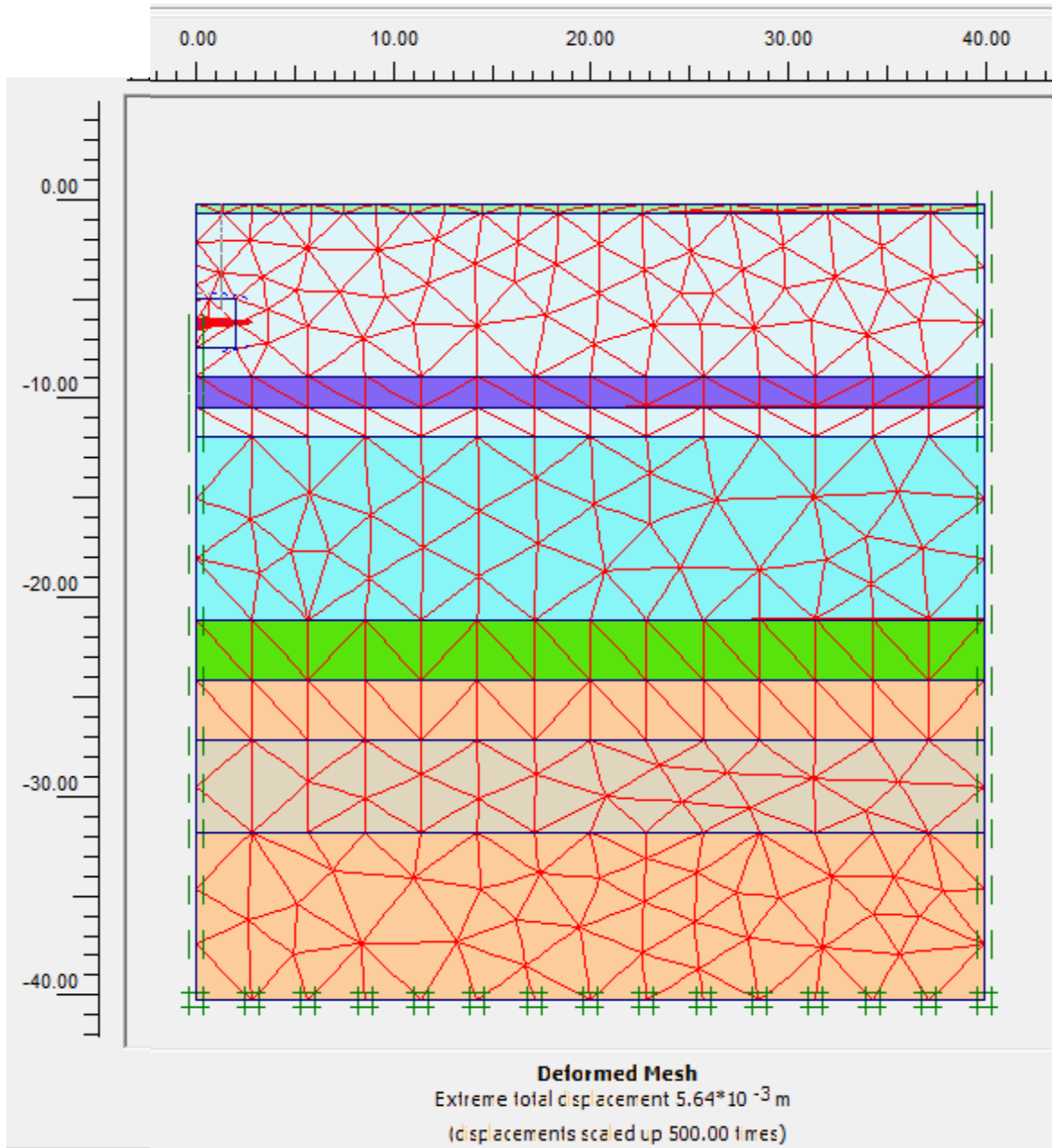


Figure 4.18 Typical deformed meshes @ 6.0 m depth at MD Station

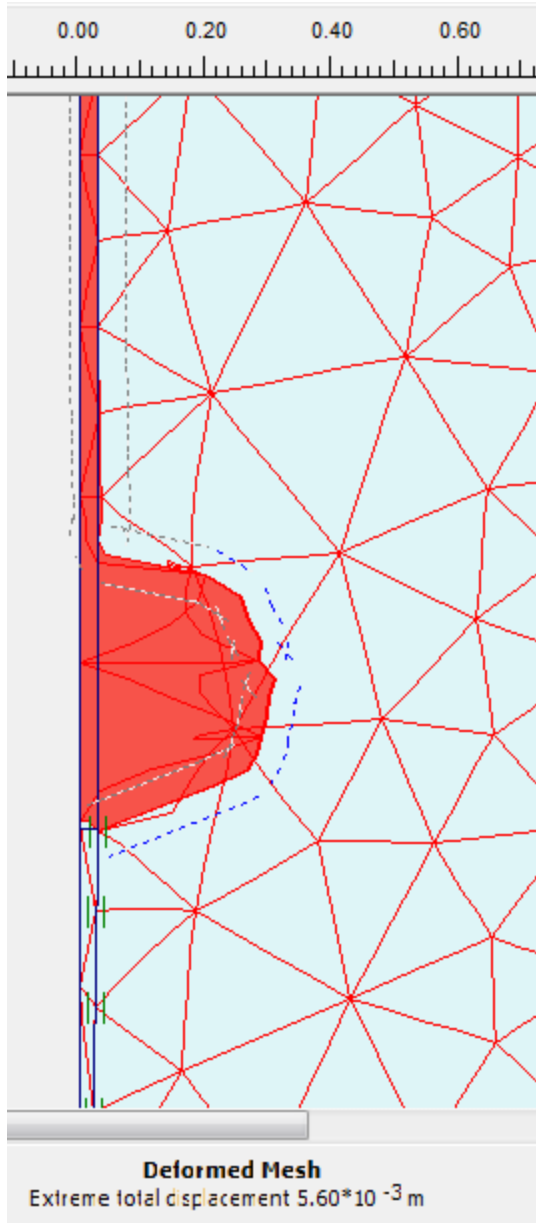


Figure 4.19 Zoomed views of the deformed meshes diagram@ 6.0 m depth at MD station

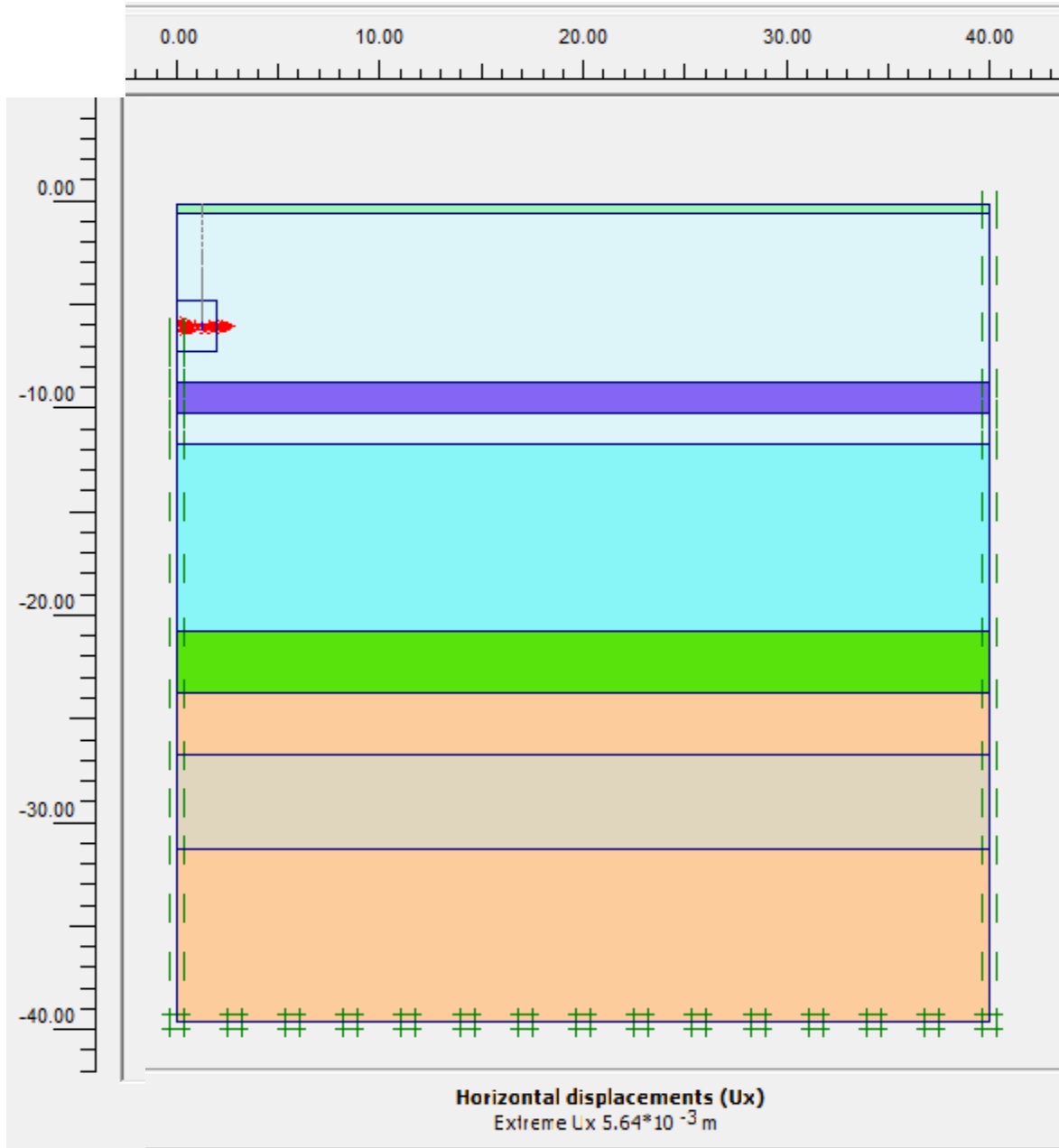


Figure 4.20 Typical horizontal displacement arrow diagram @ 6.0m depth at MD Station

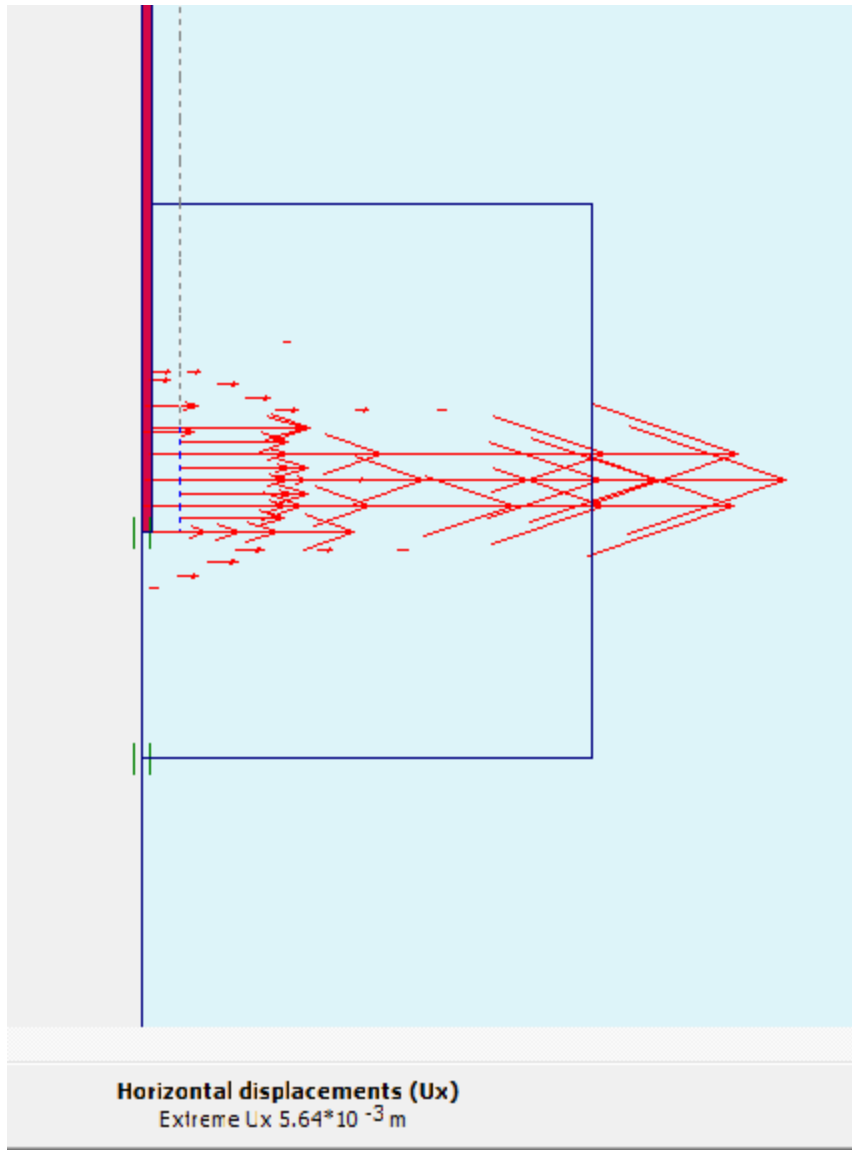


Figure 4.21 Zoomed view of the horizontal displacement arrow diagram @ 6.0m depth at MD Station

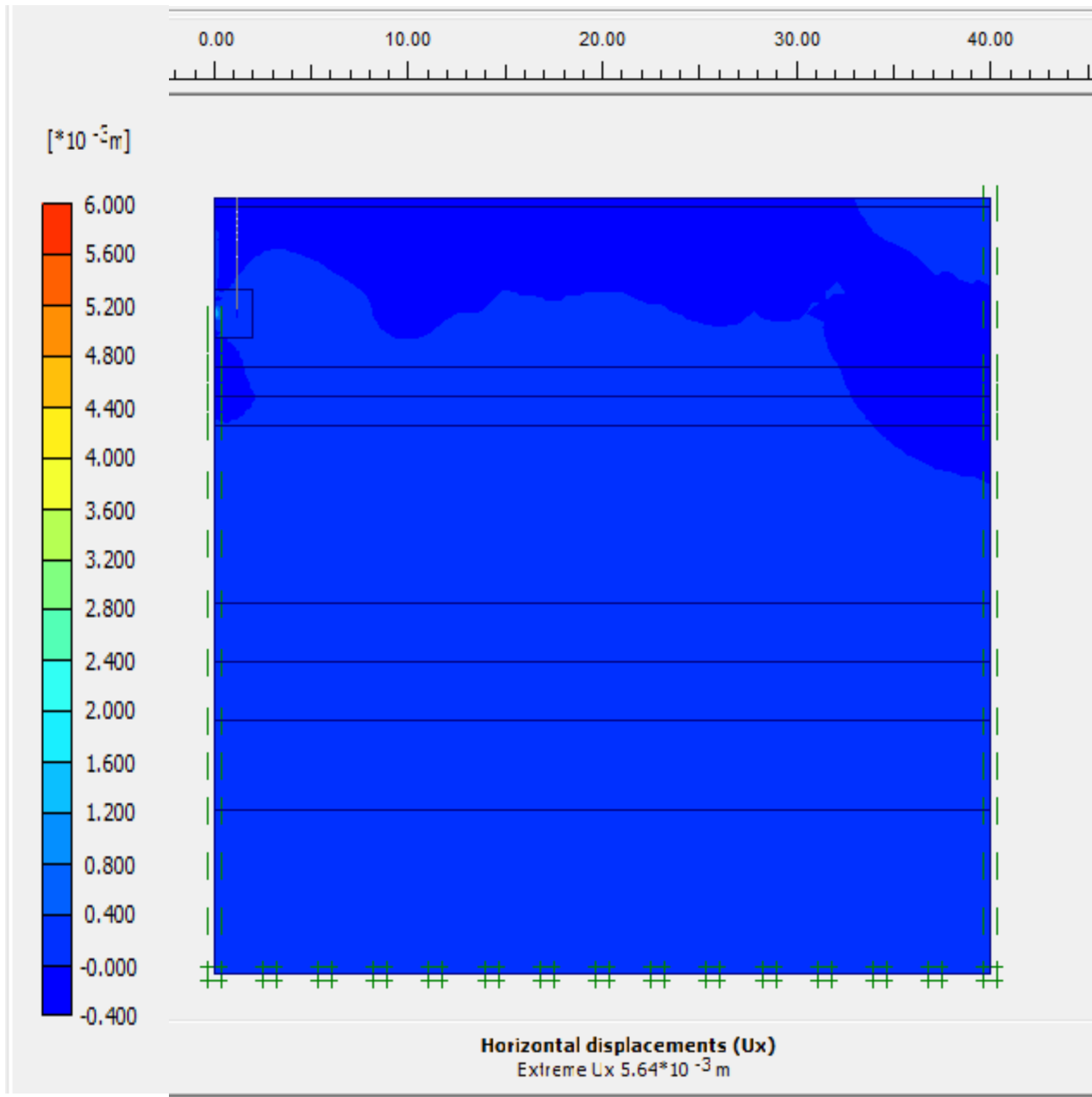


Figure 4.22 Typical horizontal displacement shaded diagram @ 6.0m depth at MD Station

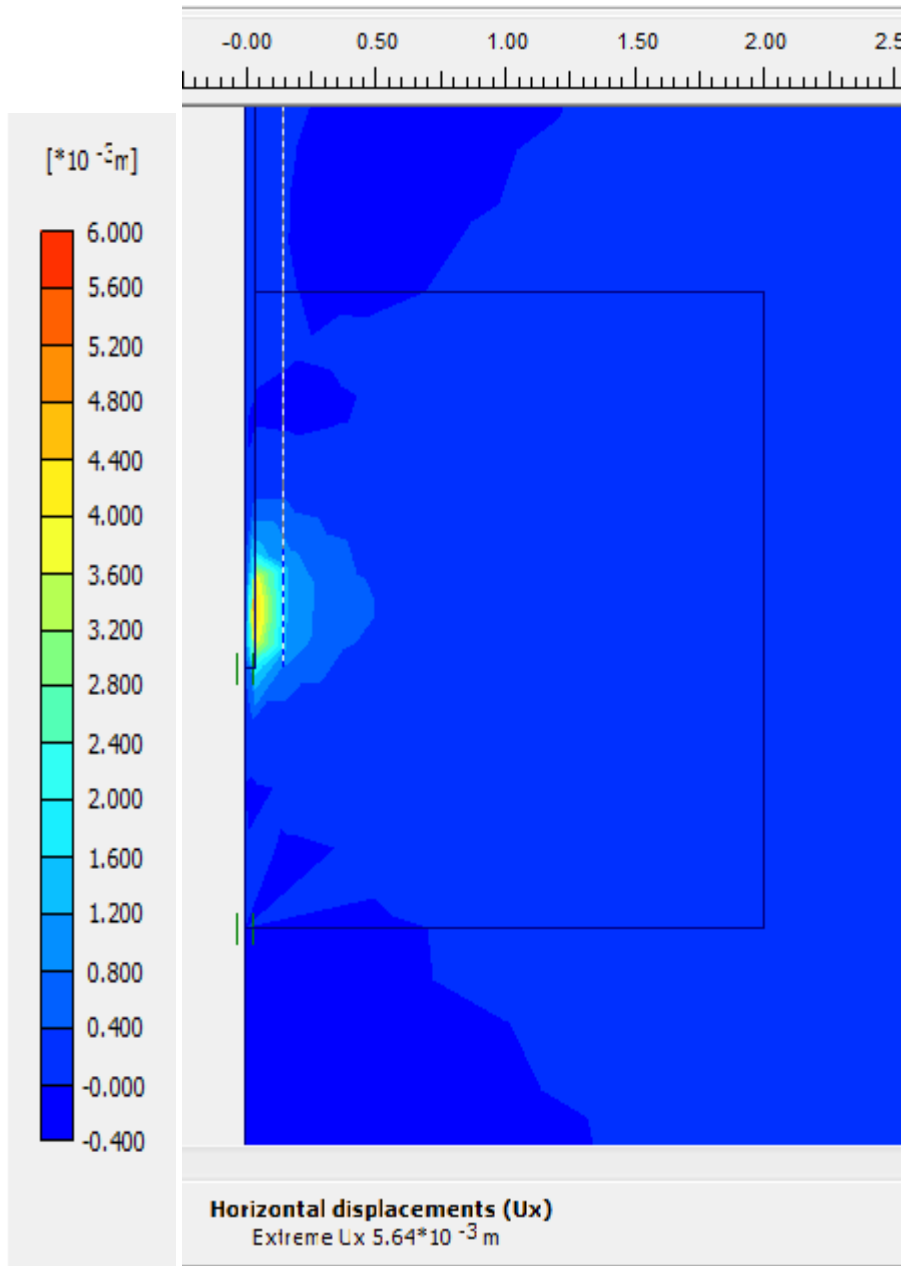


Figure 4.23 Zoomed view of horizontal displacement shaded diagram @ 6.0 m depth at MD Station

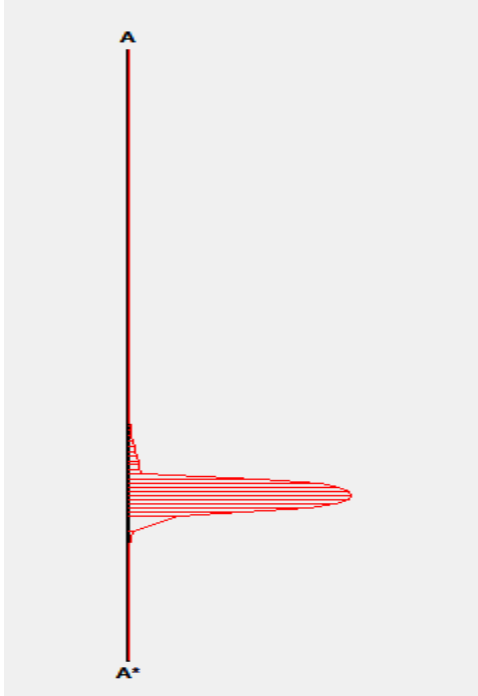


Figure 4.24 Typical horizontal displacement cross section @ 6.0 m depth at MD Station

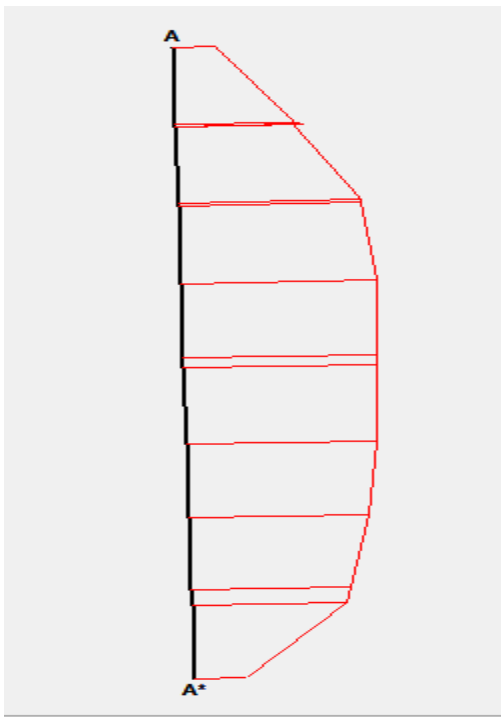


Figure 4.25 Zoomed view of horizontal displacement cross section (along the probe) @ 6.0 m depth at MD Station

4.6.3 COMPARISON OF PRESSURE VS RADIAL STRAIN CURVES FROM PMT AND PLAXIS

It is instructive to compare the results of PMT with those obtained from our numerical results. Figure 4.26 shows the typical pressure vs radial strain graphs for field PMT measurement and simulated PMT curves at 6.0 m depth with different values of Young's modulus. It can be seen that the measured PMT curves and the numerical curves obtained using the proposed numerical model are more or less similar for each depth that was investigated. During the simulation, it is seen that the curves obtained from simulations are not best fit with the field curves. There should be a many reasons for that, those are listed below:

- (i) The diameter of the probe has an impact on the quality of the test. That is a diameter of drilling bit should be equal to the diameter of the probe.
- (ii) Rotation should be slow to minimize enlargement of borehole.
- (iii) Mud circulation should be slow to minimize erosion.
- (iv) Borehole walls left behind the bit may be disturbed.
- (v) The Poisson's ratio was taken as 0.33 for whole soil profile but not at all. For saturated soils Poisson's ratio vary from 0.33 to 0.45. The Menard PM modulus means Poisson's ratio is 0.33. In this project whole calculations were performed for Poisson's ratio 0.33.
- (vi) The soil mass was assumed to be continuum, uniform and isotropic.
- (vii) Special training is required for drillers to prepare a good PMT borehole as drilling for PMT.

In addition to the reasons above the field curve initially starts horizontally then increased, but numerical simulation curves increased vertically. The reason is that in the field PMT the volume is increased then the pressure was measured, but in the simulation the pressure is applied then the deformation is measured. Due to that, in the initial the field PMT curve is going horizontally until it touches the borehole wall and after it has touched the borehole wall, it will increase. But in the simulation, the pressure vs radial curve is going vertically until it touches the borehole wall and after it has touched the wall, it will increase as well.

For each simulation, back-calculation is done for the values of E_{PMT} by using Equation 2.8 in the section 2.2.2.3, in Chapter 2, for each Young modulus and tabulated in Table 4.6. In this calculation a special attention is paid to that the two slopes of the experimental and numerical curves in the elastic phase should be similar. The portion of the curves that are used for the calculation is shown by an arrow in Figure 4.26. Then the calculated PMT modulus (E_{PMT}) vs Young modulus (E) graphs that are plotted for various depths are shown in Figure 4.27 for cohesionless glacial tills and Figure 4.28 for cohesive glacial tills respectively. The correlation equations between the modulus above with their coefficients are also tabulated in Table 4.6. The Menard “ α ” factors are calculated at each depth for different types of glacial tills at MD Station are also shown in Table 4.6. This study shows a very good agreement with Menard “ α ” factors.

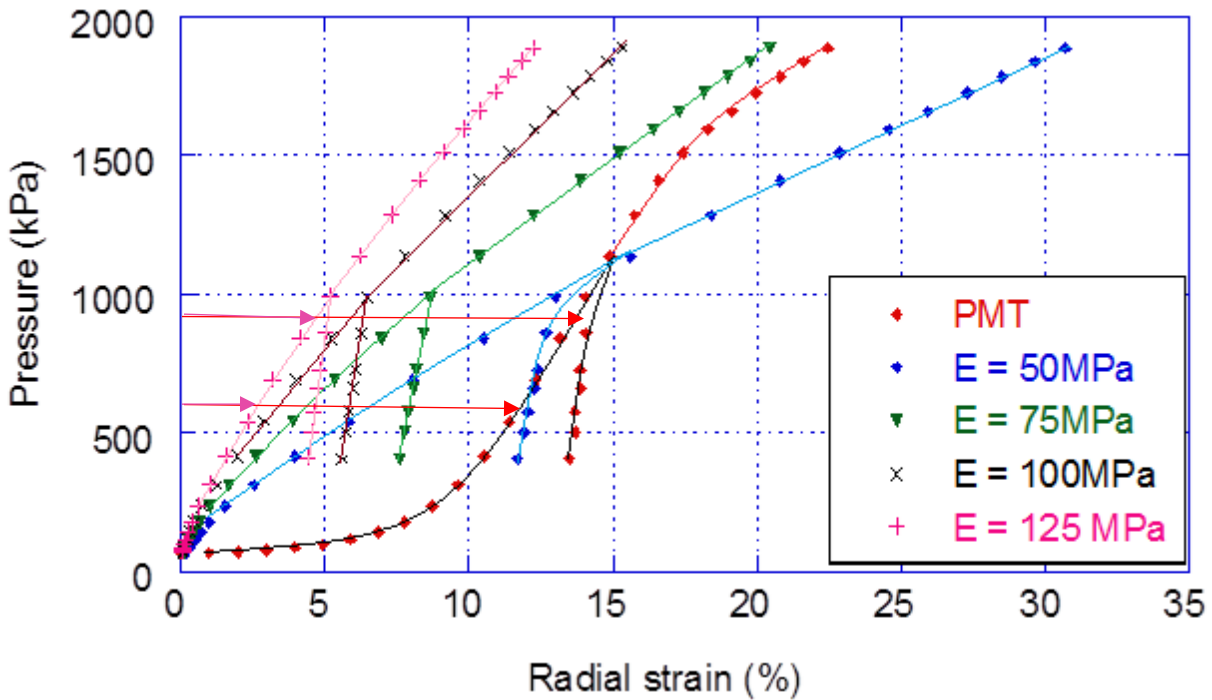


Figure 4.26 Pressure vs radial strain graphs at 6m depth for MD Station

Table 4.6 Linear correlation equations for glacial tills at MD Station

Depth (m)	Soil type	Young's modulus (E) (MPa)	PMT modulus (E_{PMT}) (Mpa)	Correlation equation	Correlation coefficient (R^2)	$\alpha = \frac{E_{PMT}}{E}$
3.8	Sand	25	7.95	$E_{PMT} = 0.34E$	1.0	0.32
		50	18.77			0.38
		75	25.91			0.35
		100	34.68			0.35
		125	43.26			0.35
		150	50.24			0.34
6	Sand	25	4	$E_{PMT} = 0.15E$	1.0	0.16
		50	8			0.16
		75	12			0.16
		100	15			0.15
		125	19			0.15
		150	22			0.15
9.4	Sandy silt	25	7.4	$E_{PMT} = 0.28E$	1.0	0.30
		50	14.4			0.29
		75	21.4			0.29
		100	28.4			0.28
		125	35.2			0.28
		150	42.2			0.28
13.9	Sandy silt	25	9.44	$E_{PMT} = 0.35E$	1.0	0.38
		50	19.32			0.39
		75	29.43			0.39
		100	36.18			0.36
		125	43.16			0.35
		150	50.85			0.34
15.2	Sandy silt	25	8.22	$E_{PMT} = 0.31E$	1.0	0.33
		50	15.84			0.32

		75	23.70			0.32
		100	31.44			0.31
		125	39.01			0.31
		150	46.74			0.31
18.3	Sandy silt	25	9.03	$E_{PMT} = 0.35E$	1.0	0.36
		50	17.78			0.36
		75	26.77			0.36
		100	35.47			0.36
		125	43.90			0.35
		150	52.61			0.35
21.3	Sand	25	10	$E_{PMT} = 0.39E$	1.0	0.40
		50	20			0.40
		75	29			0.39
		100	39			0.39
		125	49			0.39
		150	58			0.39
24.5	Silty clay	20	9.06	$E_{PMT} = 0.43E$	1.0	0.45
		40	17.80			0.45
		60	26.36			0.44
		80	34.51			0.43
		100	43.04			0.43
27.3	Clayey silt till	20	7.12	$E_{PMT} = 0.34E$	1.0	0.36
		40	13.76			0.34
		60	20.23			0.34
		80	27.12			0.34
		100	33.32			0.33
30.4	Clayey silt till	20	5.13	$E_{PMT} = 0.23E$	1.0	0.26
		40	9.64			0.24
		60	14.16			0.24
		80	18.80			0.24

		100	23.10			0.23
35	Silty clay	20	8.93	$E_{PMT} = 0.43E$	1.0	0.45
		40	17.30			0.43
		60	25.76			0.43
		80	34.21			0.43
		100	42.70			0.43

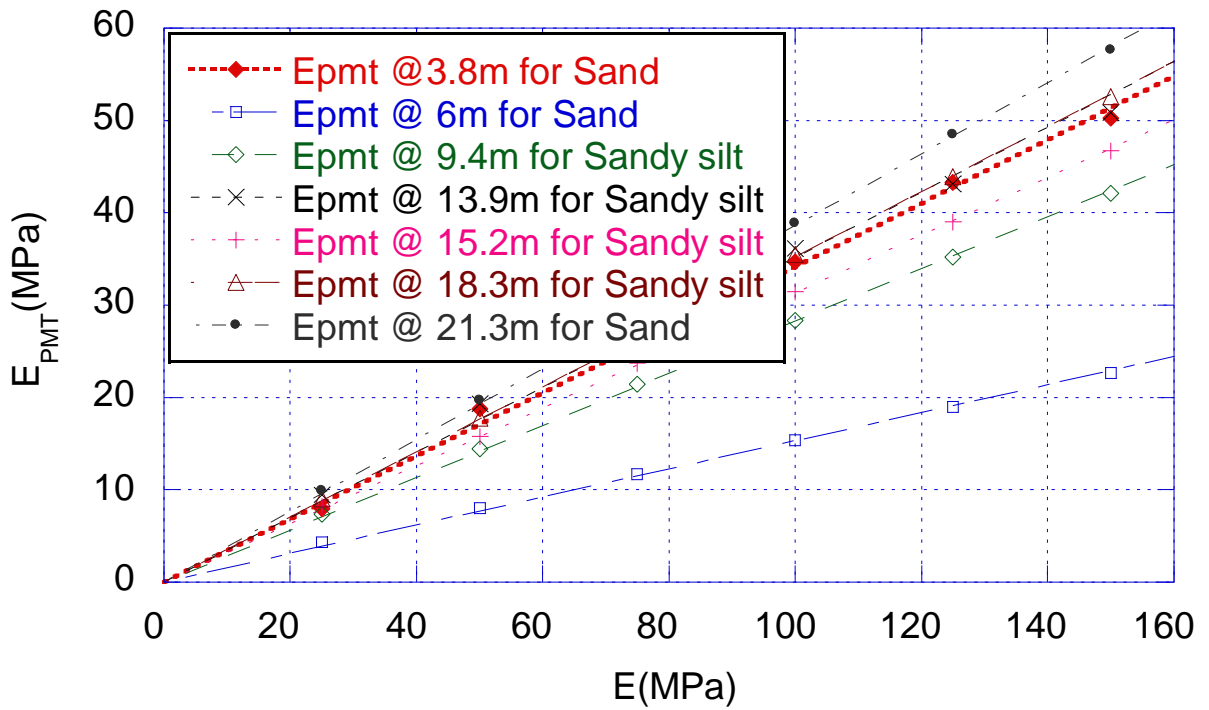


Fig 4.27 Linear relationships for E_{PMT} vs E for cohesionless glacial tills at MD Station

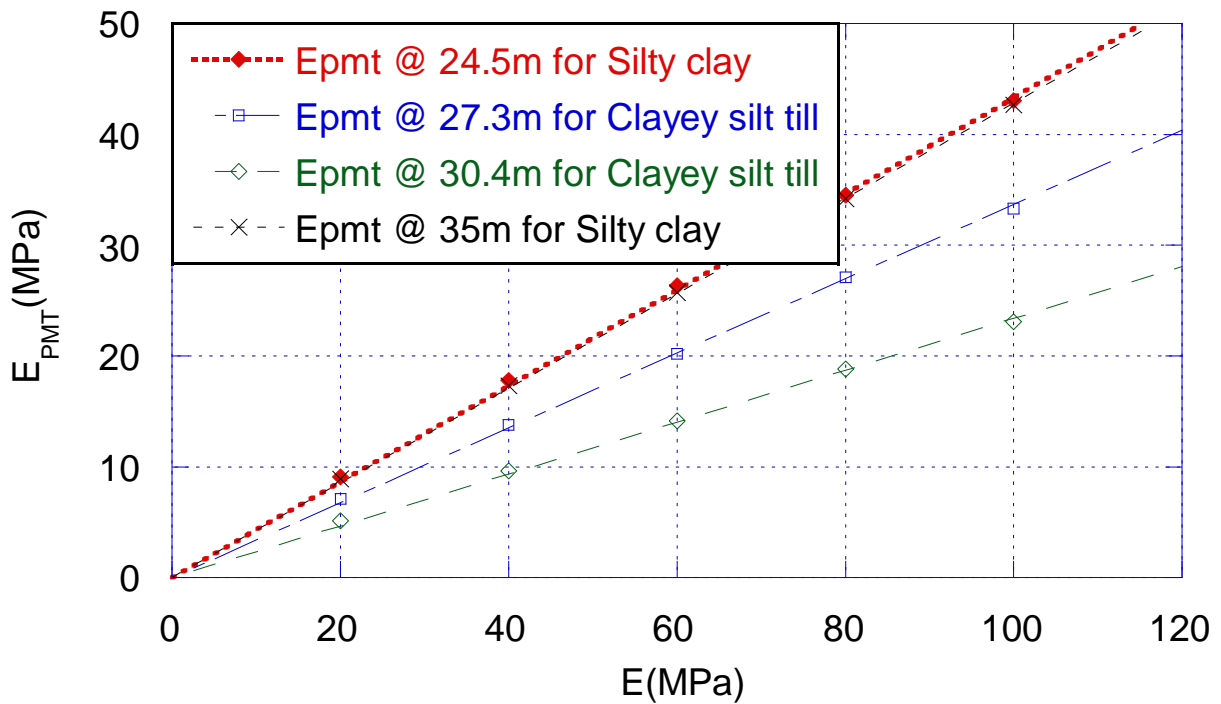


Fig 4.28 Linear relationships for E_{PMT} vs E for cohesive glacial tills at MD Station

In order to compare with Sedran et al. (2013), the linear relationship with intercept correlation equations are developed between PMT and Young modulus. The Sedran et al. (2013) suggested that, if a relation between E and E_{PMT} exists, it would be similar to $E = a + b E_{PMT}$. In this study, the same format of the equation is achieved, and is tabulated in Table 4.7.

Table 4.7 Linear with intercept correlation equations for glacial tills at MD Station

Depth(m)	Soil type	Correlation equation	R^2
3.8	Sand	$E = 2.97 E_{PMT} - 1.99$	1.0
6.0	Sand	$E = 6.85 E_{PMT} - 4.96$	1.0
9.4	Sandy silt	$E = 3.60 E_{PMT} - 1.83$	1.0
13.9	Sandy silt	$E = 3.07 E_{PMT} - 8.79$	1.0
15.2	Sandy silt	$E = 3.24 E_{PMT} - 1.63$	1.0
18.3	Sandy silt	$E = 2.87 E_{PMT} - 1.24$	1.0
21.3	Sand	$E = 2.62 E_{PMT} - 1.29$	1.0
24.5	Silty clay	$E = 2.36 E_{PMT} - 1.75$	1.0

27.3	Clayey silt till	$E = 3.04 E_{PMT} - 1.77$	1.0
30.4	Clayey silt till	$E = 4.44 E_{PMT} - 2.82$	1.0
35	Silty clay	$E = 2.37 E_{PMT} - 1.07$	1.0

4.6.4 VALIDATE THE RESULTS

To validate the results the developed correlation equations are used to predict the Young's modulus for the field PMT modulus (E_{PMT}) which is conducted in the MD Station in the ECLRT project. Then these predicted Young's modulus are used as input parameters in the simulation model in the Plaxis 2D. These simulations are carried out at each depth according to MD Station borehole #101 soil profiles. Then PMT modules (E_{PMT}) are calculated by using the Equation 2.8 in the Chapter 2(Section 2.2.2.3) from the linear portion of the pressure vs radial strain curves. The calculated PMT modules (E_{PMT}) are same as the field values. In addition, the E values are calculated analytically by using Pasturel's formula which is shown in the Chapter 2 (Section 2.3.8). Analytical E values seem to be similar to the predicted values for cohesionless glacial soil but not the same for cohesive glacial soil. Analytical and predicted E values are both tabulated in Table 4.8. The predicted E values for sand vary from 75 to 172 MPa. According to Bowles (1996), E value for dense sand is 50 to 81 MPa. But E values vary for loose glacial tills from 10 to 150 MPa and dense glacial tills from 150 to 720 MPa. From this study the predicted E values vary from 53 to 234 MPa. The studied values are within the Bowles' (1996) range.

Table 4.8 Summary of predicted and analytical E and calculated E_{PMT} at MD Station

Depth (m)	Soil type	Field PMT E_{PMT} (MPa)	Predicted E (MPa)	Calculated E_{PMT} from the FEM Simulation (MPa)	Analytical E from Pasturel's formula (MPa)	$\alpha = \frac{E_{PMT}}{E}$
3.8	Sand	0.2	0.60	0.24	1.05	0.34
6.0	Sand	25.8	172	25.90	200	0.15
9.4	Sandy silt	40.8	146	41.06	144	0.28
13.9	Sandy silt	38.6	110	39.03	104	0.35

15.2	Sandy silt	27.8	90	28.30	52	0.31
18.3	Sandy silt	28.9	83	29.50	23	0.35
21.3	Sand	29.1	75	29.20	28	0.39
24.5	Silty clay	36.2	84	36.20	8	0.43
27.3	Clayey silt till	46.2	136	45.30	3	0.34
30.4	Clayey silt till	53.9	234	53.30	3	0.23
35.0	Silty clay	22.7	53	22.50	5	0.43

4.7 SUMMARY

In this chapter, the PMT modulus (E_{PMT}) is back calculated for glacial tills at MD Station in the ECLRT project in Toronto. The PMT is investigated using FEM analysis. The FEM analysis is performed with Mohr-Coulomb models which is linear elastic perfectly plastic constitutive model. This model requires five parameters (E , c , ϕ , ψ and ν). These parameters are used from ECLRT geoengineering factual data reports to simulate the model for each types of soil in the MD Station. The site contains glacial tills which consist of cohesionless glacial till such as sand and sandy silt from 3.8m to 21.3m and cohesive glacial tills such as silty clay and clayey silt till from 21.3m to 35m.

First the model is created by using Plaxis 2D then validated by using one of the literature model Levasseur et al. (2009). The simulation is done to get the pressure (p) vs volumetric strain ($\frac{\Delta v}{V}$) curve which show that curve is well best fit to the literature curve. Further to evaluate the mesh dependency, the same model is used. The fine mesh coarseness gave exactly the same curve which is compared with the literature model Levasseur et al. (2009).

Then the PMTs are analyzed numerically using Plaxis 2D. After the simulations are executed, pressure (p) vs radial strain curves are obtained to calculate the PMT modulus (E_{PMT}) for different values of Young's modulus in each depth according to MD borehole 101-PMT soil profile. The correlation equations are developed between PMT (E_{PMT}) and Young's (E) modulus

in each depth for different types of glacial tills. Then the Young's modulus (E) is predicted by using the correlation equation for the field PMT modulus (E_{PMT}). The predicted E values for the glacial till vary from 53 to 243 MPa. These values are very good agreements with Bowles' (1992) ranges. The Bowles (1992) suggested E values for glacial tills that vary from 10 to 720 MPa.

Then the Menard “ α ” factors are suggested for different types of glacial tills at MD Station. According to Menard, the “ α ” factors are between 0 and 1. In this study, these factors are retrieved by the results of the numerical simulations of the PMT. There is a good agreement with the Menard “ α ” factors. The summary of the E_{PMT} , E and Menard “ α ” factors for glacial tills at MD Station are shown in Table 4.9.

Further the linear relationship with intercept correlation equations are developed between PMT and Young modulus. There is a very good agreement with Sedran et al. (2013) due to the similar equation format of $E = a + b E_{PMT}$.

Table 4.9 Summary of the E_{PMT} , E and Menard “ α ” factors for MD Station

Depth(m)	Soil types	PMT modulus (E_{PMT}) (MPa)	Young's modulus (E) (MPa)	$\alpha = \frac{E_{PMT}}{E}$
3.8	Sand	0.20	0.60	0.34
6.0	Sand	25.8	172	0.15
9.4	Sandy silt	40.8	146	0.28
13.9	Sandy silt	38.6	110	0.35
15.2	Sandy silt	27.8	90	0.31
18.3	Sandy silt	28.9	83	0.35
21.3	Sand	29.1	75	0.39
24.5	Silty clay	36.2	84	0.43
27.3	Clayey silt till	46.2	136	0.34
30.4	Clayey silt till	53.9	234	0.23
35.0	Silty clay	22.7	53	0.43

CHAPTER 5: CONCLUSIONS AND RECOMMENDATIONS FOR FUTURE RESEARCH

5.1 MAIN CONCLUSIONS

This study is performed based on a comprehensive geotechnical investigation program for a light rail transit (LRT) project in the City of Toronto. The following main conclusions are made from this investigation.

- (1) The field SPT-N values are corrected and the ratio of corrected SPT-N to field measured SPT-N which is $(\frac{N_1}{N_F})_{60}$ is recommended for glacial tills.
- (2) The ranges of SPT-N, E_{PMT} and P_L with all data and corrected and filtered data format for glacial tills are suggested.
- (3) The statistical correlation equations between SPT-N values with PMT parameters such as PM modulus (E_{PMT}) and pressure limit (P_L) with whole data as well as the corrected and filtered data format for glacial tills are developed.
- (4) The E_{PMT}/P_L ratios for sand and glacial till are also recommended.
- (5) The correlation equations between PM modulus with Young's modulus for glacial tills are also suggested.
- (6) The Menard "α" factors for glacial tills are also recommended.

5.2 RECOMMENDATIONS FOR FUTURE RESEARCH

The following recommendations are made for future research:

- (1) There are many possible applications to correct the field measured SPT-N. Since there is not any general agreement on these application of correction of field measured SPT-N. In contrast to heavy criticisms about the SPT-N correction, there is strong need and necessity to carry out a suitable research on correction methods which are more suitable for local conditions.
- (2) This study also proves once more, the correlation between in-situ test parameters still involves a large amount of uncertainties as presented by many researchers and they should not be preferred unless there is not any other data available. Therefore it is recommended to carry out another study in the glacial tills in these areas in the future in order to provide a good relationship.
- (3) The correlation between SPT-N and PMT has been investigated by many researchers in the past. They mentioned that the scatter in the data is considerably large which makes the correlation essentially useless in design. Due to that more theoretical study is needed to develop a sound rationale to filter the data to minimize the scatters.
- (4) The future study was recommended to predict the undrained shear strength from net limit pressure of PMT and suggest the β factor for glacial tills. Then develop the correlation equations between undrained shear strength and SPT-N for glacial tills.
- (5) In the case of FEM simulation of PMT, the FEM provides efficient results. Even though the program needs many input parameters and may be complicated to use. Due to that the research is recommended, in order to develop a best curve fitting methodology to derive the soil strength parameters quickly and more accurately.

(6) Model the PMT in glacial tills by using other constitutive models such as hardening soil model for sand and soft soil creep model for silty clay. But it is more time consuming to compare the results from different constitutive models.

REFERENCES

- ASTM D 4719–00 (2000). *Standard tests method for pre-bored pressuremeter testing in soils*. Annual book of ASTM standards, vol 04.08.
- ASTM D 1586–11 (2014). *Standard test method for standard penetration test (SPT) and split – barrel sampling of soils*. Annual book of ASTM standards.
- Baguelin, F., Jezequel, J. F. and Shields, D.H. (1978). *The Pressuremeter and foundation engineering*, Trans Tech. Publications, Clausthal, Germany. 617p.
- Baker, C.L., Lahti, L.R., and Roumbanis, D.C. (1998). Urban Geology of Toronto and surrounding area. Urban Geology of Canadian Cities. Edited by: P.F. Karrow, 42, 323-352.
- Bolton, M.D. and Whittle, R. W. (1999). A nonlinear elastic/perfectly plastic analysis for plane strain undrained expansion tests. *Geotechnique*, 49(1), 133-141.
- Boone, S. J., Shirlaw, J.N. et al. (1996). Boulder assessment report for TTC Sheppard Subway, *Golder associates report no: S-GIR3-R. Toronto*.
- Boone, S. J. and Westland, J. (2008). Geotechnical summary report for tunnel boring machine procurement for the Toronto–York Spadina Subway extension (TYSSE), *Golder associates report no: 08-111-0039-R01*.
- Bowles, J.E. (1997). *Foundation analysis and design*. The McGraw–Hill Co., Inc., Singapore, 5th edition.
- Bozbey, I. and Togrol, E. (2010). Correlation of standard penetration test and pressuremeter data. A case study from Istanbul, Turkey. *Bull eng geol environ*.
- Braja, M. Das. (1990). *Principles of Foundation Engineering, 5th ed.*, Cole engineering division.
- Briaud, J.L. (1992). *The pressuremeter*, A. A. Balkema, Rotterdam, Netherlands.
- Brinkgreve, R.B.J. and Vermeer, P.A. (1998). Plaxis. Finite element code for soil and rock analysis, Balkema, Rotterdam, The Netherlands.
- Burd, H. (1999). *The history of PLAXIS*. Beyond 2000 in computational geotechnics: 10 years of PLAXIS international; Proceedings of the international symposium beyond 2000 in computational geotechnics, Amsterdam, The Netherlands, 18-20 March 1999, Taylor & Francis group.
- Cambou, B. and Bahar, R. (1993). Utilisation de l'essai pressiometrique pour l'identification de parametres intrinseques du comportement dusol. *Revue Francaise de Geotechnique*, 63, 39-50.

- Campanella, R.G., Berzins, W.E. and Shields, D.H. (1979). A preliminary evaluation of Menard pressuremeter, cone penetrometer and standard penetration test in the lower main land, British Columbia. *Soil mechanics series* no: 40.
- Canadian Geotechnical Society, (2006). *Canadian Foundation Engineering Manual*. 4th ed., The Canadian Geotechnical Society Co & Bi Tech, publishers Ltd. Canada.
- Cao, L., Peaker, S. and Ahmad, S. (2015). Pressuremeter tests in glacial tills in Toronto, *Symposium International ISP7/Pressio*.
- Clarke, B.G. (1995). *Pressuremeter in Geotechnical Design*. 1st ed., Chapman & Hall, Glasgow.
- Eglinton Cross Town (LRT), *Geoengineering factual data report*.
- Fawaz, A., Hagechegade, F. and Farah, E. (2014). A study of the pressuremeter modulus and its comparison to the elastic modulus of soil. *Study of civil engineering and architecture (SCEA)*.
- Finn, P.S., Nisbet, R.M. and Hawkins, P.G. (1984). Guidance on pressuremeter, flat dilatometer and cone penetration tests in sand, *Geotechnique*, vol.34, no:1, pp.81-97.
- Gibson, R.E. and Anderson, W.F. (1961). In – situ measurement of soil properties with the pressuremeter. *Civil Eng.*
- Houari, O. and Abdeldjalil, Z. (2015). Numerical modeling of the test on slope pressuremeter. *International journal of emerging technology and advanced engineering*. vol 5, issue5.
- Jacques, M. (2007). Numerical validation of an elastoplastic formulation of the conventional limit pressure measured with the pressuremeter test in cohesive soil. *Journal of Geotechnical and Geoenvironmental Engineering*. ASCE. September.
- Karrow, P.F. (1967). Pleistocene geology of the Scarborough area. *Ontario department of mines, Geological reports* 46.
- Karrow, P.F. and White, O.L. (1998). Urban geology of Canadian cities, *Geological association of Canada, GAC special paper* 42.
- Kovacs, W.D. and Salomone, L.A. (1982). SPT hammer energy measurements. *American Society of Civil Engineers, ASCE, Journal of the Geotechnical Engineering Division*, vol.108, GT4, pp.599-620.
- Kovacs, W.D., Yokel, F.Y., Salomone, L.A and Holtz, R.D. (1984). Liquefaction potential and the international SPT; Proceeding of the 8th world conference on earthquake engineering, San Francisco, CA.
- Kulhawy and Mayne (1990). Manual on estimating soil properties for foundation design, *Electric power research institute, Palo Alto, CA*

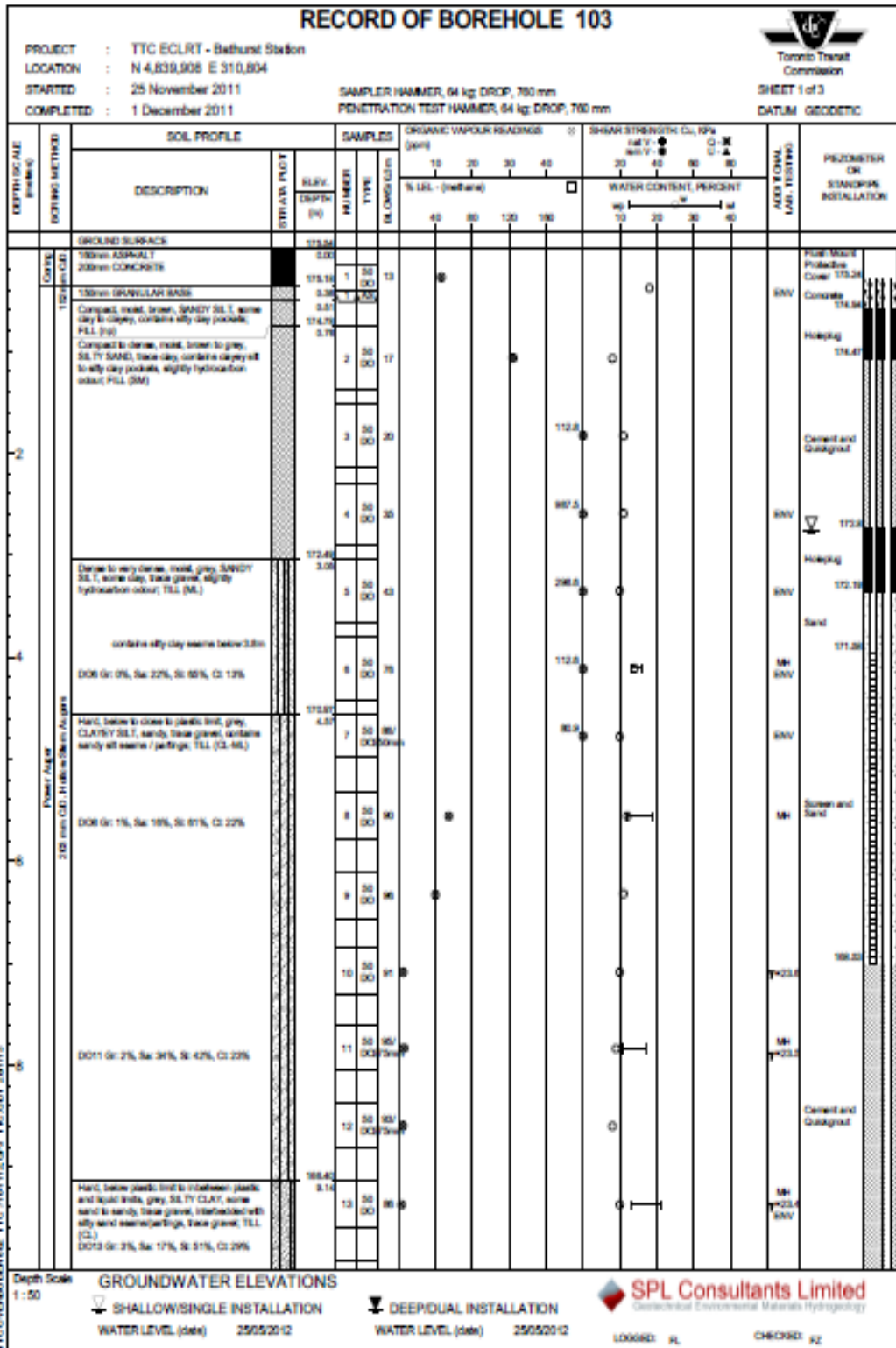
- Levasseur, S., Malecot, Y., Boulon, M. and Flavigny, E. (2009). Statistical inverse analysis based on genetic algorithm and principal component analysis. Application to excavation problems and pressuremeter tests. *International journal for numerical and analytical methods in geomechanics*. 34: 471-491.
- Levasseur, S., Malecot, Y., Boulon, M. and Flavigny, E. (2008). Statistical inverse analysis based on genetic algorithm and principal component analysis. Methods and developments using synthetic data. *International journal for numerical and analytical methods in geomechanics*. 33: 1485-1511.
- Manzari, M., Drevininkas, A., Olshansky, D. and Galaa, A. (2014). Behavioral modelling of Toronto glacial soils and implementation in numerical modeling. *67th Canadian Geotechnical Conference, Geo Regina*.
- Menard, L. (1965). Règle pour le Calcul de la Force Portante et du Tassement des Foundation en Fonction des Resultats Pressiometriques, *Proceedings 6th ICSMFE*, Montreal, vol., pp. 295- 299.
- Michel, G., Armando, A. and Antonio, G.C. (2008) Using a nonlinear constitutive law to compare Menard PMT and PLT E-moduli.
- Monnet, J. (2007). Numerical validation of an elastoplastic formulation of the conventional limit pressure measured with the pressuremeter test in cohesive soil. *Journal of geotechnical and geoenvironmental engineering*. September.
- Monnet, J. (2012). Elasto-plastic analysis of the pressuremeter test in granular soil part 2. Numerical study. *European journal of environmental and civil engineering*. vol 16, no.6 715 – 729.
- Nahra, R. and Frank, R. (1986). Contributions numeriques et analytiques a l' etude de la consolidation autour du pressiometre. Research Rep. LPC No: 137, Laboratoire Central des Ponts et Chaussees, Paris.
- Ng, R., Xue, T., Wheeler, C. and Campo, D. (2011). The Eglinton cross town light rail transit. 14th *Pan-Am conference on Soil Mechanics and Geotechnical Engineering*. 64th *Canadian Geotechnical conference*.
- Ohya, H., Kazama, E. and Negishi, Y. (1982). Reverse osmotic concentration of aqueous ethyl-alcohol solutions. Analysis of data obtained with composite membranes (PEC), *Kagaku Kogaku Ronbunshu*, 8 (2): 144-149.
- Owen, D.R.J. and Hinton, E. (1980). *Finite elements in plasticity. Theory and practice*. Pinerridge press limited, Swansea, U.K.
- Phoon, K.K. and Kulhawy, F.H. (1999). Evaluation of geotechnical variability. *Canadian geotech J* 36:625-639.
- Plaxis 2D. (2012). Material Model Manual.

- Plaxis 2D. (2012). Reference Manual.
- Plaxis 2D. (2012). Tutorial Manual.
- Potts, D. M. and Zdravkovic, L. (2001). *Finite Element Analysis in Geotechnical Engineering*. Thomas Telford, London.
- Prapaharan, S., Chameau, J. L. and Holtz, R.D.(1989). Effect of strain rate on undrained strength derived from pressuremeter tests. *Geotechnique*, 39(4), 615-624.
- Raquel, R. (2008). Characterization of Material Behavior by the pressuremeter test.
- Robertson, P. K., Campanella, R. C. and Wightman, A.(1983). SPT-CPT correlations, *American society of civil engineers, ASCE, Journal of the geotechnical engineering division*, vol.109, GT11, pp. 1449-1459.
- Schanz, T., Vermeer, P.A. and Bonnier, P.G. (2000). The hardening soil model. Formulation and verification. *Beyond 2000 in computational geotechnics. 10 years of Plaxis @ Balkema*, Rotterdam, ISBN 90 5809 040 X.
- Schmertmann, J.H. and Palacios, A. (1979), Energy dynamics of SPT, *American society of civil engineers, ASCE, Journal of the geotechnical engineering division*, vol. 105, GT8, pp. 909-926.
- Sedran, G., Failmezger, R.A. and Drevininkas, A. (2013). Relationship between Menard E_M and Young's E moduli for cohesionless soils. *Proceeding of the 18th International conference on soil mechanics and geotechnical engineering, Paris 2013*.
- Seed, H.B., Tokimatsu, K., Harder, L.F. and Chung, R.M. (1984). Influence of SPT procedures in soil liquefaction resistance evaluations. Report no: UCB/EERC-84/15, Berkeley. *Reprinted in journal of geotechnical engineering, ASCE*, vol. 111, no.12, pp 1425-1445.
- Sharp, D.R. (1980). Quaternary geology of Toronto and surrounding area. *Ontario geological survey*, Geological series preliminary map, p 2204.
- Sharpe, D.R., Barnett, P. J. et al. (1999). Regional Geological Mapping of Oak Ridges Moraine – Greater Toronto Area – Southern Ontario, in current research 1999– E, *Geological Survey of Canada*, pp 123-136.
- Silvestri, V. (2003). Assessment of self – boring pressuremeter tests in sensitive clay. *Can. Geotech. J.*, 40, 362-387.
- Silvestri, V. (2004). Disturbance effects in pressuremeter tests in clay. *Can. Geotech. J.*, 41, 738-759.
- Sivrikaya, O., Togrol, E., (2007), Turkiye de SPT N Degeri ile Dnce Daneli Zeminlerin Drenajsiz Kayma Mukavemeti A rasindaki Ddiskiler, *Technical magazine of chamber of civil engineers*, pp 4229 – 4246, paper no: 279.

- Skempton, A.W. (1986). Standard penetration test, procedures and effects in sands of overburden, relative density, particle size, aging and over- consolidation. *Geotechnique*, vol.36, no. 3, pp. 425-447.
- Terzaghi, K. and Peck, R.B. (1967). *Soil mechanics in engineering practice*, second edition, John Wiley and Sons, New York, 729p.
- Thorburn, S. (1986). Field testing: standard penetration test, engineering geology special publication, no: 2, *Geological society*.
- Timoshenko, S and Goodier, J.N. (1951). *Theory of elasticity*. McGraw Hill, New York.
- Toronto transit commission *geotechnical standards*. (2014). version 8
- Yagiz, S., Akyol, E. and Sen, G. (2008). Relationship between the standard penetration test and the pressuremeter test on sandy silty clays. A case study from Denizli. *Bulletin of engineering geology and the environment*, 67(3), 405-410.

APPENDICES

APPENDIX 3.1



RECORD OF BOREHOLE 103



PROJECT : TTC ECLRT - Bathurst Station
 LOCATION : N 4,839,908 E 310,804
 STARTED : 25 November 2011
 COMPLETED : 1 December 2011

SAMPLER HAMMER, 64 kg DROP, 760 mm
 PENETRATION TEST HAMMER, 64 kg DROP, 760 mm

SHEET 2 of 3
 DATUM GEODETIC

DEPTH (SCALE) meters (ft)	BORING METHOD	SOIL PROFILE		SAMPLES		ORGANIC VAPOUR READINGS (ppm)				SHEAR STRENGTH (kPa)				ADDITIONAL LAB. TESTING	PIEZOMETER OR STANDPIPE INSTALLATION	
		DESCRIPTION	STRAIN FACT	SURF. DEPTH (m)	NUMBER	TYPE	% SOL. (predom)				WATER CONTENT, PERCENT					
12	Penetration 210 mm O.D. In-line Open Augers	contains sand layers at 9.3m Hard, below plastic limit to in-between plastic and liquid limits, grey, SILTY CLAY, some sand to sandy, some gravel, interbedded with silty sand marlstone partings, trace gravel, T.S.L. (C.) (Continued)		14	30	OC										
				14	30	OC										
				15	30	OC										
				16	30	OC										
				17	30	OC										
				18	30	OC										
				19	30	OC										
				20	30	OC										
				21	30	OC										
				22	30	OC										
				23	30	OC										
				24	30	OC										
				25	30	OC										
				26	30	OC										
18		Hard, close to plastic limit to in-between plastic and liquid limits, grey, SILTY CLAY, trace sand, contains sandy silt waste / partings, (C.)		17.25	30	OC										
				18.25	30	OC										
				18.25	30	OC										
		occasional gravel at 18.1m		26	30	OC										
				27	30	OC										

Depth Scale 1:50

GROUNDWATER ELEVATIONS

SHALLOW SINGLE INSTALLATION
 DEEP/DUAL INSTALLATION

WATER LEVEL (date) 25052012
 WATER LEVEL (date) 25052012

Geological Environmental Materials Hydrology

LOGGED: JL CHECKED: JZ

RECORD OF BOREHOLE 103



PROJECT : TTC ECLRT - Bathurst Station
 LOCATION : N 4,839,908 E 310,804
 STARTED : 25 November 2011
 COMPLETED : 1 December 2011

SAMPLER HAMMER, 64 kg; DROP, 760 mm
 PENETRATION TEST HAMMER, 64 kg; DROP, 760 mm

SHEET 3 of 3
 DATUM: GEODETIC

DEPTH SCALE (meters)	SOIL PROFILE DESCRIPTION	STRAIN FACT	SAMPLES		ORGANIC VAPOUR READINGS (Depth)	SHANK STRENGTH (CL, kPa)	WATER CONTENT, PERCENT	LABORATORY TESTS	PENETRATION OR STANDARD INSTALLATION
			NO.	DEPTH (m)					
22	DC27 Gr: 3%, Ss: 15%, Sl: 47%, Cl: 31% Hard, close to plastic limit to 9.60m; plastic and liquid limits, grey, silty CLAY, trace sand, contains sandy silt seams / partings; (Cl) (Continued) contains silt and sand layers at 20.6m	100	27	20.00	30				SHV
			28	20.50	30				SHV
			29	21.00	30				SHV
			30	21.50	30				SHV
			31	22.00	30				SHV
			32	22.50	30				SHV
			33	23.00	30				SHV
			34	23.50	30				SHV
			35	24.00	30				SHV
			36	24.50	30				SHV
24	Compacted to very dense, saturated, grey, SAND, trace to some silt, trace clay, contains silt clay seams (SH) DC28 Gr: 1%, Ss: 50%, Sl: 4%, Cl: 45% silty sand at 24.5m	100	29	24.00	30				MH
			30	24.50	30				MH
			31	25.00	30				MH
			32	25.50	30				MH
			33	26.00	30				MH
			34	26.50	30				MH
			35	27.00	30				MH
			36	27.50	30				MH
			37	28.00	30				MH
			38	28.50	30				MH
26	END OF BOREHOLE Note: 1) 30mm dia. monitoring well was installed, screened from 22.86m to 24.26m; 2) An additional borehole was drilled to install 30mm dia. monitoring well, screened from 3.96m to 7.21m; 3) MH denotes combined steel and hydrocylinder analysis; 4) SHV denotes environmental analysis (M152(11); C.Reg. 152(11) metal & inorganic; or MSME: C.Reg. 528 metal & inorganic). Water level measurements in deep monitoring well (screen 22.86 to 24.26m): Date: Depth (m) Reading (m) Dec. 21, 2011 18.74 136.80 Feb. 09, 2012 18.43 136.11 Feb. 27, 2012 18.89 136.60 May. 26, 2012 18.84 136.70 Water level measurements in shallow monitoring well (screen 3.96 to 7.21m): Date: Depth (m) Reading (m) Dec. 21, 2011 3.73 171.81 Feb. 09, 2012 3.58 172.96 Feb. 27, 2012 2.70 172.84 May. 26, 2012 2.73 172.79	100	39	24.50	30				SHV
			40	25.00	30				SHV
			41	25.50	30				SHV
			42	26.00	30				SHV
			43	26.50	30				SHV
			44	27.00	30				SHV
			45	27.50	30				SHV
			46	28.00	30				SHV
			47	28.50	30				SHV
			48	29.00	30				SHV

TTC COVERED UNDER TTC 7164115.00, TTC 4017 200113

Depth Scale 1:50

GROUNDWATER ELEVATIONS

SHALLOW SINGLE INSTALLATION

WATER LEVEL (date) 25/05/2012

DEEP DUAL INSTALLATION

WATER LEVEL (date) 25/05/2012

SPL Consultants Limited
 Geotechnical Environmental Materials Hydrology

LOGGED: JL CHECKED: JZ

APPENDIX 3.2

SPT-N CORRECTION

Sample calculation for SPT-N correction for Bathurst Station:

First correction is performed according to Cao et al. (2015) for field measured SPT-N for penetration depth.

$$N_F = \frac{305 N}{\Delta s}$$

Where N_F - Corrected SPT-N value

N - Field recorded SPT-N value

Δs - Measured penetration depth in mm

Table A3.1 Summary of N_C calculation

Depth(m)	Soil types	Field measured SPT-N value	Penetration depth (ΔS) in mm	$N_F = \frac{305N}{\Delta s}$
3.7	Sandy silt	43	305	$= \frac{305 \times 43}{305} = 43$
7.1	Silty clay till	91	305	$= \frac{305 \times 91}{305} = 91$
10.5	Silty clay till	98	200	$= \frac{305 \times 98}{200} = 150$
13.6	Clayey silt till	68	305	$= \frac{305 \times 68}{305} = 68$
16.4	Clayey silt till	50	100	$= \frac{305 \times 50}{100} = 153$
19.8	Silty clay	50	125	$= \frac{305 \times 50}{125} = 122$
22.8	Sand	50	125	$= \frac{305 \times 50}{122} = 122$
25.6	Silty sand	68	150	$= \frac{305 \times 68}{150} = 138$

Second correction is performed according to the CFEM (2006).

$$(N_1)_{60} = C_E C_N C_R C_B C_S N_F$$

$$(N_1)_{60} = C_N N_{60}$$

$$N_{60} = C_E N_F$$

$$C_N = \left(\frac{P}{\sigma'}$$

$$C_E = \frac{ER_R}{60}$$

Where C_E - Hammer energy correction factor

ER_R - Rod energy ratio

C_N - Overburden pressure correction factor

P - Atmospheric pressure

σ' - Effective overburden pressure

C_R - Rod length correction factor

C_B - Borehole diameter correction factor

C_S - Sampler correction factor

N_F - Corrected SPT-N value for penetration depth

N_{60} - SPT-N value corrected to 60% of theoretical free fall hammer energy

$(N_1)_{60}$ - SPT-N value correctd for both vertical effective stress and input energy

Calculation procedure for overburden pressure correction factor (C_N):

Water table is located at 2.8 m below the grade level in this borehole. Density of water (γ_w) is 9.81 kN/m³ and Atmospheric pressure (P) 100Kpa. Dry density of sandy silt is 17kN/m³

Table A3.2 Summary of C_N calculations

Depth(m)	γ (kN/m ³)	σ' (kPa)	$C_N = \left(\frac{P}{\sigma'}\right)^{0.5}$
3.7	21	$2.8*17+(3.7-2.8)*(21-9.81) = 57.671$	1.316804
7.1	23.6	$57.671 + (7.1-3.7)(23.6-9.81) = 104.557$	0.977965
10.5	22.8	$104.557 + (10.5-7.1)(22.8-9.81) = 148.723$	0.819994
13.6	22.9	$148.723 + (13.6-10.5)(22.9-9.81) = 189.302$	0.726813
16.4	23	$189.302 + (16.4-13.6)(23-9.81) = 226.234$	0.664846
19.8	23.2	$226.234 + (19.8-16.4)(23.2-9.81) = 271.76$	0.606607
22.8	23.2	$271.76 + (22.8-19.8)(23.2-9.81) = 311.93$	0.566202
25.6	23.2	$311.93 + (25.6-22.8)(23.2-9.81) = 349.422$	0.534964

Table A3.3 Summary of correction factors and $(N_1)_{60}$ calculations

Depth(m)	C_E	C_N	C_R	C_B	C_S	N_F	$(N_1)_{60}$
3.7	1	1.316804	0.7	1	1	43	39.63581
7.1	1	0.977965	0.95	1	1	91	84.5451
10.5	1	0.819994	1	1	1	150	122.5482
13.6	1	0.726813	1	1	1	68	49.42325
16.4	1	0.664846	1	1	1	153	101.3890
19.8	1	0.606607	1	1	1	122	74.00602
22.8	1	0.566202	1	1	1	122	69.07665
25.6	1	0.534964	1	1	1	138	73.96774

Table A3.4 Summary of the corrected SPT-N values and ratios of $\frac{(N_1)_{60}}{N_F}$ for Bathurst Station

Depth (m)	Soil types	Field measured SPT-N	N_F	$(N_1)_{60}$	Ratio $\frac{(N_1)_{60}}{N_F}$
3.7	Sandy silt	43	43	40	0.9
7.1	Silty clay till	91	91	85	0.9

10.5	Silty clay till	98	150	123	0.8
13.6	Clayey silt till	68	68	49	0.7
16.4	Clayey silt till	50	153	101	0.7
19.8	Silty clay	50	122	74	0.6
22.8	Sand	50	122	69	0.6
25.6	Silty sand	68	138	74	0.5

(1) Allen Station

Table A3.5 Summary of the corrected SPT-N values and ratios of $\frac{(N_1)_{60}}{N_F}$ for Allen Station from Borehole AL12-PMT

Depth (m)	Soil types	Field measured SPT-N	N_F	$(N_1)_{60}$	Ratio $\frac{(N_1)_{60}}{N_F}$
4.95	Clayey silt till	33	33	26	0.8
7.62	Clayey silt till	51	51	37	0.7
10.87	Silty clay	58	58	37	0.6
13.92	Silty clay	89/250mm	109	62	0.6
16.97	Silty clay	50/75mm	203	110	0.5
20.02	Sand	83/250mm	101	52	0.5
23.06	Sand	57/150mm	116	57	0.5
26.01	Silty sand	51/150mm	104	48	0.5
30.68	Sand	50/150mm	102	45	0.4

Table A3.6 Summary of the corrected SPT-N values and ratios of $\frac{(N_1)_{60}}{N_F}$ for Allen Station from Borehole AL20-PMT

Depth (m)	Soil types	Field measured	N_F	$(N_1)_{60}$	Ratio $\frac{(N_1)_{60}}{N_F}$
-----------	------------	----------------	-------	--------------	--------------------------------

		SPT-N			
4.72	Clayey silt till	152	152	123	0.8
7.77	Silty clay till	41	41	29	0.7
10.82	Silty clay	49	49	31	0.6
13.36	Clayey silt till	55/150mm	112	67	0.6
14.63	Clayey silt till	72/150mm	146	85	0.6
17.09	Sand	88/10mm	2684	1476	0.6
19.71	Sand	104/225mm	141	74	0.5
22.81	Sand	150/150mm	305	152	0.5
25.98	Sand	50/75mm	203	97	0.5
30.02	Silty clay	84	84	38	0.5

(2) Avenue Station

Table A3.7 Summary of the corrected SPT-N values and ratios of $\frac{(N_1)_{60}}{N_F}$ for Avenue Station from Borehole MD101-PMT (i.e AV101A)

Depth (m)	Soil types	Field measured SPT-N	N_F	$(N_1)_{60}$	Ratio $\frac{(N_1)_{60}}{N_F}$
5.33	Silty clay till	37	37	31	0.8
8.31	Silty clay till	38	38	28	0.7
13.11	Silt	56	56	34	0.6
14.76	Silty clay	38	38	22	0.6
17.6	Sandy silt	50/100mm	153	80	0.5
20.6	Sand/Silty sand	50/100mm	153	73	0.5
23.93	Sand	50/130mm	117	54	0.5
26.9	Sand	50/280mm	55	24	0.4
30.02	Silty sand	50/130mm	117	50	0.4
32.72	Silty sand	50/100mm	153	63	0.4
34.82	Sandy silt/Silt	82	82	33	0.4

37.44	Silty clay	47	47	19	0.4
40.31	Clayey silt till	50/150mm	102	39	0.4
43.23	Clayey silt till	50/100mm	153	57	0.4
47.93	Silty clay	91/230mm	121	44	0.4

(3) Bathurst Station

Table A3.8 Summary of the corrected SPT-N values and ratios of $\frac{(N_1)_{60}}{N_F}$ for Bathurst Station
Borehole 103-PMT

Depth (m)	Soil types	Field measured SPT-N	N_F	$(N_1)_{60}$	Ratio $\frac{(N_1)_{60}}{N_F}$
3.7	Sandy silt	43	43	47	1.1
7.1	Silty clay till	91	91	92	1.0
10.5	Silty clay till	98/200mm	149	130	0.9
13.6	Clayey silt till	68	68	52	0.8
16.4	Clayey silt till	50/100mm	153	105	0.7
19.8	Silty clay	50/125mm	122	76	0.6
22.8	Sand	50/125mm	122	71	0.6
25.6	Silty sand	68/150mm	138	76	0.6

(4) Bayview Station

Table A3.9 Summary of the corrected SPT-N values and ratios of $\frac{(N_1)_{60}}{N_F}$ for Bayview Station
Borehole BV100-PMT (i.e BV100B)

Depth (m)	Soil types	Field measured SPT-N	N_F	$(N_1)_{60}$	Ratio $\frac{(N_1)_{60}}{N_F}$
-----------	------------	-------------------------	-------	--------------	--------------------------------

7.16	Sandy silt	57	57	58	1.0
10.36	Silt	43	43	38	0.9
13.31	Sandy silt	58	58	46	0.8
16.36	Sand/Sandy silt	74	74	52	0.7
19.33	Sandy silt/Silty clay	75	75	49	0.7
22.86	Silty clay	36	36	22	0.6
25.78	Clayey silt till	58	58	33	0.6
28.58	Clayey silt till	85	85	46	0.5
31.8	Silt	70/150mm	142	72	0.5
34.7	Silt	78	78	38	0.5

(5) Bermondsey Station

Table A3.10 Summary of the corrected SPT-N values and ratios of $\frac{(N_1)_{60}}{N_F}$ for Bermondsey Station
Borehole BE05-PMT

Depth (m)	Soil types	Field measured SPT-N	N_F	$(N_1)_{60}$	Ratio $\frac{(N_1)_{60}}{N_F}$
3.2	Silty clay till	20	20	17	0.9
5.97	Silty clay till	13	13	10	0.8
9.3	Silty clay till	15	15	10	0.7
11.89	Silty clay till	10	10	6	0.6
15.6	Silty clay till	08	08	4	0.5
18.62	Silty clay till	12	12	6	0.5
21.59	Silty clay till	13	13	6	0.5
24.41	Clayey silt till	15	15	7	0.5
27.69	Silty clay till	26	26	12	0.5
30.68	Silty clay	14	14	6	0.4

(6) Blackcreek Station

Table A3.11 Summary of the corrected SPT-N values and ratios of $\frac{(N_1)_{60}}{N_F}$ for Blckcreek Station
Borehole BH7 – PMT

Depth (m)	Soil types	Field measured SPT-N	N_F	$(N_1)_{60}$	Ratio $\frac{(N_1)_{60}}{N_F}$
6.05	Gravelly sand	7	7	9	1.3
8.69	Silty clay	14	14	15	1.0
11.84	Silty clay	9	9	8	0.9
15.09	Silty clay till	14	14	11	0.8
18.06	Silty clay	8	8	6	0.8
20.85	Clayey silt till	6	6	4	0.7
24.03	Clayey silt till	20	20	12	0.6
27.53	Clayey silt till	13	13	7	0.5
30.53	Silt	8	8	4	0.5
33.60	Sandy silt	8	8	4	0.5
36.17	Sandy silt till	34	34	16	0.5

(7) Birchmount Station

Table A3.12 Summary of the corrected SPT-N values and ratios of $\frac{(N_1)_{60}}{N_F}$ for Birchmount Station
Borehole BM01 – PMT

Depth (m)	Soil types	Field measured SPT-N	N_F	$(N_1)_{60}$	Ratio $\frac{(N_1)_{60}}{N_F}$
3.78	Sandy silt till	46	46	38	0.8
6.55	Sandy silt till	86/275mm	95	79	0.8
8.99	Sandy silt till	53/150mm	108	80	0.7
11.94	Clayey silt till	50/100mm	153	106	0.7
15.06	Sandy silt till	51/150mm	104	66	0.6
18.14	Sandy silt till	54/150mm	110	64	0.6

21.34	Sandy silt/Sand	72/150mm	146	80	0.6
24.41	Sandy silt	61/150mm	124	64	0.5
27.69	Silt	50/75mm	203	98	0.5

(8) Caledonia Station

Table A3.13 Summary of the corrected SPT-N values and ratios of $\frac{(N_1)_{60}}{N_F}$ for Caledonia Station

Borehole CA203 – PMT

Depth (m)	Soil types	Field measured SPT-N	N_F	$(N_1)_{60}$	Ratio $\frac{(N_1)_{60}}{N_F}$
3.91	Sand and gravel fill	18	18	15	0.8
6.76	Clayey silt fill	4	4	3	0.8
9.37	Silty clay fill	10	10	7	0.7
12.14	Silty sand	38	38	26	0.7
15.34	Sand	27	27	17	0.6
18.44	Silty sand, silt to sandy silt	86	86	51	0.6
21.59		67	67	38	0.6
24.64		46	46	25	0.5
27.71		52	52	27	0.5
30.68		Silty clay	31	31	15
33.68	25		25	12	0.5
36.75	20		20	9	0.5
39.88	40		40	18	0.5

Table A3.14 Summary of the corrected SPT-N values and ratios of $\frac{(N_1)_{60}}{N_F}$ for Caledonia Station

Borehole CA205A – PMT

Depth (m)	Soil types	Field measured SPT-N	N _F	(N ₁) ₆₀	Ratio $\frac{(N_1)_{60}}{N_F}$
4.01	Silty clay fill	03	3	3	1.0
5.74	Silty clay fill	06	6	5	0.8
8.92	Silty clay fill	09	9	7	0.8
11.79	Silty sand	55	55	40	0.7
14.86	Silty sand	85/250mm	104	70	0.7
19.30	Sandy silt	50/100mm	153	91	0.6
21.82	Sandy silt	85	85	48	0.6
24.77	Silty sand	52	52	28	0.5
27.89	Silty sand	58	58	30	0.5
30.89	Silty clay	38	38	19	0.5
33.68	Silty clay	17	17	8	0.5
36.81	Silty clay	16	16	7	0.4

(9) Don Mills Station

Table A3.15 Summary of the corrected SPT-N values and ratios of $\frac{(N_1)_{60}}{N_F}$ for Don Mills Station

Borehole DM06 – PMT

Depth (m)	Soil types	Field measured SPT-N	N _F	(N ₁) ₆₀	Ratio $\frac{(N_1)_{60}}{N_F}$
4.22	Silty clay till	50/100mm	153	174	1.1
7.92	Silty clay	42	42	40	1.0
9.42	Silty clay	35	35	31	0.9
11.91	Sand	66	66	56	0.9
14.99	Sand	54	54	41	0.8
17.58	Silty clay	27	27	19	0.7
21.01	Silty clay	32	32	21	0.7
24.44	Silty clay	28	28	17	0.6

27.58	Silty clay	30	30	17	0.6
30.18	Silty clay	28	28	16	0.6

(10) Kennedy Station

Table A3.16 Summary of the corrected SPT-N values and ratios of $\frac{(N_1)_{60}}{N_F}$ for Kennedy Station

Borehole BH7 – PMT

Depth (m)	Soil types	Field measured SPT-N	N_F	$(N_1)_{60}$	Ratio $\frac{(N_1)_{60}}{N_F}$
4.11	Sandy silt till	Disturbed	-	-	-
6.65	Sandy silt till	93/275mm	103	79	0.8
9.80	Silty sand till	46	46	29	0.6
12.07	Silty sand	127/200mm	194	116	0.6
15.52	Clayey silt	115/250mm	140	78	0.6
19.2	Silt	123/200mm	188	98	0.5
21.39	Silty clay	59	59	30	0.5
24.79	Silty sand	79	79	38	0.5
27.74	Sand	50/125mm	122	57	0.5
30.89	Silty sand	50/100mm	153	69	0.5

(11) Lesile Station

Table A3.17 Summary of the corrected SPT-N values and ratios of $\frac{(N_1)_{60}}{N_F}$ for Lesile Station

Borehole LE02 – PMT

Depth (m)	Soil types	Field measured SPT-N	N _F	(N ₁) ₆₀	Ratio $\frac{(N_1)_{60}}{N_F}$
3.51	Silty clay (Fill)	9	9	8	0.9
6.40	Silty clay (Fill)	8	8	7	0.9
12.9	Silty clay	25	25	16	0.6
15.7	Silty clay	24	24	14	0.6
18.75	Silty clay	35	35	18	0.5
21.79	Silty clay	43	43	21	0.5
24.84	Silty sand	93/250mm	114	54	0.5
27.89	Sand	50/125mm	122	56	0.5
30.94	Sand	98/250mm	120	53	0.4

(12) Mount Dennis Station

Table A3.18 Summary of the corrected SPT-N values and ratios of $\frac{(N_1)_{60}}{N_F}$ for Mount Dennis Station Borehole MD101 – PMT (i.e MD 101C1)

Depth (m)	Soil types	Field measured SPT-N	N _F	(N ₁) ₆₀	Ratio $\frac{(N_1)_{60}}{N_F}$
3.8	Sand	33	33	27	0.8
6.0	Sand	35	35	30	0.9
9.4	Sand silt	43	43	35	0.8
13.9	Sand silt	25	25	18	0.7
15.2	Sand silt	39	39	28	0.7
18.3	Sand silt	26	26	17	0.7
21.3	Sand	51	51	31	0.6
24.5	Silty clay	12	12	7	0.6
27.3	Clayey silt till	29	29	16	0.6
30.4	Clayey silt till	45	45	23	0.5
35	Silty clay	38	38	19	0.5

(13) Victoria Station

Table A3.19 Summary of the corrected SPT-N values and ratios of $\frac{(N_1)_{60}}{N_F}$ for Victoria Station
Borehole VP01 – PMT

Depth (m)	Soil types	Field measured SPT-N	N_F	$(N_1)_{60}$	Ratio $\frac{(N_1)_{60}}{N_F}$
4.37	Silty clay till	37	37	31	0.8
6.83	Clayey silt till	14	14	11	0.8
9.83	Clayey silt till	24	24	15	0.6
13.61	Sand	21	21	13	0.6
16.18	Silt	123	123	69	0.6
19.46	Silt	79/150mm	161	85	0.5
22.25	Silt	70	70	35	0.5
25.86	Silt	15	15	7	0.5
28.88	Silt	92	92	42	0.5
31.06	Silt	34	34	15	0.4
35	Silt	88	88	37	0.4

(14) Warden Station

Table A3.20 Summary of the corrected SPT-N values and ratios of $\frac{(N_1)_{60}}{N_F}$ for Warden Station
Borehole WA04 – PMT

Depth (m)	Soil types	Field measured SPT-N	N_F	$(N_1)_{60}$	Ratio $\frac{(N_1)_{60}}{N_F}$
3.63	Silty clay till	29	29	22	0.8
5.82	Silty clay till	17	17	13	0.8
8.97	Gravelly sand	23	23	17	0.7

11.71	Silty clay till	53/150mm	108	74	0.7
15.67	Sandy silt till	50/75mm	203	126	0.6
18.44	Silty sand	86/250mm	105	61	0.6
21.01	Sandy silt	50/100mm	153	85	0.6
24.08	Silt	50/100mm	153	80	0.5
27.03	Silty sand	50/75mm	203	102	0.5
30.3	Silty sand	50/125mm	122	58	0.5

(15) West Portal Station

Table A3.21 Summary of the corrected SPT-N values and ratios of $\frac{(N_1)_{60}}{N_F}$ for West Portal Station
Borehole C3 – PMT

Depth (m)	Soil types	Field measured SPT-N	N_F	$(N_1)_{60}$	Ratio $\frac{(N_1)_{60}}{N_F}$
1.7	Sand to silty sand fill	28	28	32	1.1
3.84	Sand to silty sand fill	32	32	24	0.8
9.19	Sandy silt	06	06	4	0.7
13.77	Silty clay till	15	15	9	0.6
15.42	Silty clay till	05	05	3	0.6

(16) Wynford Station

Table A3.22 Summary of the corrected SPT-N values and ratios of $\frac{(N_1)_{60}}{N_F}$ for Wynford Station
Borehole WY03 – PMT

Depth (m)	Soil types	Field measured SPT-N	N_F	$(N_1)_{60}$	Ratio $\frac{(N_1)_{60}}{N_F}$
3.68	Silty clay till	28	28	21	0.8
5.84	Silty clay till	23	23	17	0.7
8.79	Silty clay	10	10	7	0.7
12.14	Clayey silt till	32	32	19	0.6
14.71	Silty clay	83/275mm	92	52	0.6
18.14	Silty clay till	50/125mm	122	64	0.5
20.88	Silty clay till	50/250mm	61	31	0.5
24.38	Silty sand	50/100mm	153	73	0.5
27.64	Silty sand	50/100mm	153	70	0.5
30.2	Inferred sandy soil	50/100mm	153	67	0.4

RECORD OF BOREHOLE MD101C3



PROJECT : ECLRT - Mount Dennis WLS
 LOCATION : N 4,838,370 E 305,877
 STARTED : February 4, 2013
 COMPLETED : February 15, 2013

SAMPLER HAMMER, 64 kg DROP, 750 mm
 PENETRATION TEST HAMMER, 64 kg DROP, 750 mm

SHEET 2 of 4
 DATUM GEODETTIC

DEPTH (SCALE BORING METHOD)	SOIL PROFILE DESCRIPTION	STRATA FACT	SAMPLED			ORGANIC VAPOUR READINGS (ppb)				SHAW STRENGTH CL, KPa				ADDITIONAL LAB TESTING	PROBETTER OR STANDPIPE INSTALLATION	
			SLUR DEPTH (m)	NUMBER	TYPE	% LUL - (methane)				WATER CONTENT, PERCENT						
						10	20	30	40	20	40	60	80			
12	Dense, saturated, dark brown, sandy, some gravel, trace silty and clay; (SM) DO12 Gr: 15%, Ss: 70%, W & C: 15% Contact to dense, saturated, brownish grey, sandy silt, trace clay; (SP)		11230 11231													
14	DO13 Gr: 2%, Ss: 38%, W & C: 5% grey below 15.2m		11241 11242													
16	DO15 Gr: 2%, Ss: 47%, W & C: 4%		11251 11252													
18			11261 11262													

METROLINX ON/ENB/BE/ENH/LO/2013 7101/DO-POR/MS/LJ/BE/WL/01/TTC/DET 6/0/0/13
 Depth Scale 1:50
GROUNDWATER ELEVATIONS
 SHALLOW SINGLE INSTALLATION WATER LEVEL (date) DEEP DUAL INSTALLATION WATER LEVEL (date)
 SPL Consultants Limited
 Geotechnical Engineering Materials Hydrogeology
 LOGGED: LJ CHECKED: RJ

RECORD OF BOREHOLE MD101C3



PROJECT : ECLRT - Mount Dennis WLS
 LOCATION : N 4,838,370 E 305,677
 STARTED : February 4, 2013
 COMPLETED : February 15, 2013

SAMPLER HAMMER, 64 kg DROP, 760 mm
 PENETRATION TEST HAMMER, 64 kg DROP, 760 mm

SHEET 3 of 4
 DATUM GEODETIC

DEPTH SCALE (metres)	BOTTING METHOD	SOIL PROFILE		SAMPLES		ORGANIC VAPOUR READINGS (ppm)		SHOAR STRENGTH CL. Rtg (kPa)		ADDITIONAL LAB. TESTS	PIEZOMETER OR STAINLESS INSTALLATION
		DESCRIPTION	STRATA PLLOT	RUN DEPTH (m)	NUMBER TYPE	% LAL - (methane)	% LAL - (methane)	SHOAR STRENGTH CL. Rtg (kPa)	SHOAR STRENGTH CL. Rtg (kPa)		
		Compact to dense, silty, brownish grey, SANDY SILT, trace clay. (py) (Continued)		18	50 DO						
		Compact to very dense, silty, brownish grey, SAND, some sil, trace clay. (SM)		19	50 DO						
-22		DC04 Gr-2%, Sk 34%, Sl 15%, Cl 1%		20	50 DO						
		contains clayey silty sands at 22.0m		21	50 DO						
-24		Soft to very soft, (softener) (mass) and (sand) (silty) grey, SILTY CLAY, trace silty. (CL)		22	50 DO						
		DC01 Gr-2%, Sk 5%, Sl 47%, Cl 28%		23	50 DO						
-26		Very soft to soft, below sands silty, grey, CLAYEY SILT, sandy trace gravel, LL (CL-M)		24	50 DO						
		DC04 Gr-4%, Sk 22%, Sl 46%, Cl 17%		25	50 DO						

Depth Scale 1:50

GROUNDWATER ELEVATIONS

SHALLOW SINGLE INSTALLATION
 WATER LEVEL (date)

 DEEP DUAL INSTALLATION
 WATER LEVEL (date)

SPL Consultants Limited
 Geotechnical Environmental Materials Hydrogeology
 LOGGED: LJ CHECKED: RJ

RECORD OF BOREHOLE MD101C3



PROJECT : ECLRT - Mount Dennis WLS
 LOCATION : N 4,838,370 E 505,877
 STARTED : February 4, 2013
 COMPLETED : February 15, 2013

SAMPLER HAMMER, 64 kg; DROP, 750 mm
 PENETRATION TEST HAMMER, 64 kg; DROP, 750 mm

SHEET 4 of 4
 DATUM : GEODEIC

DEPTH SCALE (metres)	BORING METHOD	SOIL PROFILE		SAMPLES		ORGANIC VAPOUR READINGS (ppm)				SHAW STRAINING CL. FOR				ADDITIONAL LAB. TESTING	PIEZOMETER OR SANDPIPE INSTALLATION
		DESCRIPTION	STRAIN FACT	SLV. DEPTH (m)	NUMBER	TYPE	% L.L. - (methane)				WATER CONTENT, PERCENT				
		Very soft to hard, brown to black, grey, CLAYEY SILT, sandy, trace gravel; TEL (C, M); (continued)			36	SO	DO								
		Very soft to hard, close to plastic limit, grey, SILTY CLAY, trace sand, occasional gravel; (C, L)		30.00	36	SO	DO								
		DO07 Gr: 2%, Ss: 2%, Sk: 67%, Cl: 24%		30.00	37	SO	DO								
				30.00	38	SO	DO								
		END OF BOREHOLE Note: 1) Casing (75mm PVC) was installed for close-hole seismic survey 2) Two additional boreholes were drilled for close-hole seismic survey in adjacent borehole MD101C1 and MD101C2, with 75mm PVC casings. Piezometer testing was conducted in borehole MD101C1. 3) SW describe combined sieve and hydrometer analysis. 4) SW describe environmental analyses (per DSD 11; O Reg. 152(11) metal & inorganic; or MSDR; O Reg. 559 metal & inorganic).		30.00											

METROLINX OVERBURDEN/SHOULDER TIGER/BEFORE/MAJURE/BLU/1/TIGER/BLU/1

Depth Scale 1:50

GROUNDWATER ELEVATIONS

SHALLOW SINGLE INSTALLATION
WATER LEVEL (date)

DEEP DUAL INSTALLATION
WATER LEVEL (date)

SPL Consultants Limited
 Geotechnical/Environmental/Materials/Hydrogeology

LOGGED: LJ CHECKED: RJ

APPENDIX 4.2

Table D1: Summary of Pressuremeter Test Results from Borehole MD101-PMT (i.e. MD101C1)

Test No.	Test Depth (m)	Test Elev. (m)	Soil Type*	E_{PMT} (MPa)	$E_{Unload\ 1}$ (MPa)	$E_{Reload\ 1}$ (MPa)	p_y (kPa)	p^*_t (kPa)
1	3.8	118.7	Sand	0.2	0.6	0.6	84	214
2	6.0	116.5	Sand	25.8	160.4	9.1	989	2421
3	9.4	113.1	Sandy silt	40.8	159.1	67.0	582	2735
4	13.9	108.6	Sandy silt	38.6	209.7	100.4	700	3126
5	15.2	107.3	Sandy silt	27.8	151.5	68.5	596	2657
6	18.3	104.2	Sandy silt	28.9	139.6	58.2	533	1940
7	21.3	101.2	Sand	29.1	125.2	63.6	638	2428
8	24.5	98.0	Silty clay	36.2	116.0	45.0	676	1520
9	27.3	95.2	Clayey silt till	46.2	140.0	65.5	789	994
10	30.4	92.1	Clayey silt till	53.9	148.5	83.4	1063	1110
11	35.0	87.5	Silty clay	22.7	145.2	97.9	786	1373

Notes: * Soil type is based on the information in adjacent Borehole MD101C3.